Aerosol Particle Electroscavenging by Droplets

A DISSERTATION
SUBMITTED TO THE FACULTY OF THE GRADUATE SCHOOL
OF THE UNIVERSITY OF MINNESOTA
BY

Meng Zhang

IN PARTIAL FULFILLMENT OF THE REQUIREMENTS
FOR THE DEGREE OF
Doctor of Philosophy

Thomas H. Kuehn, Advisor

June, 2012

Acknowledgements

Many people have helped and encouraged me during my doctoral study.

First, I would like to thank my classmates and lab mates in the Mechanical Engineering department. Daniel Thomas, Guang Yang, Nick Stanley, Jim Wang and Christof Asbach, thanks for all the advice and assistance.

My gratitude also goes to the Mechanical Engineering computer lab for supporting me with all hardware and software issues. There are not enough words to describe their excellent work.

I am thankful to members of my exam committee including Professors James Ramsey, Virgil Marple and Peter Raynor. I would especially like to thank my advisor, Professor Thomas Kuehn who was abundantly helpful and offered invaluable assistance, support and guidance. His enthusiasm in research will continue to influence me along my career path.

Finally, my deepest gratitude goes to my family for their love and encouragement throughout my life. My parents have given me their unequivocal support. It would not have been possible to write this doctoral thesis without their help. Most of all, I would like to thank my wife, Hao Shen, who is always supportive and patient to help me through those years towards my degree.

Dedication

I would like to dedicate this dissertation to my beloved parents.

Abstract

When water droplets precipitate under the action of gravity and frictional forces, they will collide with smaller aerosol particles and fall to the ground. Usually, either droplets or aerosol particles carry some electric charges, and some may be highly charged. Therefore, the electrostatic effect is a very important factor in particle scavenging.

Wet scrubbers as air pollution control devices use the same theory as scavenging to remove both particulate and gas contaminants from the industrial exhaust streams. Electrostatic wet scrubbers were developed in an attempt to improve collection efficiency by raising the attraction force between droplets and particles. Very few numerical models have been developed to describe the phenomenon of particle collection by highly charged droplets when electrostatic force is dominant.

In an attempt to understand the physics of scavenging, a new three-dimensional model has been developed to simulate neutral or charged particles collected by a group of neutral or charged droplets. The model can simulate the particle traveling through a matrix of droplets. Both the inertial effect and the electrostatic effect on particle scavenging have been considered. The collection efficiency can be estimated by utilizing this developed model. The effect on the collection efficiency by the size of the particle and of the droplet, the charges of the particle the droplet, and droplet distance have been investigated. A validation approach has also been developed and the study results have achieved good agreement with published data.

Contents

List of Tables

List of Figures

Nomenclature

γ	surface tension
e	elementary charge
λ	mean free path
μ	dynamic viscosity
μ	kinematic viscosity
ρ	air density
ρ_d	droplet density
ρ_p	particle density
τ	characteristic relaxation time
ε_0	dielectric permittivity of free space
A	area
C_c	Cunningham correction factor
C_D	drag coefficient
D	droplet diameter
d	particle diameter
E	collection efficiency

F_e	electrostatic force
g	acceleration of gravity
g^*	net gravitational acceleration
Kc	the Coulomb number
L	droplet distance
M	particle mass
m	mass flow rate
n_L	Rayleigh limit
p	pressure
Q	droplet charge
q	particle charge
R	droplet radius
r	particle radius
Re_d	droplet Reynolds number
Re_p	particle relative Reynolds number
S	distance between droplet and particle
St	the Stokes number
U	flow velocity
u	air velocity in x direction
v	air velocity in y direction
V_{dt}	droplet settling velocity
V_{pt}	particle settling velocity

V_p	particle velocity
w	air velocity in z direction

Chapter 1

Introduction

The study of particle collection by droplets can be applied to two major areas, air atmospheric aerosol scavenging and industrial pollution control. The atmospheric aerosol is very important to global climate and human health. The most common method of atmospheric aerosol removal is by precipitation washout. For pollution control, wet scrubbers have been used widely to remove particulate pollutants by applying the mechanisms of particle and droplet collision.

In atmospheric environments, below-cloud particle scavenging by falling droplets is the most common mechanism of atmospheric aerosol particle clean-out. Therefore, it has always been of concern to researchers. Many studies, for example, field studies [4, 5] and numerical simulations [6, 7, 8, 9] have been done since the 1970s. The droplets and particles usually can be charged in nature. The droplet and particle interaction caused by the electrostatic effect has also been included in some studies. Recently, in-cloud scavenging has also attracted attention. In-cloud scavenging refers to the droplet collision to form raindrops. Some studies [10, 11] develop rain enhancement and fog elimination methods by injecting charged droplets into clouds. The charged droplets can greatly increase the possibility of droplet collision.

From the viewpoint of wet scrubber design, collection efficiency and energy consumption are two major concerns. The venturi scrubber, the most commonly used high-energy scrubber, is efficient in larger particle removal by use of an impaction mechanism. For submicron particles, the Venturi scrubber cannot provide the required collection efficiency. The Venturi scrubber has high gas velocity, the abrasion of the scrubber shell

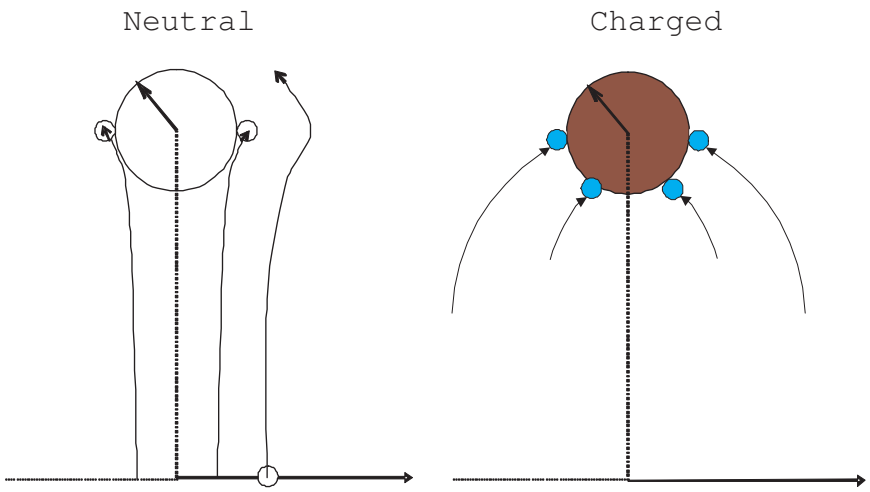

Figure 1.1: Schematic of electrostatic force collection mechanism

is a primary maintenance problem. In addition, the Venturi scrubber can be costly because of high energy consumption. A Low-energy scrubber, such as air washer, is adequate for the collection of coarse particles and gas contaminants. It is a very useful and inexpensive control device but it cannot provide enough collection efficiency for submicron particles. To overcome this problem, Penney [12] proposed the idea of a wet electrostatic scrubber. By charging droplets in air washers, the collection efficiency for submicron particles can be greatly improved. Therefore, an electrostatic wet scrubber is a very economic and promising way for separation of submicron particles. Figure 1.1 shows the efficiency enhancement by oppositely charging droplets and particles. Some previous studies also show that the collection efficiency can be improved even though the droplets and particles are charged to the same polarity. This is because the repulsive force between droplets and particles will repel the particles to the walls of scrubbers. Several experimental studies [13, 14, 15, 16, 17] on electrostatic wet scrubbers have been conducted. Those experimental data only provide a short range of results in terms of particle and droplet size and charges. Moreover, those experiments are designed for industrial purposes; they are difficult to compare with numerical results to know the fundamental physics.

Estimating the collection efficiency of particles scavenged by droplets is the core concern for both atmospheric aerosol scavenging and wet scrubber performance. Several theoretical correlations are proposed by [18, 19]. However, a large discrepancy exists between correlations and numerical or experimental results. Many numerical studies have used a method of determining the particle trajectory around the droplet to calculate the collection efficiency. However, those numerical studies simplified the model to be only a two-dimensional one droplet and one particle situation. It is unrealistic in real cases where a population of particles is usually washed out by a group of droplets. The effects on scavenging by the interaction between droplets needs to be investigated. In addition, most previous studies concentrated on the effects of droplet or particle size and several mechanisms on collection efficiency. There are very few studies on collection efficiency caused by electrostatic effects especially in cases when the collector or the small particle is highly charged.

The objective of this work is to develop a three-dimensional numerical model for describing the phenomenon of particle collection by multiple droplets. Particles start from different positions and travel into a droplet matrix. A portion of the particles can be collected by the droplets, and the rest of the particles can pass through the matrix. The electrostatic effect and droplet spacing are considered in the model. The collection efficiency will be determined by counting the portion of collected particles.

Chapter 2

Background

2.1 Application of particle and droplet interaction physics

Studying the particle and droplet interaction physics is very important to pollution control. Wet scrubbers have been used widely in removing pollutants. Generally, they utilize the physics of a liquid in direct contact with a contaminated gas. For particle removal, the capture mechanisms include:

1. Inertial impaction
2. Direct interception
3. Diffusion
4. Electric forces
5. Condensation
6. Thermal gradients

There are many types of wet scrubbers. In general, they can be categorized by energy consumption. Typically, low-energy scrubbers have a pressure drop less than 1200 Pa; medium-energy scrubbers have a pressure drop from 1200 to 3700 Pa and high-energy scrubbers have a pressure drop greater than 3700 [20].

The most common high-pressure wet scrubber is the Venturi scrubber. To achieve high collection efficiency for particles by impaction, it uses a high-velocity gas flow to

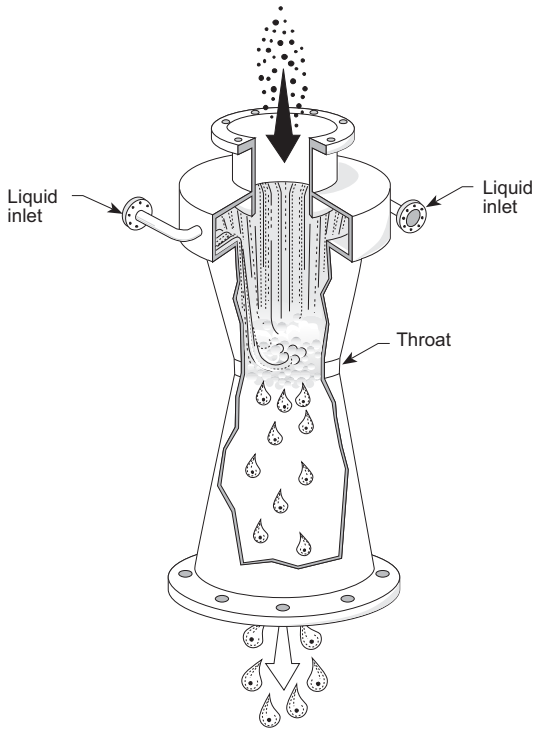

Figure 2.1: Schematic of a typical Venturi scrubber [2]

atomize the liquid. As shown in Figure 2.1, the high velocity gas flow impacts with the scrubbing liquid and small water droplets are formed. The particles are collected by the water droplets and separated from the gas flow. Higher gas velocity can cause greater turbulence, which increases the efficiency of particle collection. The Venturi scrubber can have very high particle collection efficiency, but it is energy consuming and causes significant maintenance problems, such as the abrasion of the scrubber shell caused by high velocity gas flows.

Figure 2.2 shows a typical design of a plate tower, a medium-energy scrubber. The gas flow enters at the bottom and flows upward, contacts and atomizes the liquid falling several plates. Plate towers are efficient in removing gaseous pollutants. However, they are not appropriate for particle removal, because particles can accumulate in the holes in the plates.

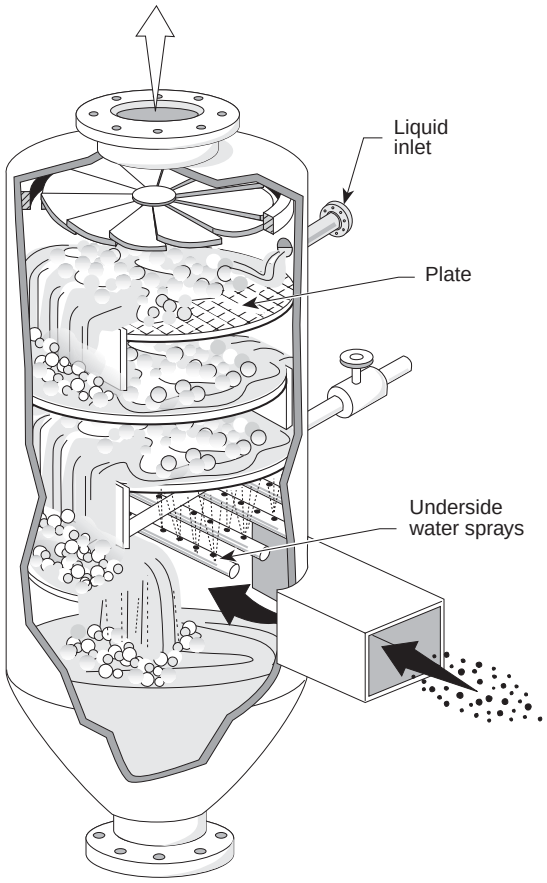

Figure 2.2: Schematic of a typical plate tower scrubber [2]

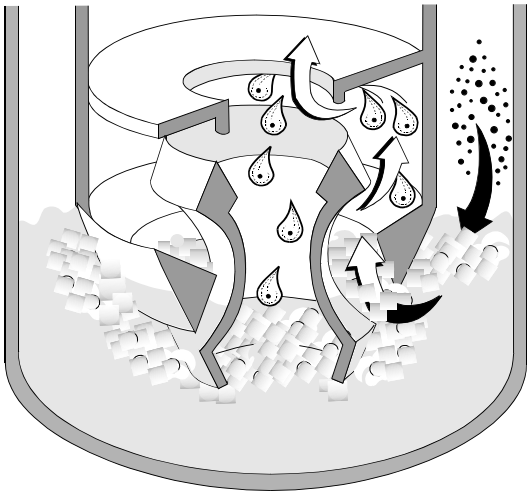

Figure 2.3: Schematic of a typical orifice scrubber [2]

The orifice scrubber is another example of a medium-energy scrubber with moderate collection efficiency. As shown in Figure 2.3, the gas flow with particles passes through a pool of liquid, and creates a large number of droplets when leaving the liquid surface. Large particles in the gas flow can be collected by impaction in the pool, while small particles may be collected by droplets generated by the gas liquid interaction.

Compared to the previous scrubbers, spray towers are low-energy. Figures 2.4 and 2.5 show two different designs, counter-current flow and cross-current flow scrubbers. They have the same particle collection mechanisms. Nozzles produce liquid droplets washing out particles by colliding droplets and particles. The energy needed for spray towers is much lower than for Venturi scrubbers. The pressure drop across spray towers is generally 250 Pa, while the pressure drop for Venturi scrubbers ranges from 1200 to 25000 Pa. However, the particle collection efficiency of spray towers is lower than for the Venturi scrubber.

For Venturi scrubbers, the performance of particle removal strongly depends on pressure drop, which is related to the power requirement and the size of auxiliary equipment. Several studies have been done to predict pressure drop numerically. The most

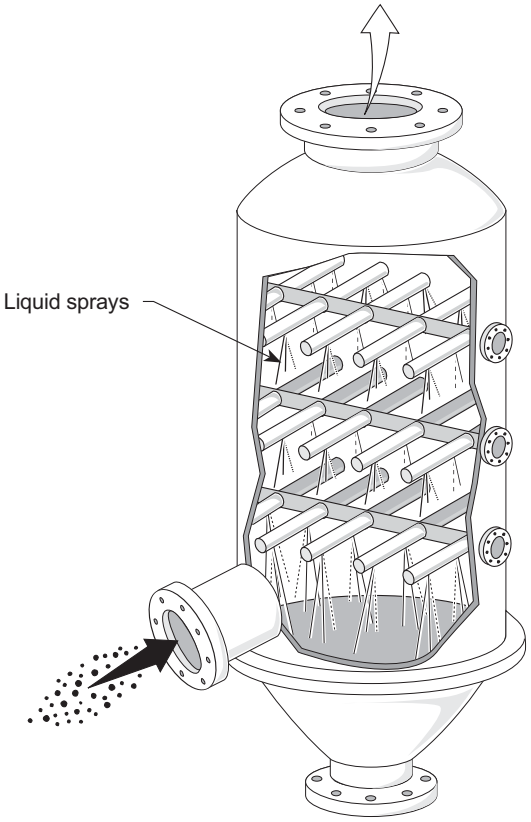

Figure 2.4: Schematic of a typical counter-current flow scrubber [2]

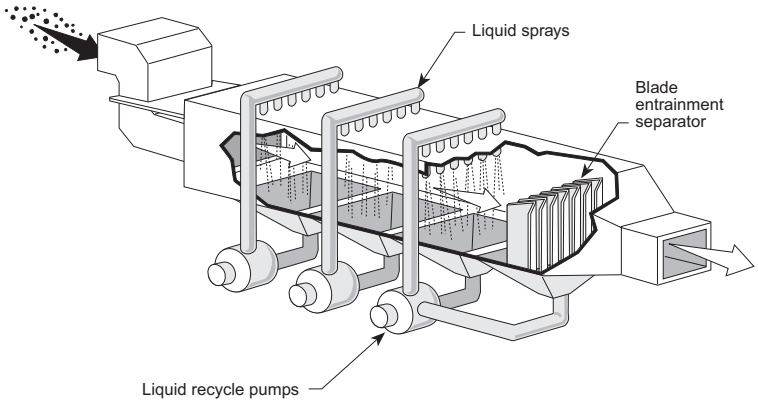

Figure 2.5: Schematic of a typical cross-current flow scrubber [2]

widely used model was proposed by Calvert [21]. This model used a very simple one-dimensional momentum balance equation to describe the gas liquid system. However, this model overestimated pressure drop because it assumed that droplets always reach the gas velocity at the throat, which might not be true in real cases. Yung [22] and Leith [23] extended Calvert's model using some correlations to fix the overestimation. Hesketh [24] derived an empirical equation that fit experimental data to predict pressure drop. Boll [25] was the first one to solve the pressure problem numerically. He used a differential equation of one-dimensional flow for the momentum balance along the scrubber. Azzopardi [26, 27, 28] and Pulley [29] developed a model using annular two-phase flow knowledge. The model assumes a situation where a gas flow with droplets is surrounded by a film flowing on the walls of the Venturi scrubber. The advantage of this model is that it considers the exchange of liquid between the film and gas flow.

Low energy wet scrubbers, such as air washers, are efficient for gas contaminant removal. They can usually reach above 90% removal efficiency depending on the gas material properties [30, 31]. However, the particle removal efficiency is not as high as gas contaminant removal efficiency, especially for small aerosol particles in the size range of the "Greenfield gap" ($0.2 \ll d \ll 2\ \mu m$). Several approaches were attemped to solve this problem.

Schaber and Koch [32] conducted the experiment to study the behavior of acid aerosols in humid air. They found that the size of acid aerosols can grow by humidification even without supersaturation. The size of submicron particles can increase by a factor of two, and therefore improve the scavenging of these particles.

Sun [33] proposed a new approach that used injection of steam in a wet scrubber to achieve a supersaturation environment. The test showed that 90% of submicron particles can grow to micron size particles, and thereby are easily removed by the impaction mechanism.

Electrostatic wet scrubbers are another approach that uses electrosatic scavenging mechanism to improve collection efficiency. Penney [12] was the first to propose the idea of a wet electrostatic scrubber. Aerosol particles and scrubbing droplets are electrically charged to the same or opposite polarities. The particles charged oppositely to the droplets will be collected by coulomb attraction forces. If the particles and droplets have the same polarity, the particles can be repelled to the scrubber walls. Electrostatic

wet scrubbers were selected as the best technology in the future for submicron particle control [34]. Sheppard [35] made a comparison of the operating costs for an electrostatic wet scrubber and a Venturi scrubber at the same performance level. The electrostatic wet scrubber showed significant savings compared to the Venturi scrubber.

Particle and droplet interaction physics is also utilized to study atmospheric aerosol scavenging. Atmospheric aerosol is very important to global climate and human health. The scavenging of atmospheric aerosol is mainly by clouds and precipitation. There are two types of scavenging, in-cloud and below-cloud scavenging. In-cloud scavenging refers to collision of cloud drops. Recently, in-cloud scavenging has attracted concern because it can be applied to rain enhancement and fog elimination. Rain enhancement is a practical way for solving water shortage problems in some countries. Fog elimination is to increase visibility in certain areas such as runways of airports. For those purposes, a portion of droplets is taken from clouds, charged, and then injected back to clouds to accelerate droplet collision. Below-cloud scavenging occurs when atmospheric aerosols are removed from the air by precipitation. It is a very important factor, which affects atmospheric aerosol population.

2.2 Numerical and analytical study of aerosol scavenging

Greenfield (1957) [36] was one of the first to study various scavenging mechanisms, including Brownian diffusion, turbulent shear diffusion and inertial impaction. He found that the aerosol particles of diameter $d \gg 2\ \mu m$ are easier to be captured by inertial impaction, while the particles of $d \ll 0.2\ \mu m$ can be collected by Brownian diffusion. The particles with diameter $0.2 \ll d \ll 2\ \mu m$, defined as the "Greenfield gap", have the minimum collection efficiency.

Many studies considered only one collection mechanism and calculated the collection efficiency. Walton and Woolcock derived an equation for the collection efficiency by inertial impaction [37]. Fuchs provided the analytical solutions for the collection efficiencies by diffusion and interception [38]. Waldman and Schmidt [39] studied the collection efficiency contributed from thermophoresis.

Several studies on the overall scavenging efficiency by combining several collection mechanisms were made by Slinn and Hales [40, 41], Davenport[42] and Young [43]. In

their approach, they assumed that the total collection kernel can be determined from a summation of the collection kernels for each of the individual scavenging mechanisms.

$$E = 1 - (1 - E_{imp})(1 - E_{int})(1 - E_{dif})(1 - E_{th})(1 - E_{dph}) \tag{2.1}$$

where E_{imp}, E_{int}, E_{dif}, E_{th} and E_{dph} are the efficiency caused by impaction, interception, diffusion, thermophoresis and diffusiophoresis efficiency respectively.

However, this approach neglected the coupling of different mechanisms, and therefore inaccurately estimated the overall collection efficiency.

There were some approximate formulas proposed by Langmuir and Blodgett [44], Walton and Woolcok [37] and Viswanathan [45] for roughly estimating the particle collection efficiency. Kraemer and Johnstone [18] proposed a collection efficiency correlation for the highly charged droplets and particles. Based on that, Nielson and Hill [19] proposed a new correlation by incorporating the Stokes number.

$$E = (2(-Kc)^{1/2} - 0.8St)^2 \tag{2.2}$$

where E is the collection efficiency, Kc is the Coulomb number and St is the Stokes number. However, it was found that all theoretical correlations had a large discrepancy with experiment and numerical results [46].

Quantitative studies have used a method where the total collection efficiency was obtained by determining the trajectory of a particle around a droplet. To calculate particle trajectories, the important step is to solve the problem of the hydrodynamic interaction between two particles moving in an airflow. Pruppacher and Klett [47] proposed the superposition method to overcome this problem. Basically, this method assumed that each particle moved in a flow caused by the other particle alone.

When using this method, the velocity fields induced by moving particles must be known. Several studies, including Hocking [48], Hocking and Jonas [49], Davis [50], and Davis and Sartor [51] used the analytical Stokes solution for the flow field [52]. The Stokes flow, also called creeping flow, neglects the flow inertial force and is only applicable to a low Reynolds number ($Re << 1$). Therefore, the droplet diameter considered in those studies was limited to less than 60 μm.

Oseen [47] obtained the stream function for viscous flow by linearizing inertial force in the Navier-Stokes equation. Oseen's approximation is applicable to a Reynolds number less than 2. Klett and Davis [53] took inertial effect into account by using analytical flow field results from Oseen's equations by Carrier [54]. The droplet size was limited to less than 140 μm.

For a Reynolds number larger than 1000, the viscous force is negligible to the inertial force. The potential flow assumption fits in this situation. Viswanathan [45] took potential flow assumption into the calculation of flow field for solving the particle trajectory.

Another approach is to solve the velocity field numerically. Dau [55], Schmidt and Loffler [14], and Adamiak [56] solved the Navier-Stokes equations by assuming two-dimensional axisymmetric flow around a droplet. Lin [6] and Beard [7] used the numerical results for viscous flow around a sphere at intermediate Reynolds numbers published by Le Clair [57]. The droplet size was extend to 1200 μm and the scavenging mechanisms included impaction and interception.

In 1977, Grover and Pruppacher [9] computed the collection efficiency with which aerosol particles ($1 \ll d \ll$ 20 μm) collided with droplets of diameters ranging from 80 to 800 μm. The flow field around the water droplet was from LeClair's numerical results. The mechanisms considered in the study included impaction, interception, thermophoresis, diffusiophoresis and external electric field. Schlamp and Grover [58] also used the same approach to investigate the effect of electric charges and vertical external electric fields on the collection efficiency. In 1978, to investigate the collection of relatively small particle ($d <$ 1 μm), Wang [8] proposed a method of determining the particle flux to a droplet. The model considered Brownian diffusion, thermophoresis, diffusiophoresis and electric effects but neglected inertial effects.

In 2000, Pinsky and Khain [59] numerically calculated the collection efficiency in a wide range of droplet (from 2 to 500 μm) and particle (from 2 to 500 μm) sizes. In their study, the flow field results were obtained by interpolating two analytical solutions based on the Reynolds number. The Stokes solution was considered for a low Re number ($Re << 1$) while the Hamielec and Johnson solution [60] was for an intermediate Reynolds number ($Re < 100$).

In their study, only the inertial effect was considered but thermophoresis, diffusiophoresis, and electric forces have not been accounted for. In a recent study, Pinsky and Khain also explained the turbulence effect on collection efficiencies [61]. They found that the collection efficiencies in a turbulent flow are greater than those in a calm atmosphere.

In 2004, Khain et al. [10] studied the electric charging effect on collection efficiency. Because the study focused on rain formation in clouds, both the droplets and particles ranged from 0 to 40 μm and the Stokes solution was used for the flow field. The charges ranged from neutral to their Rayleigh limits. Their results showed that high collection efficiency can be obtained by charging the droplets and particles oppositely.

Tinsley and Rohrbaugh [62] investigated image charging effects on scavenging. The results showed that image charge forces provide an attraction when the particle size is large and neutral or only charged with a few elementary charges. That attraction can increase the collection efficiency, which is important for the scavenging of aerosol particles in the size range of the "Greenfield gap".

In 2002, Jaworek and his coworkers [63] proposed a three-dimensional model to calculate the collection efficiency for scavenging particles by charged droplets. They used the methodology of predicting the particle trajectory similar to previous one droplet two-dimensional models. However, the flow field results were for three-dimensional models, as well as particle trajectory determination. It was claimed that three-dimensional results can provide much more information on the complex nature of the scavenging process than two-dimensional results.

All of the models reviewed above concentrate on the physics of collision between only one droplet and one particle. However, in many real cases, such as wet electrostatic scrubbers or rain scavenging, a cluster of droplets might exist. The trajectory of a small particle in a group of droplets may be quite different from the case of only one droplet. This is because the flow field within a group of droplets can be different and all of the droplets near the particle can affect its motion.

Kojevnikova and Zimmels [3, 64, 65] conducted a series of studies on the collection of aerosol particles by an array of oppositely charged droplets from 1999 to 2002. It was assumed that the charged droplets were distributed uniformly and had the same size and charge. A small particle started below the droplet matrix, and then entered

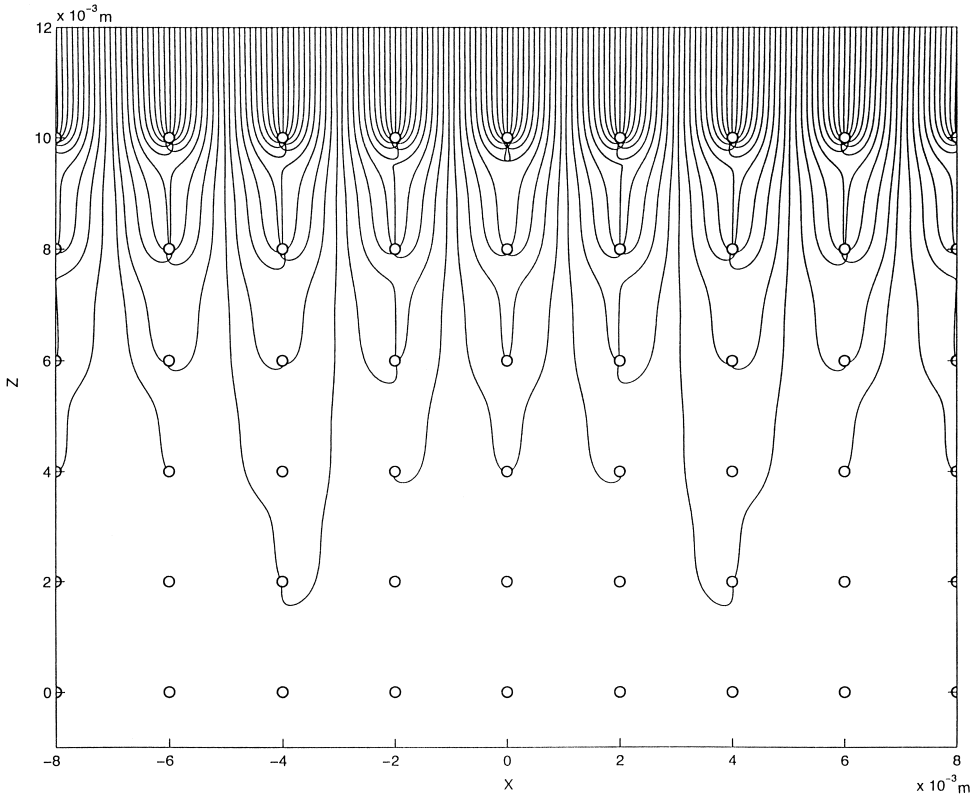

Figure 2.6: Trajectory results of a 10 μm particle collected by a rectangular, 8x17 array of 200 μm droplets: $Q = 1.0 \times 10^{-12} C, q = -3.0 \times 10^{-14} C$ [3]

it. The motion equation for the particle was solved to determine how many matrix rows it can pass through before collection. The particles that had greater inertia and a lower coulomb number can penetrate more rows before colliding with a droplet. Figure 2.6 shows an example of a particle trajectory solution. There were two limitations in their approach. One was that the flow field solution only accounted for a single droplet under creeping flow approximation. There was no interaction between droplets in terms of flow field. The second was that it can only explain the phenomenon of a particle traveling through the first several rows of a droplet matrix. It did not provide results for the situation in which a particle moves in the middle of a fully developed droplet matrix.

2.3 Experimental study of aerosol scavenging

Many experimental studies on aerosol scavenging have been performed over the past 30 years. All of the experiments discussed here are divided into two groups, one is for atmospheric aerosol scavenging, and the other is for electroscrubbing.

2.3.1 Atmospheric aerosol scavenging experiments

Chate [4] experimentally investigated the density of aerosol material on the collection by water drops. He used NaCl, $MgSO_4$ and $MgCl_2$ particles and considered several mechanisms including diffusion, impaction and interception. It was shown that the collection efficiency increased as the impaction parameter increased, which was caused by either a change of particle size or density. Vohl [66] studied the effects of turbulence on the scavenging of aerosol particles utilizing a wind tunnel. Song [67] conducted experiments to study aerosol scavenging by ice in supercooled clouds. It was found that the scavenging efficiency depended on the size of ice crystals and aerosols. However, the dependence of the efficiency on temperature was very small. Krasnogorskaya's study [68] focused on in-cloud scavenging. Therefore, the collision of droplets of comparable size were investigated. Several studies including Hampl [69], Adam [70], Lai [71] and Wang [72] studied submicron aerosol particles collected by falling water droplets with sizes ranging from hundreds to a thousand microns. They used different methods for particle and droplet generation. Because a single droplet can collect only very few

Table 2.1: Summary of literature on numerical scavenging studies

Reference	Droplet size	Particle size	Flow field solution	Approach	Mechanisms
Hocking [48]	$< 60\ \mu m$	12-60 μm	Stokes solution	2D one droplet	Impaction,Interception
Klett [53]	$< 140\ \mu m$,	14-140 μm	Oseen's solution	2D one droplet	Impaction,Interception
Viswanathan [45]	Unknown	Unknown	Potential flow solution	2D one droplet	Impaction,Interception
Lin [6]	40-400 μm	8-400 μm	Numerical solution	2D one droplet	Impaction, Interception
Grover [9]	84-876μm	1-20 μm	Numerical solution	2D one droplet	Impaction, Interception Phoretic and Electrical forces
Wang [8]	84- 620 μm	0.002-2 μm	NA	Particle flux	Diffusion, Thermophoresis Electrical force, diffusiophoresis
Pinsky [59]	2-500 μm	2-500 μm	Stokes solution Hamielec solution	2D one droplet	Impaction, Interception
Khain [10]	2 - 40 μm	2 - 40 μm	Stokes solution	2D one droplet	Impaction, Interception Electric force
Tinsley[62]	36-212 μm	0.2-2 μm	Stokes solution	2D one droplet	Impaction, Interception Electric force
Jaworek [63]	0.1-1 mm	1-10 μm	Numerical solution	3D one droplet	Impaction, Interception Electric force
Zimmels [3, 64, 65]	200 μm	10-80 μm	Stokes solution	2/3D array of droplets	Impaction, Interception Electric force

particles, detection has always been one of the concerns in scavenging experiments. Lai and Hampl used AgCl particles because they were easily identified. Adam used bacillus subtilis spores as the collected particles. After scavenging, the solution was incubated in a petri dish, and the colonies originating from the individual spores were counted to estimate total original collected particles. Indium can also be used as the collected particle material because it is easy to detect and analyze by means of the neutron activation technique. Lai studied the effects of droplets and particles on collection efficiency. Adams concentrated on the situation in which charged droplets collected on uncharged aerosol particles.

2.3.2 Electroscrubbing experiments

Pilat [13] experimentally investigated the collection of charged aerosol particles with diameters ranging from 0.05 to 5 μm by charged water droplets in a two-chamber vertical scrubber. Results showed that the overall collection efficiency for 1.05 μm particles increased from 68.8% to 93.6% by charging the droplets and particles to opposite polarity. The collection efficiency for 0.3 μm increased from 35% to 87%.

Schmidt [14] investigated a vertical electrostatic scrubber with a pneumatic atomizer. The collection efficiency for the particles ranging from 0.3 to 10 μm charged oppositely to the droplets increased by more than 400 % compared to the uncharged condition. However, the droplet size and charge information was not provided in the literature; it was hardly compared to any theoretical results.

Yang [43] experimentally investigated an electrostatic Venturi scrubber with a pneumatic atomizer. The collection efficiency for 0.5 μm particles improved from 79% to 89% with induction charging at 2.0 kV.

Wang [75] conducted experiments for charged submicron particles collected by charged water droplets ranging from 137 to 500 μm. All experiments were conducted in a situation where the Coulomb force was dominant. The relations of the collection efficiency with the particle charge, the particle and droplet size were provided individually.

Hara [76] used a stereo microscope to visually observe trajectories of charged particles near charged collector droplets. As shown by observation, the charged droplet cloud expanded and concentration decreased in the existence of neutral particles. When droplets and particles charged oppositely, droplets migrated to the central area of the

Table 2.2: Summary of literature on atmospheric aerosol scavenging experiments

Reference	Droplet size	Particle size	Droplet generating method	Particle type and generating method
Chate [4]	20-400 μm	2-6 μm	Vibrating orifice TSI 3450	NaCl, $MgSO_4$ and $MgCl_2$
Vohl [66]	692 μm, 3.36 mm and 5.76 mm	0.32-0.46 μm	distilled water injected	Indium acelylacetonate
Song [67]	50-300 μm	0.109 and 0.551 μm	Ice crystals	Latex particles atomized by TSI 3076
Kranogorskaya [68]	50-300 μm	0.109 and 0.551 μm	Ice crystals	Latex particles atomized by TSI 3076
Lai [71]	0.62,0.82, 0.98 and 1.82 mm	0.15-0.45 μm	Blowing off droplets formed on a needle tip by constant air flow	AgCl generated by furnaces enclosing combustion tubes
Adam [70]	0.1- 2 mm	0.7-1.2 μm	dripping water from a hypodermic needle	Bacillus subtilis spores
Abbcott [73]	10-25 μm	10-25 μm	Unknown	Unknown
Hampl [69]	0.71-2.54 mm	0.7-1.2 μm	a dropping device with a hypodermic needle	AgCl generated by furnaces enclosing combustion tubes
Leong [74]	112-186 μm	0.58-3.16 μm	TSI 3050	Unknown
Wang [72]	150-2500 μm	0.5 μm	Hypodermic needle	Indium acetylacetonate

space. In contrast, droplets expanded to the wall if they carried the same polarity charge as the particles. The collection efficiency as a function of particle charge was also provided in the literature.

Smirnov [77] observed charged monodisperse particles falling onto a fixed and charged metal sphere. He varied the Reynolds number from 5 to 100 to reveal its relation to collection efficiency.

Jaworek and his coworkers [16] numerically and experimentally investigated submicron charged dust particles collected by charged droplets. They used the tip of a capillary to generate water droplets charged by induction, and the particles were charged in an AC boxer charger. They determined the particle trajectory necessary to calculate the collection efficiency. The experimental collection efficiency results compared well with the numerical results.

Krupa [15] used a multiple-nozzle electrospray system to generate charged droplets. The collected particles were charged in a DC corona discharger. The collection efficiency was higher than 90% for 5 μm particles. The liquid to gas ratio was 0.08 l/m^3, which was much lower than the one at the uncharged situation.

Jaworek [17] also investigated a multi-nozzle electrospray system for particle removal. He pointed out that the electrospray is more effective in particle charging than the pneumatic atomizer with induction electrode. Electrospray can generate smaller droplets than pneumatic atomizers, and can charge droplets to half of the Rayleigh limit.

The droplet and particle sizes, charges and relative velocities were varying for different studies. However, in general, there were several conclusions for the electroscaving mechanism.

1. The principle of electrostatic scrubbing can greatly increase the collection performance without increasing pressures.

2. Smaller droplets are much more efficient in collecting particles compared to larger droplets.

3. Higher relative velocity between droplets and particles cannot necessarily improve the collection efficiency in electrostatic scrubbers. The typical method of increasing flow speeds or coagulating the fine particles cannot apply to electrostatic scrubbers.

Table 2.3: Summary of literature on electroscrubbing experiments

Reference	Droplet size and charge	Particle size and charge	Droplet charging method	Particle charging method	Collection efficiency
Pilat [13]	50 μm, 0.56 mC/kg	0.3-1.05 μm, 53 mC/kg	Induction charging	Corona charging	35% 0.3 μm uncharged 87% charged
Schmidt [14]	Unknown, 0.4-1.2C/kg	0.3-10 μm, unknown	Pneumatic atomizer & induction	Corona charging (-18 kV)	20% for 1 μm uncharged 60% charged
Kruppa [15]	60 μm, unknown	1-14 μm, 10-20 mC/kg	Electrospraying 11 kV	Corona charging -12 kV	90% for 0.08 l/m^3
Yang [43]	30-120 μm, 1.4-2.8 mC/kg	0.5-5 μm, unknown	Pneumatic atomizer & induction 2 kV	Unknown	79% 0.5 μm uncharged 89% charged
Hara [76]	530 μm, $-3.95E^{-11}$C	4 μm, $-5E^{-16}$ -$2E^{-15}C$	Induction charging	AC Charging	Varying with particle charge
Wang [75]	137-500 μm, $3.1E^{-12}$- $3.5E^{-11}$C	0.075-0.2 μm, 1-13.5 e	Induction Charging	Diffusion charger	Varying with particle&droplet size&charge
Smirnov [77]	0.4 cm, 0-10 kV	5-40 μm, 800-10^5 e	Stationary metal sphere	Induction charging	Varying with coagulation parameters
Jaworek 1 [16]	600-3000 μm, 1-200 pC	3 μm,1fC	Electrospraying 4 & 10 kV	AC Charging	40%
Jaworek 2 [17]	80 μm, 9 mC/kg	0.5-2 μm, 53 mC/kg	Electrospraying 11kV	Corona charging -10 kV	80-90 %

Chapter 3

Approach

3.1 Introduction

The purpose of this study is to investigate the situation where a group of monodisperse droplets are falling to a set of particles in a calm air environment. Both droplets and particles are assumed to be traveling at their settling velocities. The purpose is to develop an approach to numerically model a particle traveling through droplets and estimate particle collection efficiency. There are two major steps for the numerical investigation. The first is to solve the flow field generated by droplets in a calm air environment. The second is to track particles traveling through the flow field solved in the first step. The following sections describe the modeling assumptions and the whole numerical process in detail.

3.2 Model assumptions

- The droplets were assumed to be monodispersed and formed a simple cubic system as shown in Figure 3.1. A simple cubic system consists of one droplet on each corner of the cube. The assumption is realistic for monodisperse droplets with the same magnitude and polarity charge. Although Figure 3.1 only shows 27 droplets, this study considered a domain with infinite droplets.
- The initial velocities of the collector droplets and the particles were set at their gravitational settling velocity. A droplet or particle reaches to its settling velocity

when the drag force is balanced with the gravity force.

- The effect of the flow field induced by the particles on the motion of the droplets was negligible. It was shown to be true if the ratio of the particle mass to drop mass is less than 10^{-3} [6, 9].
- The whole system was assumed to have standard ambient temperature and pressure at sea level (temperature at 25 $^{\circ}C$ and pressure at 1 atmosphere).
- Both the droplets and the particles were spherical. There were no distortions on either the droplets or the particles.
- There was no collision between the droplets.
- The mass and electrical charges on the droplets and particles were constant.

3.3 Flow field solution

3.3.1 Flow field governing equations and CFD process

The flow field needed in the study is caused by the droplets falling at their settling velocities in calm air. Since the particle is much smaller than the droplet, the existence of the particle does not alter the flow field around the droplet. The droplet settling velocity is the steady state velocity when the drag force and gravitational force are balanced during the droplet falling. It is a function of droplet density, size and air properties. Since it is a monodisperse group, all of the droplets have the same settling velocity. For modeling convenience, the droplets were treated as stationary objects while the air was traveling toward the droplets at the droplet settling speed but in the opposite direction. The droplets were assumed to be in a uniform distribution as shown in Figure 3.1.

The governing equations for the 3D model are given from Equation 3.1 to 3.4.

$$\frac{\partial u}{\partial x} + \frac{\partial v}{\partial y} + \frac{\partial w}{\partial z} = 0, \tag{3.1}$$

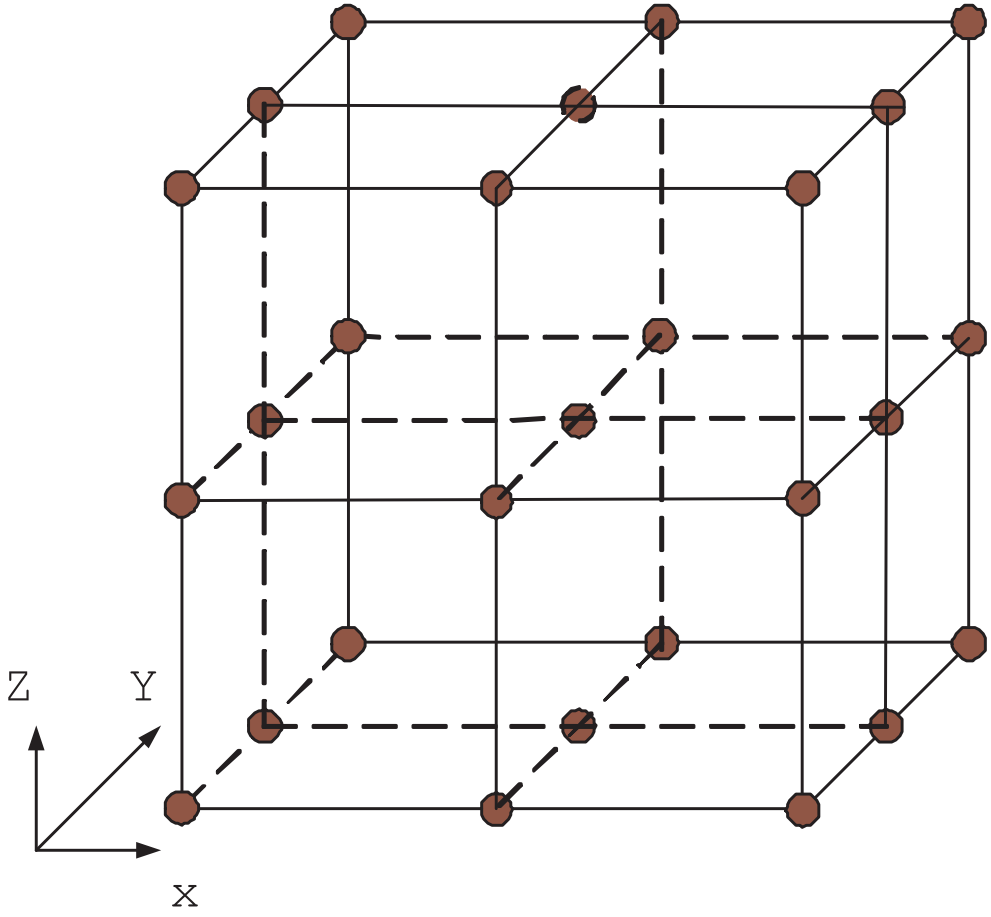

Figure 3.1: Schematic of three-dimensional model

Table 3.1: Summary of inlet conditions

Cases	Droplet size (μm)	Droplet distance (μm)	Droplet terminal velocity (m/s)	Re	Mass flow rate (kg/s)
1	50	100	$7.55e^{-2}$	0.26	$1.156e^{-10}$
2	50	250	$7.55e^{-2}$	0.26	$7.226e^{-10}$
3	50	500	$7.55e^{-2}$	0.26	$2.890e^{-9}$
4	100	200	$2.49e^{-1}$	1.65	$1.525e^{-9}$
5	100	500	$2.49e^{-1}$	1.65	$9.532e^{-9}$
6	100	1000	$2.49e^{-1}$	1.65	$3.813e^{-8}$
7	200	400	$7.08e^{-1}$	9.42	$1.735e^{-8}$
8	200	1000	$7.08e^{-1}$	9.42	$1.080e^{-7}$
9	200	2000	$7.08e^{-1}$	9.42	$4.337e^{-7}$

$$u\frac{\partial u}{\partial x} + v\frac{\partial u}{\partial y} + w\frac{\partial u}{\partial z} = -\frac{1}{\rho}\frac{\partial p}{\partial x} + \nu(\frac{\partial^2 u}{\partial x^2} + \frac{\partial^2 u}{\partial y^2} + \frac{\partial^2 u}{\partial z^2}), \tag{3.2}$$

$$u\frac{\partial v}{\partial x} + v\frac{\partial v}{\partial y} + w\frac{\partial v}{\partial z} = -\frac{1}{\rho}\frac{\partial p}{\partial y} + \nu(\frac{\partial^2 v}{\partial x^2} + \frac{\partial^2 v}{\partial y^2} + \frac{\partial^2 v}{\partial z^2}), \tag{3.3}$$

$$u\frac{\partial w}{\partial x} + v\frac{\partial w}{\partial y} + w\frac{\partial w}{\partial z} = g - \frac{1}{\rho}\frac{\partial p}{\partial z} + \nu(\frac{\partial^2 w}{\partial x^2} + \frac{\partial^2 w}{\partial y^2} + \frac{\partial^2 w}{\partial z^2}), \tag{3.4}$$

where u, v, w are the air velocity components in x, y and z direction respectively, p is the pressure, ν is the kinematic viscosity and g is the acceleration of gravity.

The flow field was solved by using a computational fluid dynamics (CFD) approach by utilizing the commercial software FLUENT®. The CFD process is described in Figure 3.2. Each step will be explained in the following sections. The study investigated the flow fields with different droplet diameter (D) and different droplet distance (L), where D can be $50, 100$ or 200 μm and L can be $2D, 5D$ or $10D$. Therefore, a total of nine flow fields were solved as shown in Table 3.1.

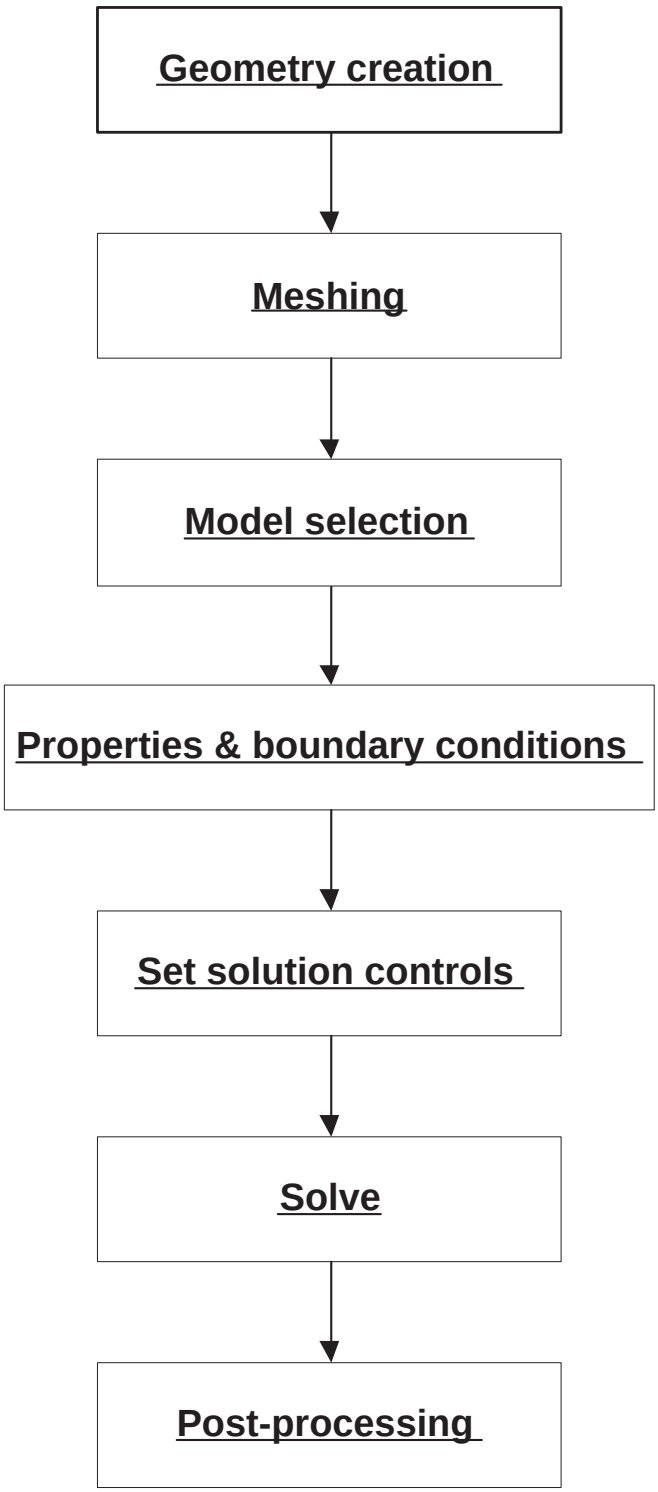

Figure 3.2: The CFD process map

3.3.2 Geometry creation and meshing

Figure 3.3 shows the process of taking advantage of symmetrical characteristic with the simulation domain simplified as in the last plot. Gambit® has been utilized as the geometry creating and meshing tool in the study. Tetrahedral and triangular prism meshes were created by Gabmit®. The droplet boundary region needs finer mesh to compute the gradient near the wall. The boundary layer mesh method has been employed for all of the cases [78].

Since the mesh quality has great effect on the accuracy and robustness of the CFD solution, the mesh quality examination was conducted for each generated mesh. Gambit provides several variables to measure mesh quality, equal-size skewness has been used in this study. The bar chart in Figure 3.4 represents the statistical distribution of mesh elements with respect to equal-size skewness. Zero equal-size skewness represents an ideal element and mesh quality decreases with increasing skewness. To guarantee quality, each mesh should have a major portion of the elements located on the right side of the histogram. Most of the elements should have skewness less than 0.4. Another important process was to check if those highly skewed elements were located in potential large gradient areas. Those elements have been fixed by adding local mesh size control [78]. The mesh density and boundary layer meshing are also important factors to evaluate quality. A sensitivity study has been performed and will be discussed in a later session.

3.3.3 Model selection and operating properties

Taneda justified that any flow with a Reynolds (Re) number lower than 24 can be assumed as a laminar flow [79]. In this study, the Re numbers for all cases are lower than 24 and therefore the laminar flow model has been chosen. The Re number calculation is described in Section 3.3.4.

As discussed in the earlier section, the study assumed standard atmosphere at the sea level. The operating condition parameters are listed in Table 4.1.

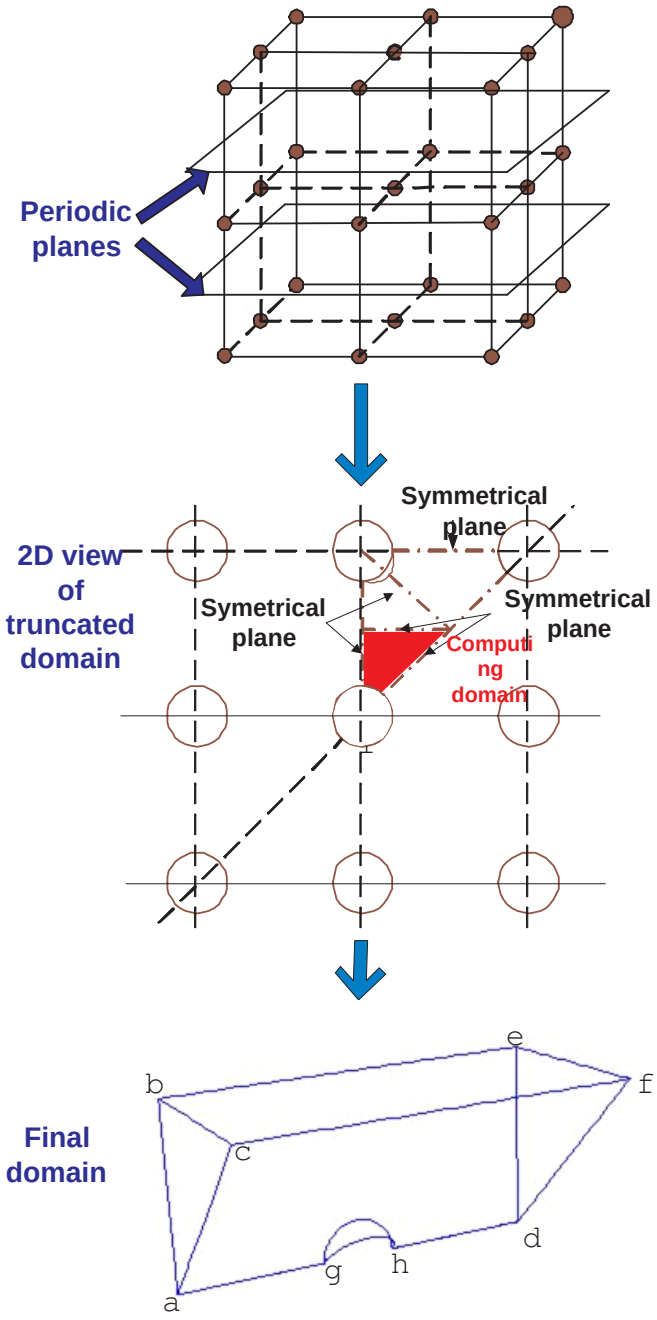

Figure 3.3: The simulation domain evolution

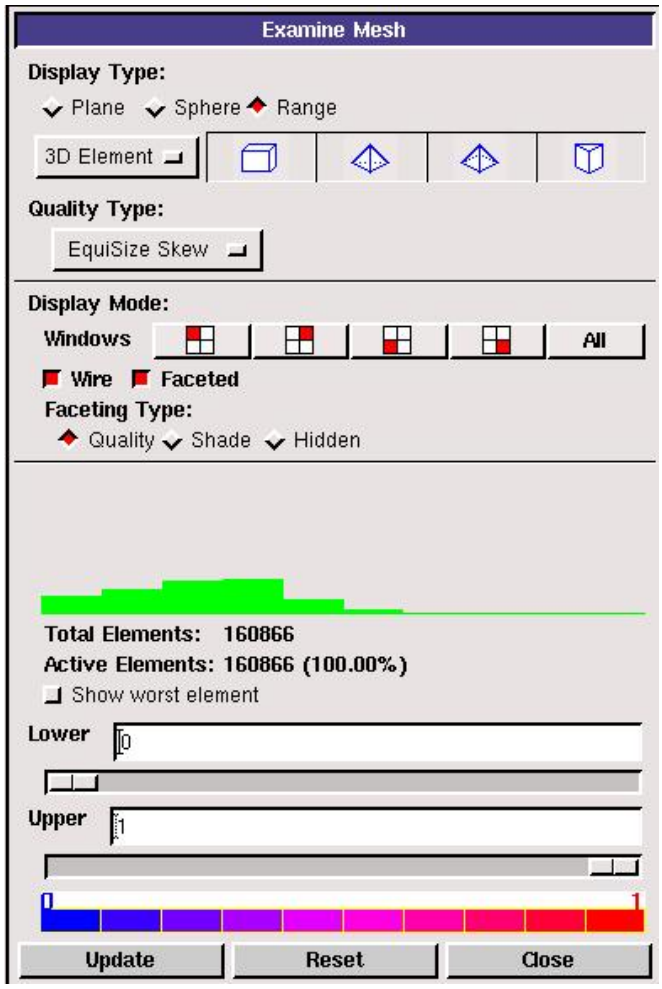

Figure 3.4: Examine mesh option in Gambit

Table 3.2: Summary of operating conditions

Operating conditions	Values
Pressure	101,325 pa
Air density	1.225 kg/m^3
Air viscosity	$1.7894e^{-5}$
Acceleration of gravity	9.8 m/s^2

3.3.4 Boundary conditions

The droplet surface was treated as a no-slip wall that result in zero air velocity on the surface. The symmetrical boundary condition was used in the cutting planes acfd, abed and bcef shown in Figure 3.5. FLUENT assumes zero flux of quantities such as normal velocity and gradient across those planes. Since the study is to investigate the scavenging in the middle of uniform distributed droplets with a simple cubic formation, it has a periodically repeating nature along the flow direction. Therefore, the periodic boundary condition was applied to the inlet and outlet. The application of the periodic boundary condition implies that the velocity and pressure drop repeat themselves in space

$$U(\overrightarrow{r}) = U(\overrightarrow{r} + L\overrightarrow{L}) = (\overrightarrow{r} + L2\overrightarrow{L}) = Constant \tag{3.5}$$

$$\triangle P = p(\overrightarrow{r}) - p(\overrightarrow{r} + \overrightarrow{L}) = p(\overrightarrow{r} + \overrightarrow{L}) - p(\overrightarrow{r} + 2\overrightarrow{L}) = Constant \tag{3.6}$$

where $\overrightarrow{r}$ is the position vector and $\overrightarrow{L}$ is the periodic length vector.

Given by Table 3.1, the inlet mass flow rates were determined based on the air density, the inlet air velocity and the area. The inlet air velocity value equaled the droplet settling velocity given by the empirical Equation 3.8 [1]. The boundary conditions are summarized in Figure 3.5 and Table 3.3.

$$m = \rho A V_{dt} \tag{3.7}$$

$$V_{dt} = \frac{\mu}{\rho D} exp(-3.070 + 0.9935J - 0.0178J^2) \tag{3.8}$$

$$J = ln[C_D(Re_d^2)] = ln(\frac{4\rho_d \rho D^3 g}{3\mu^2}) \tag{3.9}$$

where μ and ρ are the air dynamic viscosity and density, D and ρ_d are the droplet diameter and density, V_{dt} is the droplet terminal velocity, C_D is the drag coefficient, and Re is the droplet Reynolds number.

Once the droplet terminal velocity is determined by Equation 3.8, the droplet Re number can be calculated. It is noted that the droplet and flow have the same Re

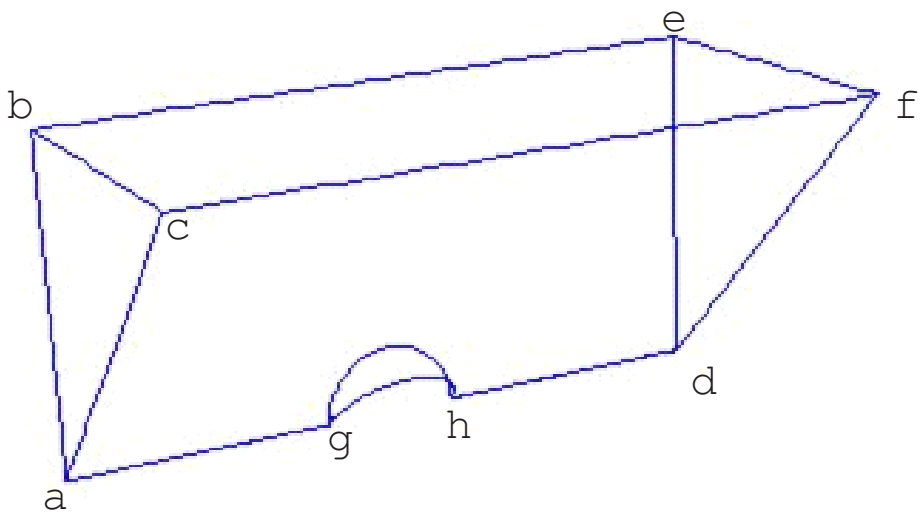

Figure 3.5: Schematic of flow domain and boundary conditions

Table 3.3: Summary of boundary conditions

Domains	Boundary conditions
Surface abc and def	Periodic
Surface $bcef$,$acfd$ and $abed$	Symmetrical
Surface gh	No-slip wall

number.

$$Re_d = \frac{V_{dt}\rho}{\mu} \tag{3.10}$$

3.3.5 Solution controls

The summary of solution controls is given by Table 3.4. There are four pressure and velocity coupling algorithms available in Fluent, SIMPLE (Semi-Implicit Method for Pressure-Linked Equations), SIMPLEC (SIMPLE-Consistent), PISO (Pressure Implicit Split Operator) and Fractional Step Method (FSM) with Non-Iterative Time Advancement option (NITA). PISO and FSM are recommended for transient analysis. PISO

may also be useful for steady-state on highly skewed meshes. All cases were steady-state analysis, so that SIMPLE and SIMPLEC were more appropriate. SIMPLEC is easier for convergence but time-consuming compared to SIMPLE. Since the SIMPLE method has no convergence problem in this study, it has been chosen for all simulation runs for the sake of consistency.

The PRESTO! (PREssure STaggering Option) scheme has been chosen for pressure discretization. The PRESTO! scheme uses the discrete continuity balance for a "staggered" control volume about the face to compute the "staggered" pressure [80]. This avoids potential numerical errors caused by using pressure difference between two alternate grid points. A detailed discussion can be found in Patankar's book [81]. The second order upwind scheme was used for momentum discretization. Generally, the second order scheme provides better accuracy but sacrifices some convergence robustness. For the tetrahedral mesh, which has been used in the study, the second order schemes should be the first selection to minimize numerical discretization error. The URF (under-relaxation factor) is to reduce the changes of ϕ during each iteration, where ϕ can represent any variable, the density, the body force and momentum in this case. The definition is shown in Equation 3.11. The chosen URF values are suggested by FLUENT and supposed to work in most flows. Those values need to be modified only if unstable or divergent behavior is observed. In this study, the default values provided stable and converged solutions for all cases.

$$\phi = \phi_{old} + \alpha \triangle \phi \tag{3.11}$$

CFD uses the iteration approach to solve non-linear equations. At each iteration, an approximate solution results in a small imbalance called "residual". The sum of residuals for the entire fluid domain will be normalized and monitored during the calculation. If the solution converges, the residual should decrease as the iteration progresses. Residuals are often used to judge if the simulation converges. Convergence criteria are pre-set residual values that indicate convergence to some extent. However, the residuals failing to meet the convergence criteria is not the only indicator suggesting convergence. True convergence means that the solution is no longer changing with iterations. Therefore, in this study, all variables including continuity and velocities in all three directions have

Table 3.4: Summary of solution controls

Control variables	Chosen values
Pressure-Velocity coupling	SIMPLE
Pressure Discretization	PRESTO!
Momentum Discretization	Second order upwind
Pressure under-relaxation factor	0.3
Density under-relaxation factor	1.0
Body force under-relaxation factor	1.0
Momentum under-relaxation factor	0.7

Table 3.5: The sensitivity study of mesh quality

Cases	Total volume	Boundary layer (BL) starting size	BL growth rate	BL size limit
A	275,284	0.5 μm	1.05	4.0 μm
B	79,934	1.0 μm	1.10	5.0 μm
C	37,332	1.3 μm	1.15	6.5 μm
D	14,339	2.0 μm	1.20	10 μm

been set to 10^{-20} as residual criteria. Such a small value can guarantee iteration streaming without ceasing. The residuals were plotted with iteration steps. The leveling-off curves eventually suggested that the flow field has stabilized and the solution has converged. Figure 3.6 shows an example of the convergence curve (Case: 50 μm droplet diameter and 500 μm droplet distance).

3.3.6 The mesh quality study

In an attempt to study the effects on the accuracy of mesh quality, the four mesh densities were tested for the case of a 100 μm diameter droplet and a 200 μm droplet distance. The mesh is given by Table 3.5 and configurations are shown by Figure 3.7. The boundary starting size is the first layer height adjacent to the wall, and the boundary growth rate is the height ratio of any row to its previous row. The boundary size limit defines the maximum layer height.

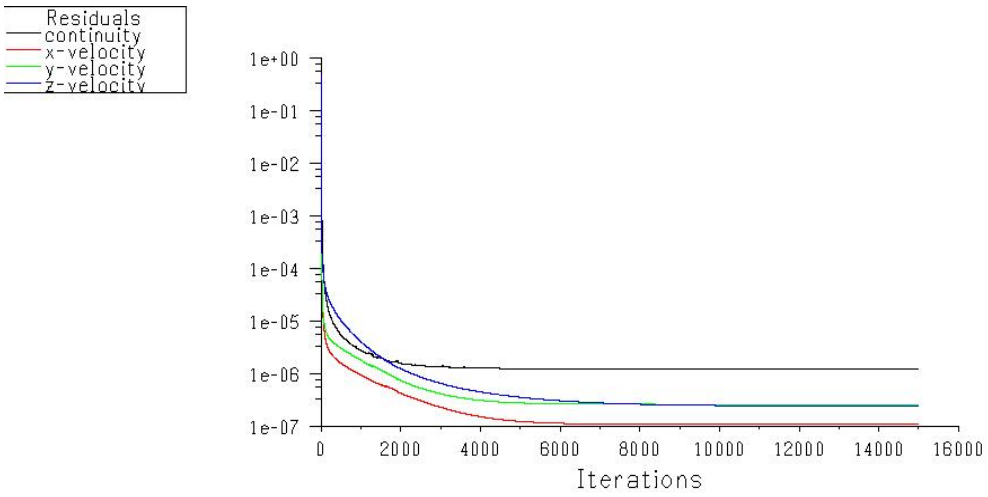

Figure 3.6: The convergence curve for the case D=50 μm and L=10D

Mesh case A was considered to have the best mesh quality to provide the most accurate results. The results of the other three cases were compared to Case A results. To perform the comparison, the flow velocity values were extracted from several surface cuts shown in Figure 3.8. The velocities for Case A from those surfaces were used as the reference. The percentages of the velocity deviation from the other three cases to the reference were calculated as in Equation 3.12 for those surface cuts.

$$\sigma = \frac{|U - U_{ref}|}{|U_{ref}|} \times 100\% \tag{3.12}$$

where σ is the deviation of the air velocity magnitudes from the reference values, U is the air velocity from each case and U_{ref} is the air velocity of case A. The maximum percentage of deviation for each case is shown in Figure 3.9. It was demonstrated that Case B deviated from Case A within only 0.01% but the computing time was one fifth of Case A. Therefore, the meshing parameters of Case B were finally selected for all of the studies.

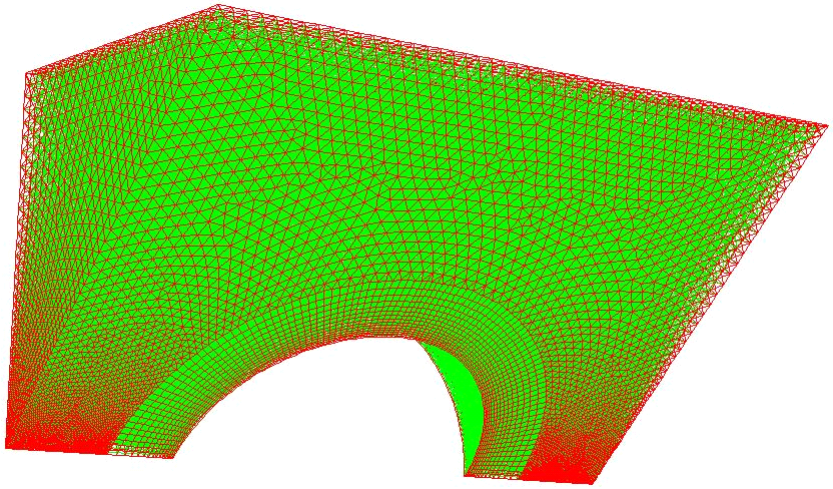

(a) Mesh case A

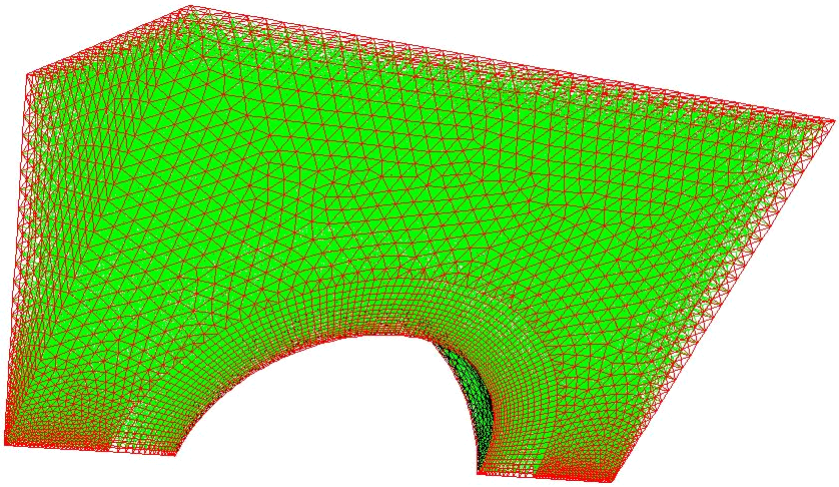

(b) Mesh case B

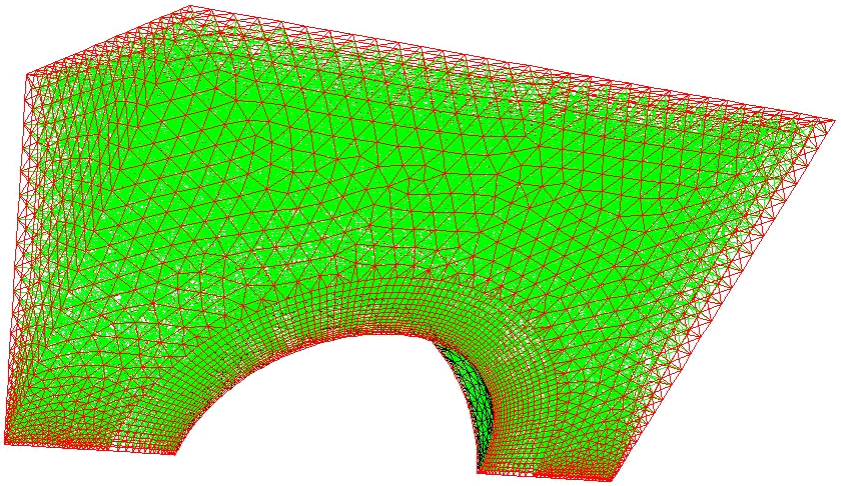

(c) Mesh case C

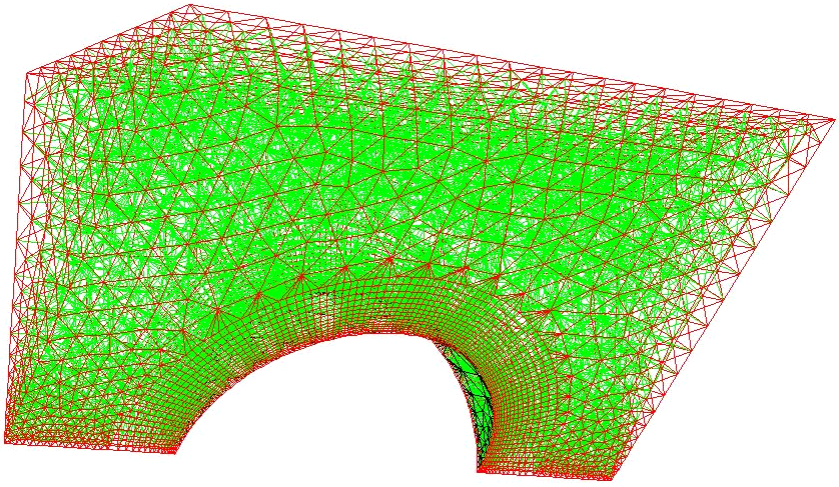

(d) Mesh case D

Figure 3.7: The configuration of mesh test

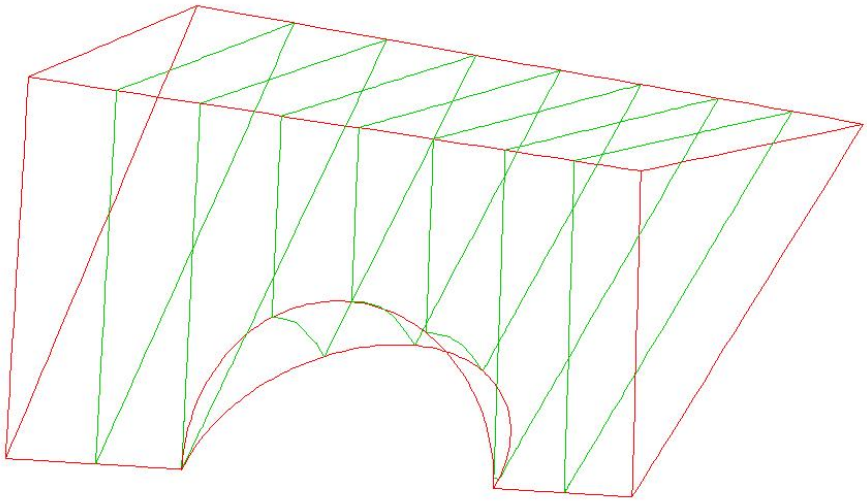

Figure 3.8: The surface cuts for air velocity result extraction

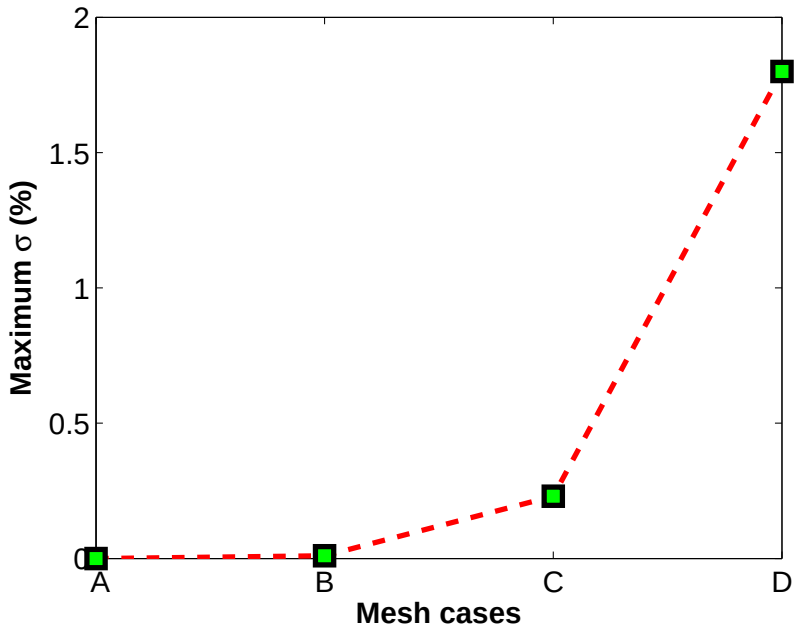

Figure 3.9: The mesh result difference

3.4 Particle tracking

Once the flow field solution is achieved, the following step is to calculate particle trajectory. The particles were released at the inlet in different locations with particle and droplet settling relative velocity ($|V_{dt} - V_{pt}|$). Each particle was tracked in the domain to determine if it could be eventually collided with the droplets or not. All particle fates finally determine the collection efficiency. The particle tracking procedure is described in Figure 3.10. The droplet and particle were assumed to have water density 1000 kg/m^{-3}

3.4.1 The particle tracking governing equation

The governing equations for a particle trajectory are

$$\frac{dV_p}{dt} = g^* + (\frac{C_D Re_p}{24\tau})(V_p - U) + \frac{Fe}{M} \tag{3.13}$$

$$\frac{dS_p}{dt} = V_p \tag{3.14}$$

where V_p is the particle velocity and U is the flow velocity, S_p is the particle position, $g^* = \frac{(\rho_p - \rho)g}{\rho_p}$ is the net gravitational acceleration, ρ_p is the particle density, ρ is the fluid density, M is the mass of a particle, $Re_p = \frac{\rho|V_p - U|d}{\mu}$ is the particle relative Reynolds number, d is the particle diameter, C_D is the drag coefficient, F_e is the electrostatic force, τ is the characteristic relaxation time and V_p is the particle velocity.

Equation 3.13 and 5.3 were solved for each particle in Fluent by using the fifth order Runge-Kutta method. It is a very typical iterative method for the approximation of solutions of ordinary differential equations. The detailed method description can be found at [82].

3.4.2 The drag force

In Equation 3.13, the term $(\frac{CdRe_p}{24\tau})(V_p - U)$ represents the acceleration caused by the drag force acting on a particle.

The drag coefficient is described by

$$C_D = \frac{24}{Re_p}(1 + 0.15Re_p^{0.687}) \tag{3.15}$$

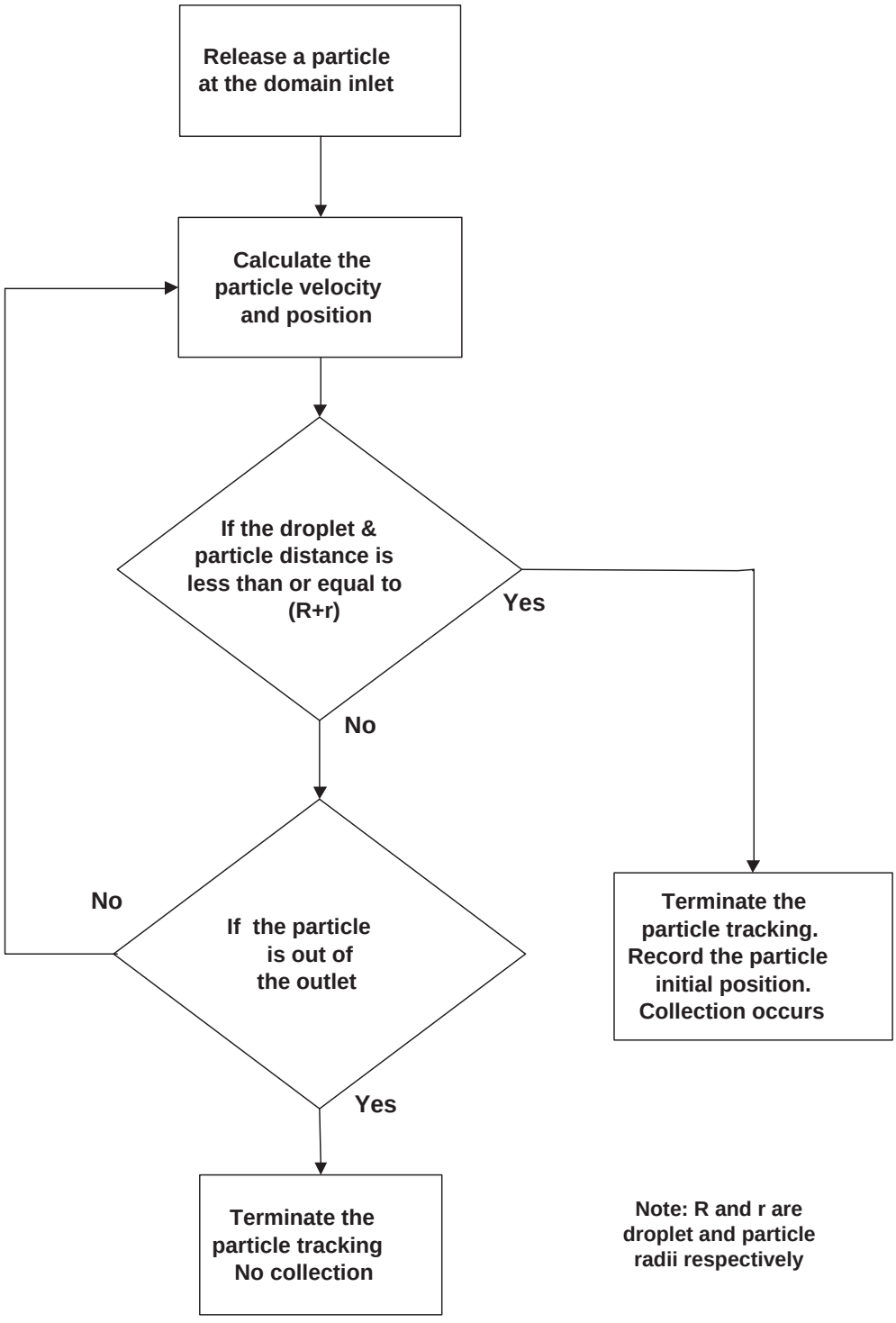

Figure 3.10: The particle tracking calculation procedure

Table 3.6: The Cunningham correction factor values [1]

Particle size (μm)	C_c
1	1.155
2	1.077
3	1.051
4	1.039
5	1.031
6	1.026
7	1.023
8	1.019
9	1.017
10	1.015

which agrees with the experimental result by Clift [83]

The particle relative Reynolds number is given by

$$Re_p = \frac{\rho|V_p - U|d}{\mu} \tag{3.16}$$

The characteristic relaxation time τ represents the time required for a particle to adjust its velocity to a new condition.

$$\tau = \frac{V_t}{g} = \frac{MC_c}{3\pi\mu d} \tag{3.17}$$

where C_c is called the Cunningham correction factor and accounts for air slippage at the surface of the particle. C_c is described by Equation 3.18 and its typical values used in the study are provide in Table 3.6

$$C_c = 1 + \frac{2.52\lambda}{d_p} \tag{3.18}$$

where λ is the mean free path.

3.4.3 The electrical force

The Coulomb force between one droplet and one particle is given by Equation 3.19

$$F_e = \frac{Qq}{4\pi\varepsilon_0 S^2} \tag{3.19}$$

where Q and q are the charges on the droplet and the particle respectively, ε_0 is the dielectric permittivity of free space and S is the distance between the droplet and the particle.

Since the study is for an infinite droplet system, the approximation of the total electric force exerted by all of the droplets on the particle needs to be considered. In reality, the infinite droplet effect cannot be modeled. Fortunately, the magnitude of the Coulomb force is inversely proportional to the square of the distance. The force from the droplets far from the particle can be neglected. Imagine in a uniform distributed droplet matrix, one droplet is in the origin of the coordinate and the matrix extends in an isotropic manner to three orthogonal directions. N is the total droplet number considered in the calculation of total electrical force. If the electric force computing domain grows in all three directions with one unit of droplet interval distance, N equals 27. It can be seen that N equals $(2W + 1)^3$, in which W is the discrete number of droplet interval distances that has been taken into account.

Figure 3.11 shows the total scaled electric force is the function of the considered droplet number. The electric force is scaled by dividing the force at $N = 531,441$. As shown in the figure, the tendency starts to level off at $N = 1,331$ and the value difference to $N = 531,441$ is within 0.3%. Because the electric force needs to be calculated for each particle at each time step, it is very time consuming. Total $N = 1,331$ was then chosen finally for all of the cases to maintain the accuracy with a reasonable computing time.

3.4.4 Particle size and electric force implementation

In Fluent, a particle is treated as a mass point, and its size is only for the purpose of mass calculation. As a result, the collection of a particle can only be considered to occur when the center of a particle arrives at the droplet surface. It cannot hold true when the particle size becomes larger. In reality, the collection occurs when the particle surface is touching the droplet surface. To take the particle size into consideration, a user-defined function (UDF) method was used. UDFs are written by users in the C programming language and loaded in Fluent solver. During the particle trajectory calculation, the UDF was executed to check if the particle collided with the droplet or left from the outlet at each time step. By using the collection judgement shown in Equation 3.20,

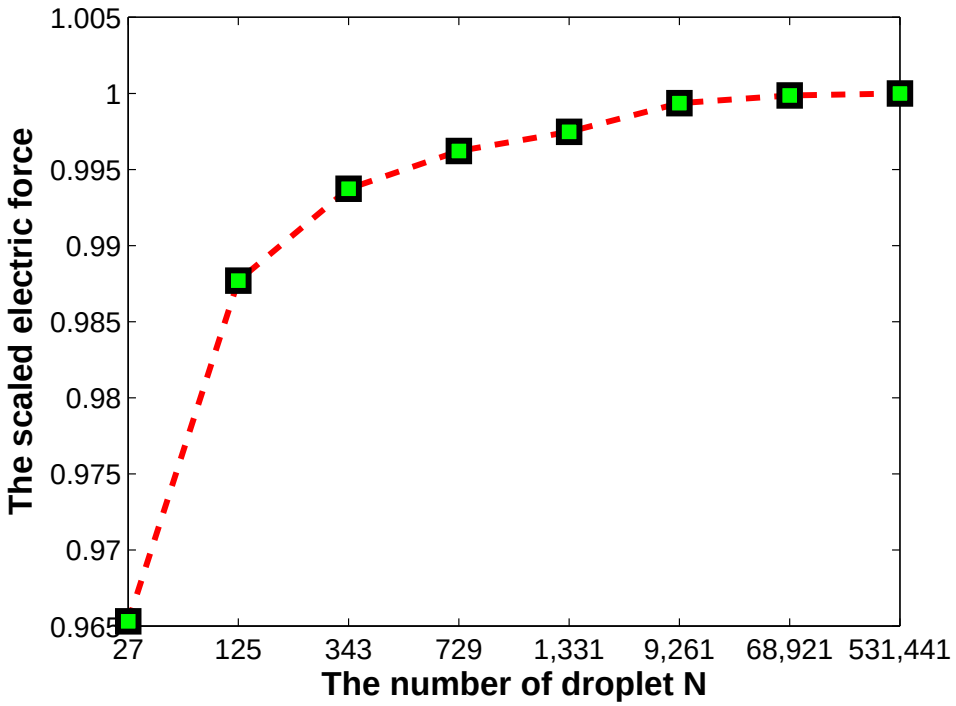

Figure 3.11: The scaled total electric force varying with the number of droplets

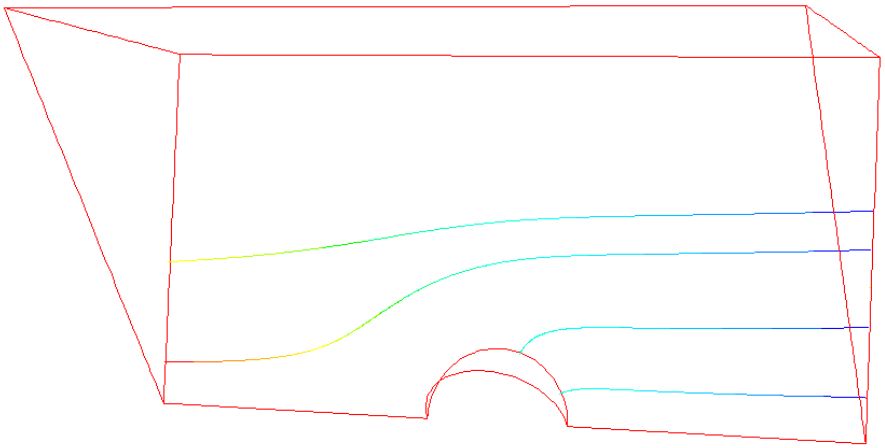

Figure 3.12: An example of particle trajectories

the particle size can be taken into consideration. The UDF C code is shown in Appendix A.

$$S <= R + r \tag{3.20}$$

where S is the distance between the centers of the particle and the droplet, r and R are the particle and droplet radii respectively.

3.4.5 The collection efficiency calculation

The particles were released from different locations at the inlet plane individually, and their fates were determined and recorded if they eventually escaped from the domain or collided with the droplets. The initial release positions were recorded as well if the particles were collected. Figure 3.13 shows the particle initial position plot in the inlet plane. The shaded area is called the collection area and the inlet plane is the equilateral triangle. All particles starting within the collection area were collected and particles out of the shaded area avoided collection. Therefore, the collection efficiency is defined as the ratio of the collection area to the inlet area shown in Equation 3.21

$$E = \frac{A_{collection}}{A_{inlet}} \tag{3.21}$$

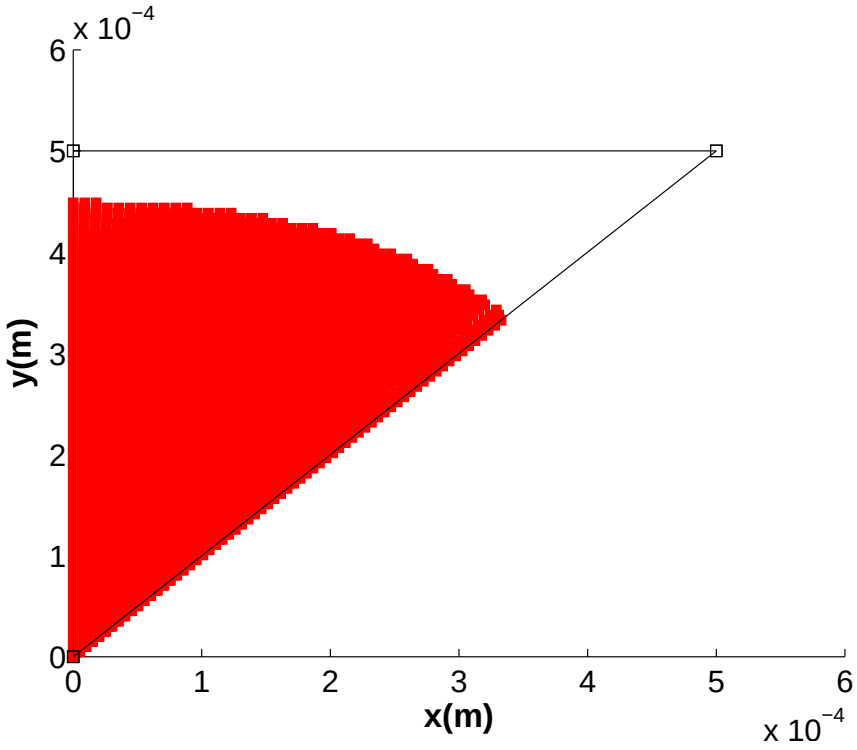

Figure 3.13: An example of collection area

There were always two simulations to determine the collection area for each case. The first simulation used 5000 particles to cover the entire entrance area. All particles were released and tracked and the collection area was calculated. Then, in the second simulation, an area slightly larger than the calculated area in the first simulation was chose. Another 5000 particles were assigned to the chosen area, and another round of particle tracking occurred. Finally the collection area was determined. In this way, high accuracy can be guaranteed.

Chapter 4

The influence of the inertial effect on collection efficiency

4.1 Overview

One objective of this study is to determine the inertial effect on particle collection efficiency. When particles are approaching droplets and not able to follow the curved streamlines of the flow because of their inertia, they can be collected by droplets. In this study, particles are traveling through the developed flow field formed by uniformly distributed droplets. The collection efficiencies from the inertial effect are calculated for several situations, including variant droplet distance, droplet size, and particle size. As a group of droplets usually settle at a lower velocity than a single droplet, the effects of the velocity hindrance on inertial collection efficiency are also studied.

4.2 Inertial effect without velocity hindrance consideration

In this section, all droplets uniformly distributed in the system are assumed to have one velocity that equals a single droplet settling velocity. All of the results shown in this section are based on this assumption. Figure 4.1 to 4.3 show the inertial effect results in terms of the collection area and the collection efficiency when droplets of diameter

(D) equals $50, 100$ and 200 μm respectively. For each of the figures, the droplet distance (L) varies from $2D, 5D$ to $10D$, and the particle diameter ranges from 1 to 10 μm . All figures show the results on a log scale. As observed, both the collection area and the collection efficiency increase as the particle diameter increases because the inertial effect plays a more important role. Note that the inlet air velocity is set as a single droplet settling velocity, a smaller droplet distance will cause the local air velocity through the droplets to accelerate more. As a consequence, the collection area and the collection efficiency are larger for a smaller droplet distance. This trend is more obvious from $L = 2D$ to $L = 5D$ and becomes less from $L = 5D$ to $L = 10D$. For 200 μm droplets (Figure 4.3(a)), the collection areas are almost identical for L = $5D$ and $10D$. It implies that the droplets are separate enough and the effect of the air velocity acceleration becomes insignificant. It should be noted that the collection efficiency is the collection area scaled by the order of $1/L^2$. Although the collection areas for L = 5D and 10D are almost identical when the droplet diameter equals 200 μm , the collection efficiency of $L = 5D$ is much larger than that of $L = 10D$ because of the smaller droplet distance L (Figure 4.3).

Figure 4.4 shows the collection area and the collection efficiency, for two cases when $L = 500$ μm ($D = 50$ μm , $L = 10D$ and $D = 100$ μm , $L = 5D$). Both cases have the same droplet distance, so the comparison is only on droplet size. For the same idea, Figure 4.5 provides the results for L= 1000 μm , which include two cases of $D = 100$ μm $L = 10D$ and $D = 200$ μm $L = 5D$. As droplet size increases, relative velocity between the droplet and the particle increases, which makes the particle hardly turn around the droplet. This causes impaction or interception to occur more easily. Therefore, both the collection area and the collection efficiency increase with the increase of the droplet size when all the conditions except the droplet size are same and only the inertial effect is considered. It can also be seen that the increasing droplet size has larger effects on larger particles than smaller ones. To explain the reason, the Stokes number (Stk), a dimensionless number, is used to define the inertial characteristics. When $Stk >> 1$, particles continue moving in a straight line as the air flow turns around the obstacle. When $Stk << 1$, particles tend to follow the air streamlines closely. The definition of the Stokes number is given in Equation 4.1. In this case, d_c is the droplet diameter D. The undisturbed air velocity U_0 is the droplet terminal velocity, which is proportional

to D^2. Note that the relaxation time τ is proportional to the particle diameter d^2. Therefore, Stk is proportional to Dd^2. This also explains why the difference of the collection area between two droplet sizes (the distance between the two curves in Figure 4.4) becomes larger as the particle size increases.

$$Stk = \frac{\tau U_0}{d_c} \tag{4.1}$$

where U_0 is the undisturbed air velocity, d_c is the characteristic dimension of the obstacle and τ is the relaxation time of the particle.

4.3 Inertial effect with velocity hindrance consideration

One important assumption in the previous section is that the terminal velocity of a single droplet in still air is assigned to each droplet in the system. In other words, the whole group of droplets has one velocity, which equals a single droplet settling velocity. This assumption might not hold true in reality when droplets are close to each other. The interaction of droplets can hinder the terminal velocity of the whole system because the presence of other droplets affects the mechanism of momentum transfer between the droplet and the air. Mertes [84], Richardson [85] and Oliver [86] respectively used experimental approaches to measure the settling velocity of multiple droplet systems V_ϕ compared to the single droplet settling velocity V_{dt}. All of the previous studies have similar conclusions:

- V_ϕ is always smaller than V_{dt}
- The ratio V_ϕ/V_{dt} is a function of droplet volume fraction ϕ and single droplet Reynolds number Re_d.

A number of theoretical approaches have also been applied to multiple droplet system settling in terms of the drag force and the system settling velocity calculation. One of the classical studies was developed by Kuwabara [87], a method to calculate the drag force on multiple spheres in a viscous flow on the basis of Stokes' approximation called the "cell model". The basic assumption is that each sphere in the system is enclosed by a larger imaginary cell. The vorticity and the normal component of velocity are assumed to be zero at the cell interfaces.

To take account of the effect of velocity hindrance in a multiple droplet system, this study used an approach to calculate the system settling velocity by checking the force balance on the droplet. As shown in Figure 4.6, the periodic flow field was initially solved by using the single droplet settling velocity. Then the drag force acted on the droplet was calculated and compared to the gravitational force. If the drag force was larger than the gravitational force, the inlet mass flow rate was lowered down and the flow field was recalculated. The final flow field was achieved by adjusting the inlet mass flow rate until the drag and gravitational forces were balanced. The final average inlet velocity represented the droplet system settling velocity.

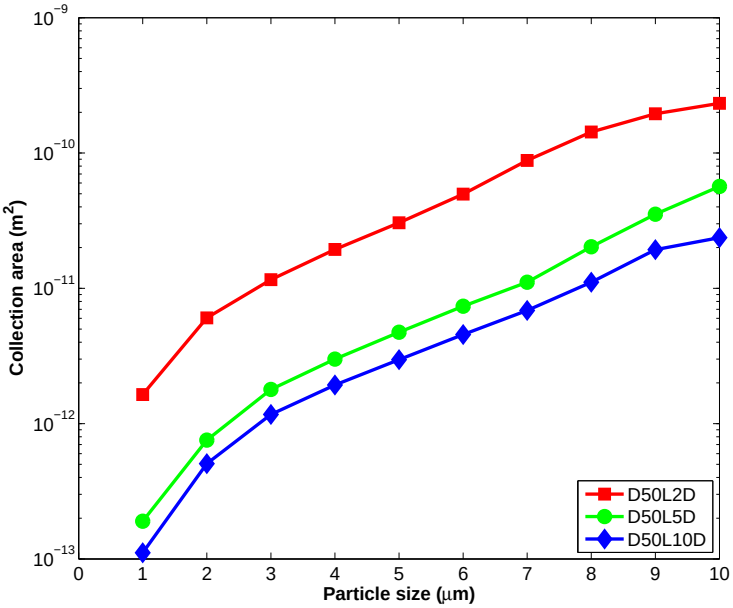

(a)

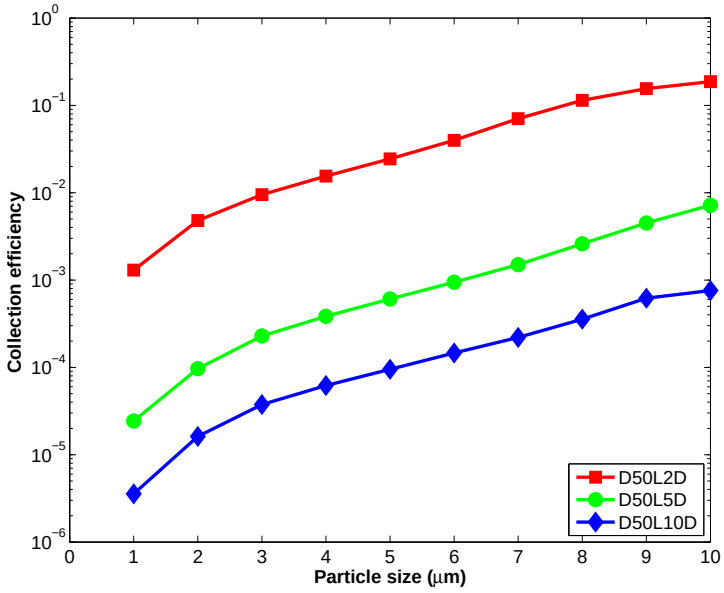

(b)

Figure 4.1: The inertial effect results from a 50 μm droplet, a 1-10 μm particle, and $L = 2D$, $5D$ and $10D$ without velocity hindrance consideration (a) the collection area plot (b) the collection efficiency plot

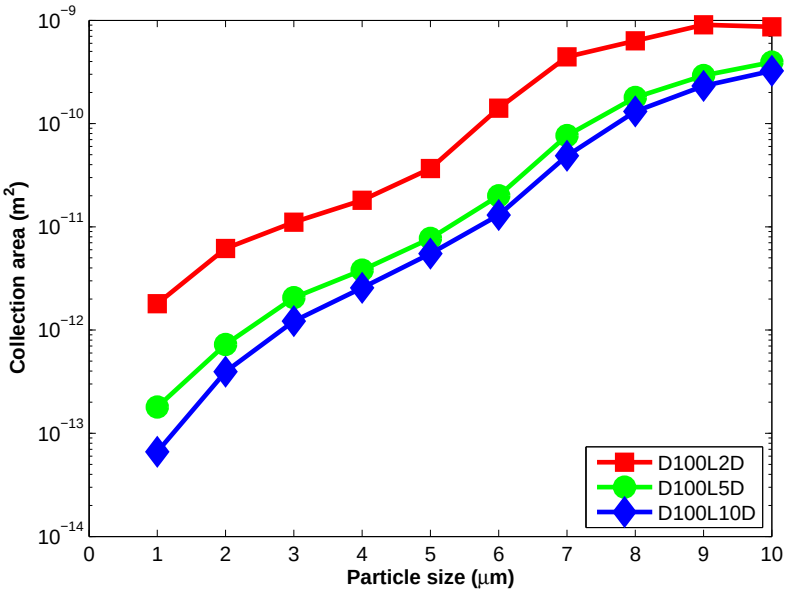

(a)

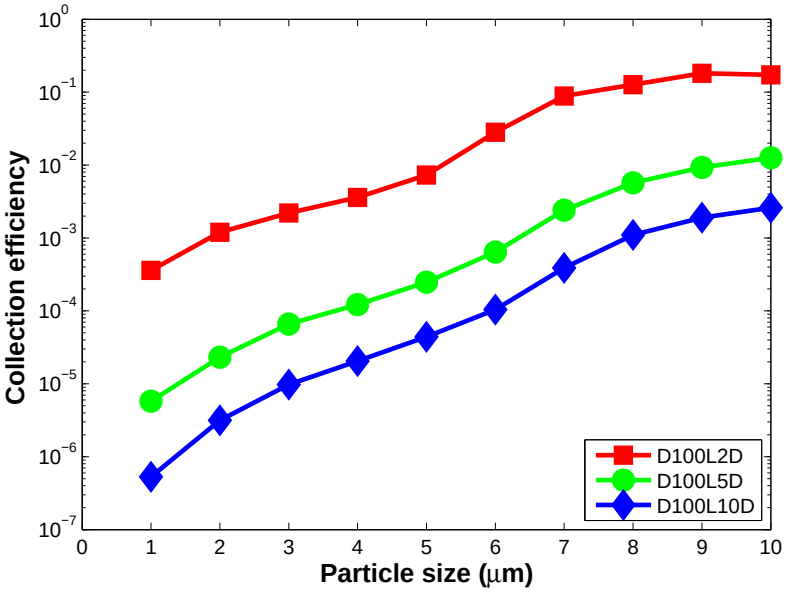

(b)

Figure 4.2: The inertial effect results from a 100 μm droplet, a 1-10 μm particle, and $L = 2D$, $5D$ and $10D$ without velocity hindrance consideration (a) the collection area plot (b) the collection efficiency plot

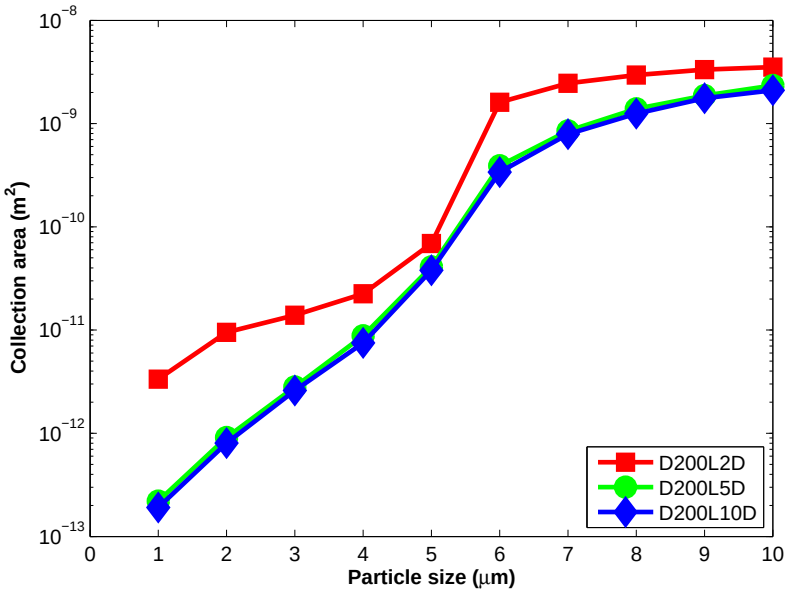

(a)

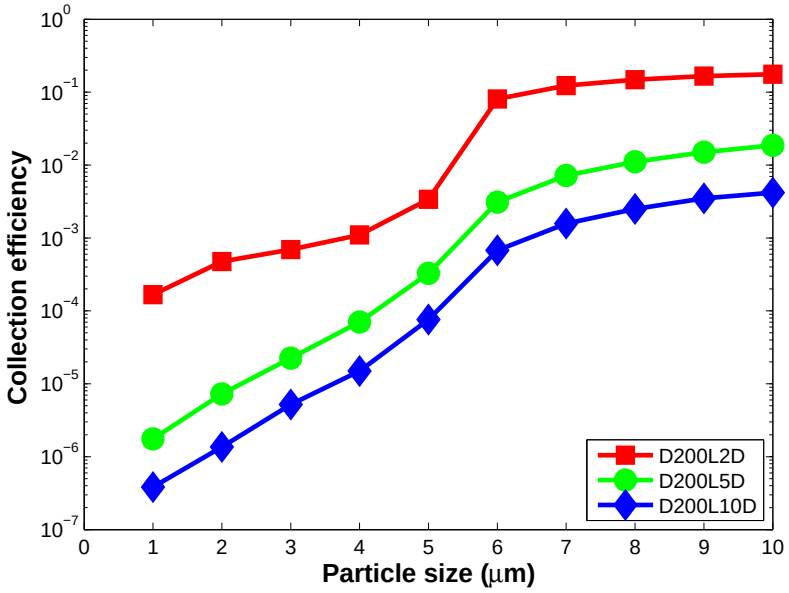

(b)

Figure 4.3: The inertial effect results from a 200 μm droplet, a 1-10 μm particle, and $L = 2D$, $5D$ and $10D$ without velocity hindrance consideration (a) the collection area plot (b) the collection efficiency plot

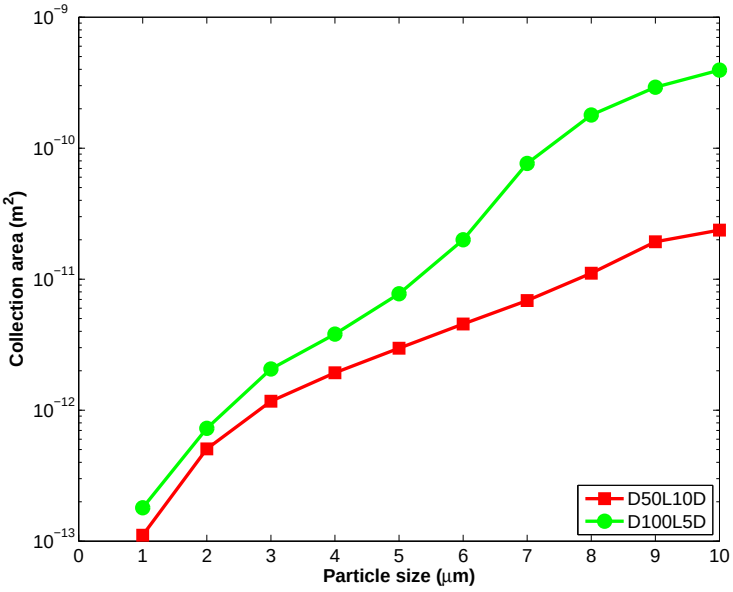

(a)

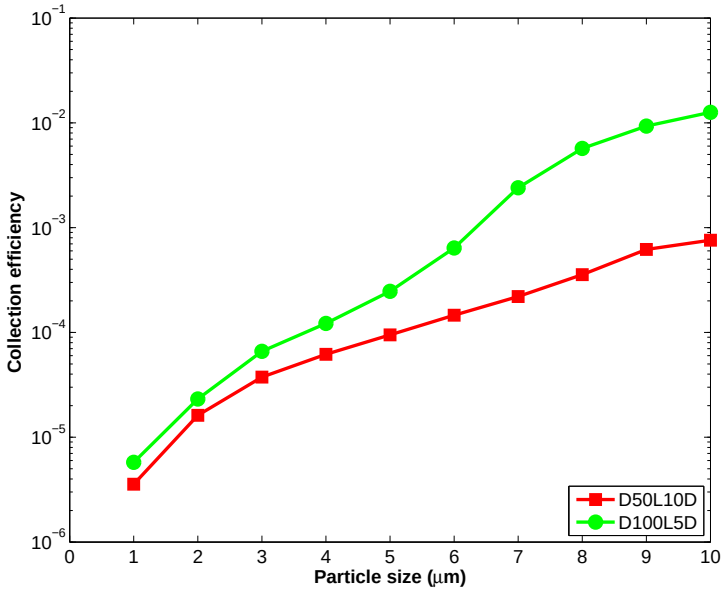

(b)

Figure 4.4: The inertial effect results for 500 μm droplet distance, 1-10 μm particle and without velocity hindrance consideration (Case 500 μm droplet $L = 10D$ and 100 μm droplet $L = 5D$) (a) The collection area plot (b) The collection efficiency plot

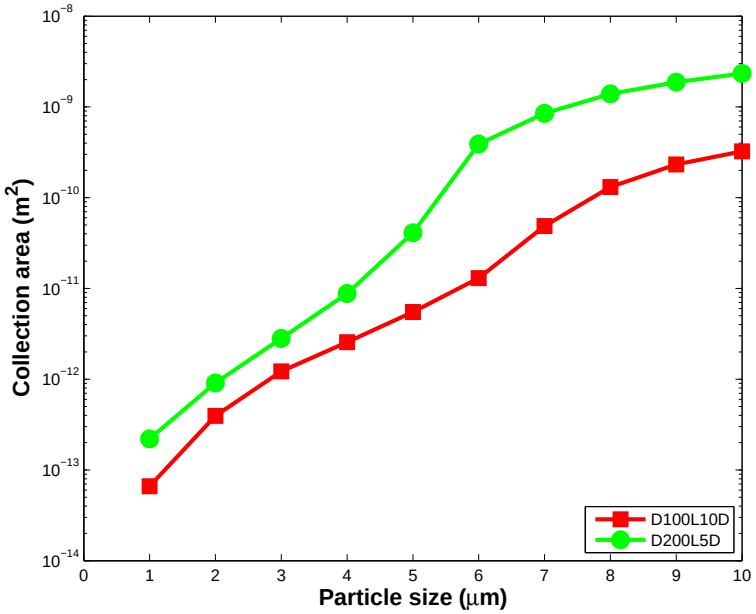

(a)

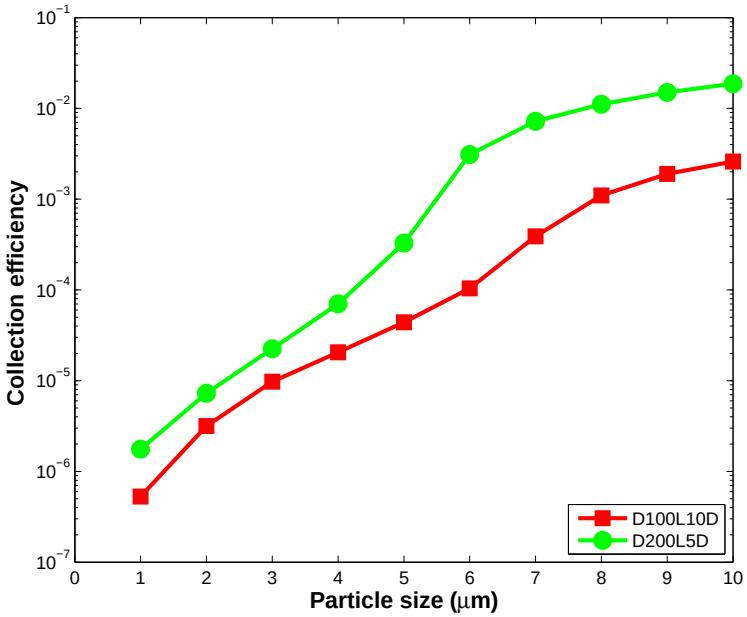

(b)

Figure 4.5: The inertial effect results from a 1000 μm droplet distance, and a 1-10 μm particle without velocity hindrance consideration (Case 100 μm droplet L=10D and 200 μm droplet L=5D) (a) the collection area plot (b) the collection efficiency plot

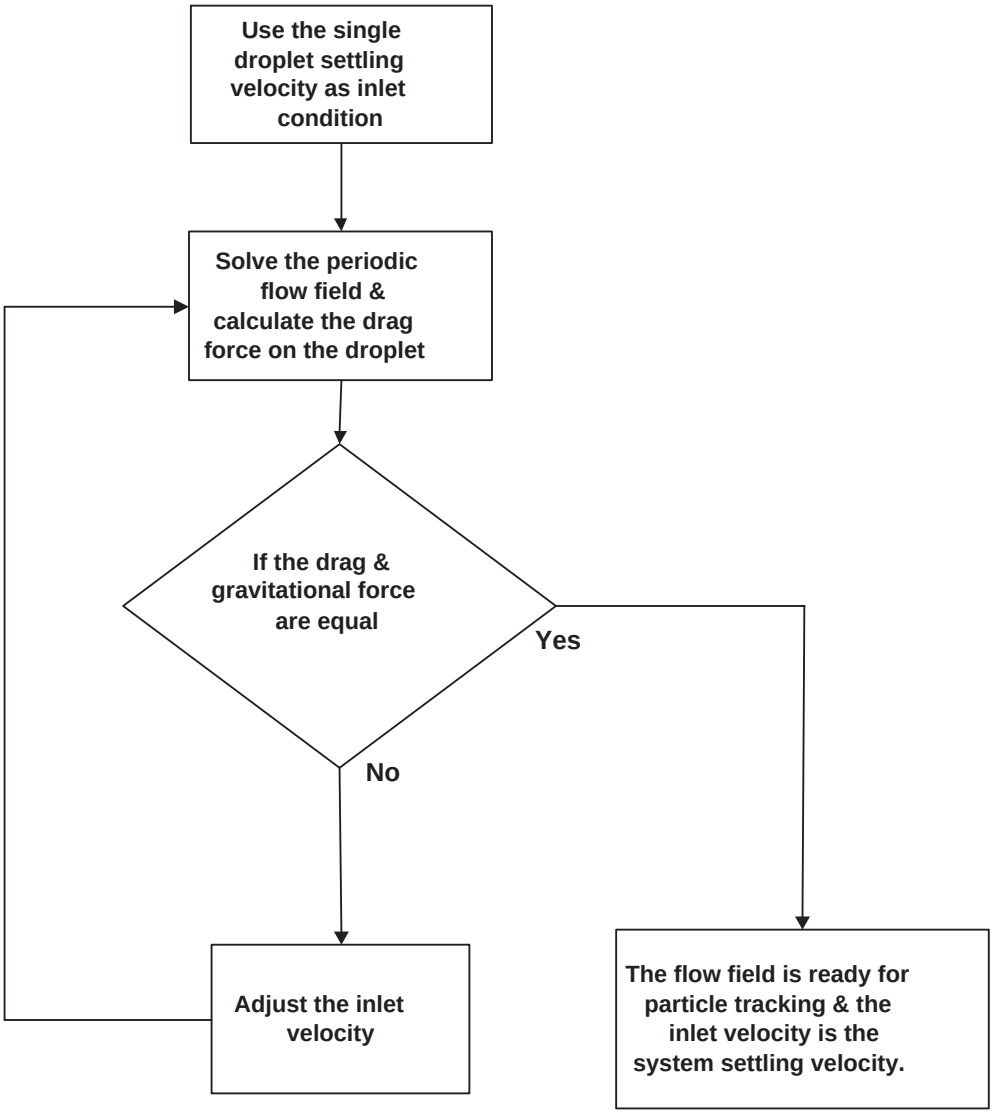

Figure 4.6: The process of calculating the droplet system settling velocity

Table 4.1: Previous analytical solutions for dilute suspension in the creeping flow region

Date	Author	Reference	Equation
1959	Kuwabara	[87]	$\frac{V_\phi}{V_{dt}} = 1 - 1.62 * \phi^{1/3} + 0.012 * \phi^{2/3} + 0.464152 * \phi$
1959	Hasimoto	[88]	$\frac{V_\phi}{V_{dt}} = 1 - 1.7601 * \phi^{1/3} + \phi - 1.5593 * \phi^2$
1957	Happel	[89]	$\frac{V_\phi}{V_{dt}} = 1 - (9/5) * \phi^{1/3} + \phi - (1/5) * \phi^2$

The results are given in Figure 4.7 in terms of the ratio of the system settling velocity to the single droplet settling velocity (V_ϕ/V_{dt}). The droplet distance can be viewed as the droplet volume fraction ϕ. The droplet distances $L = 2D$, $5D$ and $10D$ are equivalent to the droplet volume fraction 6.52%, 0.42% and 0.05%, respectively, with the simple cubic assumption. As ϕ increases, V_ϕ/V_{dt} increases as well. As shown in Figure 4.7, the results match very well with several theoretical correlations for a 50 μm droplet. Note that a 50 μm droplet has Re_d 0.26 shown in Table 3.1 and is in the creeping flow region. Most of the theoretical approaches including Kuwabara, Hasimoto and Happel's are based on analytical solutions of the differential Navier-Stokes equations with the simplifying assumption of creeping flow [87, 88, 89]. Therefore, all of those solutions are in good agreement with a 50 μm droplet in this study. A variety of studies have shown that in the creeping flow region, V_ϕ/V_{dt} is nearly independent of Re_d [90]. Clearly, as droplet size increases, the Re_d increases and the results begin to deviate from the creeping flow solution. Many experimental studies, such as Mertes and Rhodes [84], and Richardson and Zaki [85], provide the velocity ratio results with varying Re_d and ϕ. The experimental data show that V_ϕ/V_{dt} increases with Re_d in the intermediate range between Stoke's law and Netwon's Law, and this increase is moderate for low ϕ and becomes more evident with increasing ϕ. The volume fractions in those experiments are usually larger than the values in this study and V_ϕ/V_{dt} can hardly be compared. However, the tendency of V_ϕ/V_{dt} with Re_d has good agreement with this study.

Figure 4.8 to 4.10 provide the results with the consideration of reduced velocity effect. A multiple droplet system settles at lower velocity than a single droplet does. Therefore, it can be seen that the collection area and efficiency are lower as well. As the volume fraction ϕ increases, the hindrance effect becomes more evident. As a result, the reduction of the collection efficiency for droplet distance $2D$ is larger than that of droplet distance $5D$ and $10D$. For the 100 and 200 μm droplet at droplet distance $10D$,

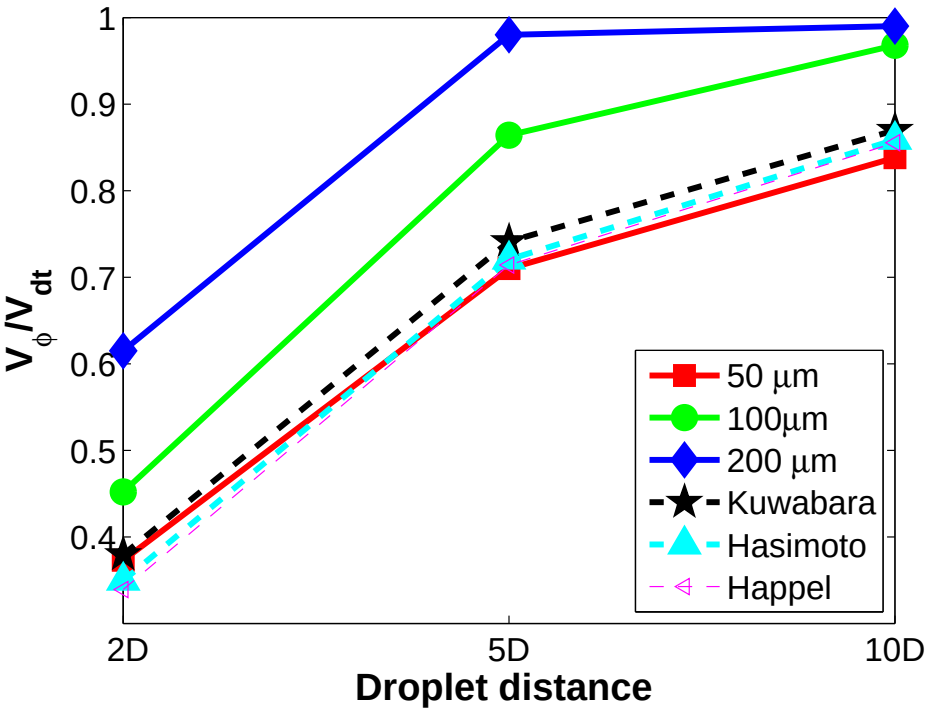

Figure 4.7: V_ϕ/V_{dt} versus droplet distance $L = 2D$, $5D$ and $10D$. Droplet diameter includes 50 μm, 100 μm and 200 μm. The validation data come from different theoretical sources (see Table 4.1)

the reduction of the collection efficiency is very trivial. It should be noted that the collection efficiencies in Figure 4.9 for particles from 7 to 9 μm with droplet distance 2D are even lower than those with distance 5D and 10D. The lower settling velocity distributes in the 2D flow domain can cause less inertial effect than 5D and 10D for the particles in this size range. Similarly, for the 200 μm droplet, the collection efficiency for particle 6 μm with droplet distance 2D is lower than that with 5D (Figure 4.10).

As shown in Figure 4.3 and 4.10, the collection area and the collection efficiency have relatively larger increases between 5 and 6 μm and between 6 and 7 μm respectively. This trend is similar to a typical characteristic efficiency curve of inertial impactor. A cutoff diameter exists when particles greater than a certain size are collected and particles smaller than the size pass through. Many published results for a single droplet simulation including Lee, Pinsky and Schlamp show that efficiency increases dramatically within an interval of one or two micrometer particle size, and then the increase becomes slow until the particle and droplet approach similar size. At that time, collection efficiency will increase largely again with particle increase. Their results also show that the larger a droplet is, the sooner the first increase occurs. This means that the efficiency jump for larger droplet occurs at relatively smaller particle size. This explains that this jump can only be seen in 200 μm droplet with 2D spacing in our case. The occurrence of dramatic increase is related to the flow field provided by droplets. The larger droplet provides the flow field, which benefits the collection due to the inertial effect. For the same reason, the reduced velocity effect hinders the collection. As shown in Figure 4.3 and 4.10, the sudden increase is postponed from 5-6 μm to 6-7 μm because of the reduced velocity effect.

4.4 Validation

Most of the previous studies on particle inertial scavenging are based on the physics of the interaction between a single droplet and a particle. To validate the approach for the multiple droplet system in this study, a single droplet model has been set up using the same processes and tools as for the multiple droplet model. An agreement on the single model results between this study and published work will provide confidence on the multiple droplet model.

The geometry configuration of the single droplet model is shown in Figure 4.13. The inlet and outlet were made of two $10D \times 10D$ right isosceles triangles. The distance from the inlet to the outlet was $20D$. The model is for a single droplet in infinite air; the domain size is chosen to be large enough that the boundary effect can be neglected. A uniform velocity equal to the droplet settling velocity was assigned to the inlet. The outlet was set to a standard atmospheric pressure at sea level. The planes ABED, ACFD and BCEF shown in Figure 4.13 were treated as the symmetrical faces. A no-slip wall boundary condition was assigned to the droplet wall. Gambit was used as the meshing tool. The meshing parameters were chosen to be the same as what had been used in the multiple droplet model. The solution control variables also matched those in the multiple droplet models. In total, three cases for the droplet diameter 50, 100 and 200 μm were modeled. The geometry and mesh were created for the 100 μm droplet case, and were scaled up and down by a factor of 2 to achieve 50 and 200 μm cases. Fluent provides the capability for geometry and mesh size scaling. The flow field solution for each case was achieved when the convergence was reached. Again, the following step was to calculate the particle trajectory. Particles were released at the inlet one by one in different locations. Each particle's position and velocity were calculated at each time step. The program checked if it was collided with the droplet or not. Eventually, those particles collected by the droplet were recorded and used to determine the collection area. This methodology is similar to the approach in some of the published studies except the flow field acquisition [6, 8, 10]. Most published studies used the theoretical solutions such as Stokes solution, while in this study the Navier-Stokes equations were solved using the numerical method with the assumption of laminar flow.

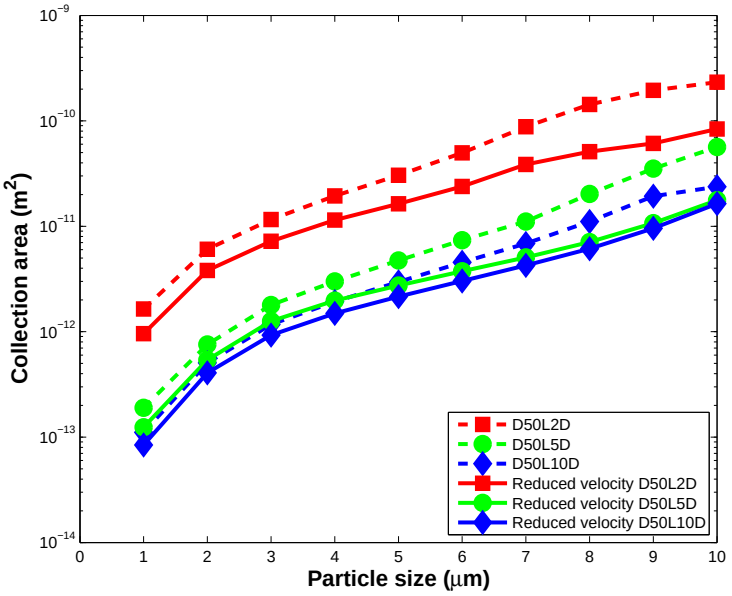

(a)

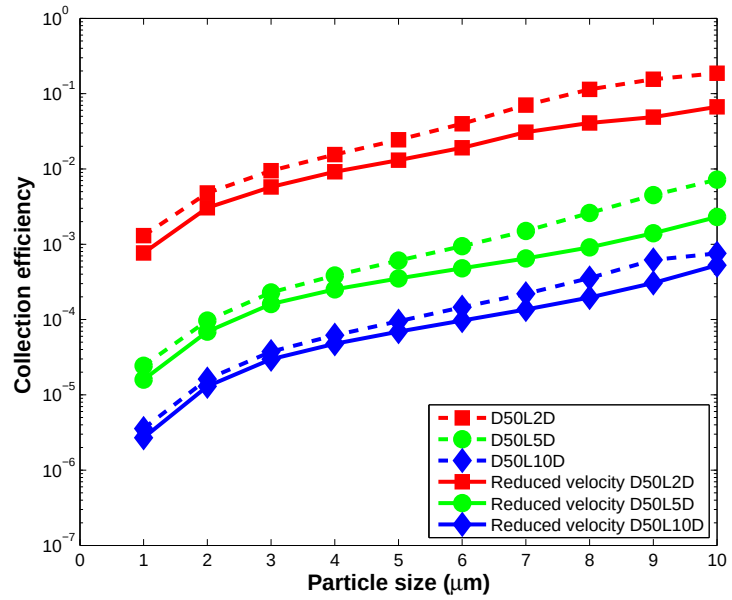

(b)

Figure 4.8: The inertial effect results from a 50 μm droplet, a 1-10 μm particle, and $L = 2D, 5D$ and $10D$ with and without velocity hindrance consideration (a) the collection area plot (b) the collection efficiency plot

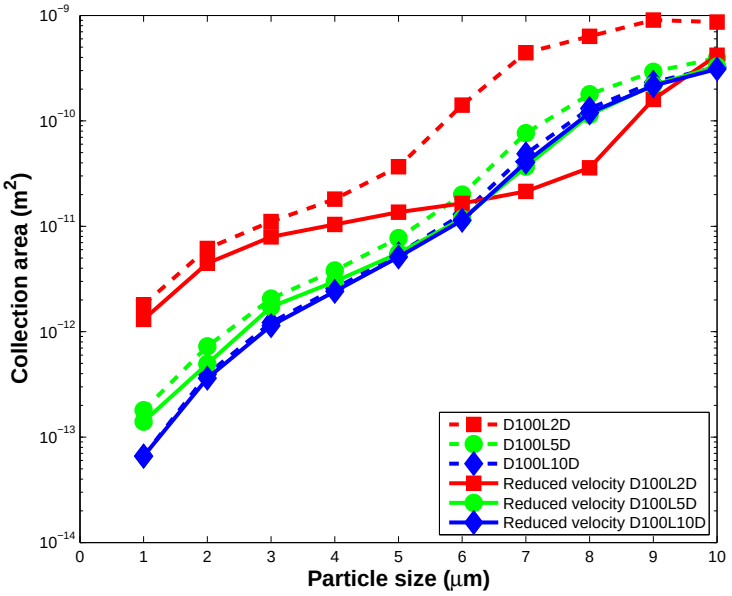

(a)

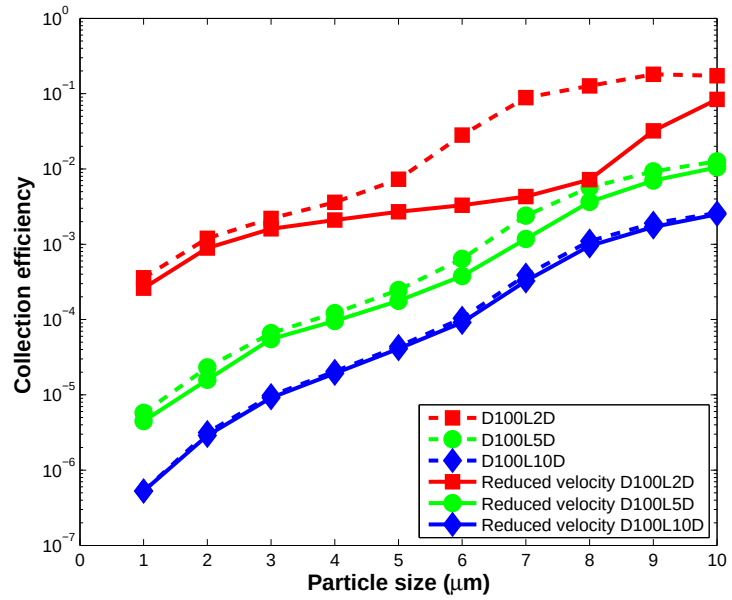

(b)

Figure 4.9: The inertial effect results from a 100 μm droplet, a 1-10 μm particle, and $L = 2D, 5D$ and $10D$ with and without velocity hindrance consideration (a) the collection area plot (b) the collection efficiency plot

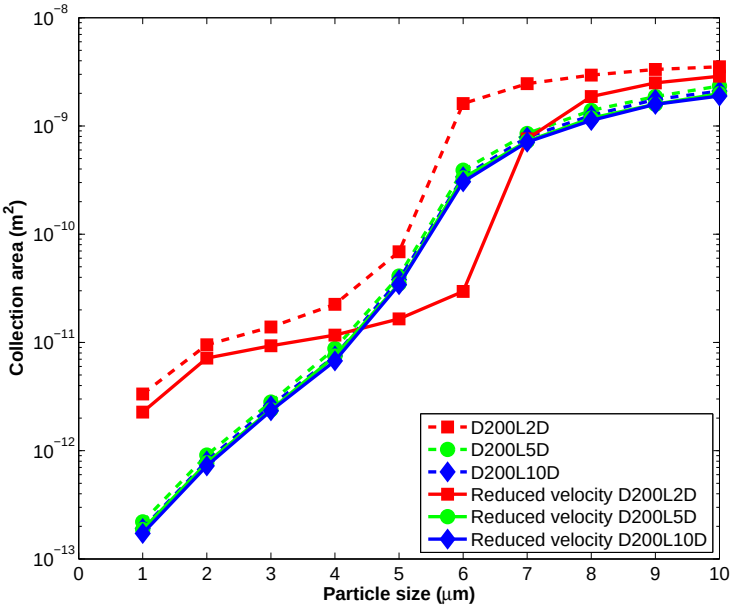

(a)

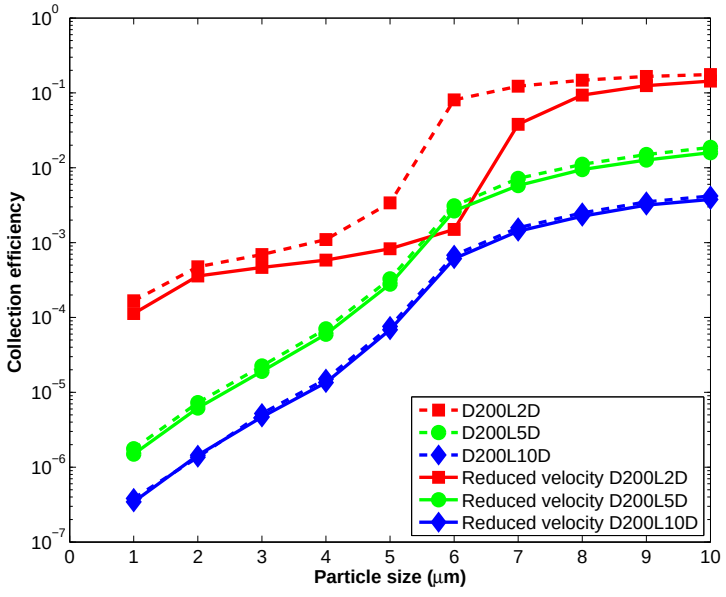

(b)

Figure 4.10: The inertial effect results from a 200 μm droplet, a 1-10 μm particle, and $L = 2D, 5D$ and $10D$ with and without velocity hindrance consideration (a) the collection area plot (b) the collection efficiency plot

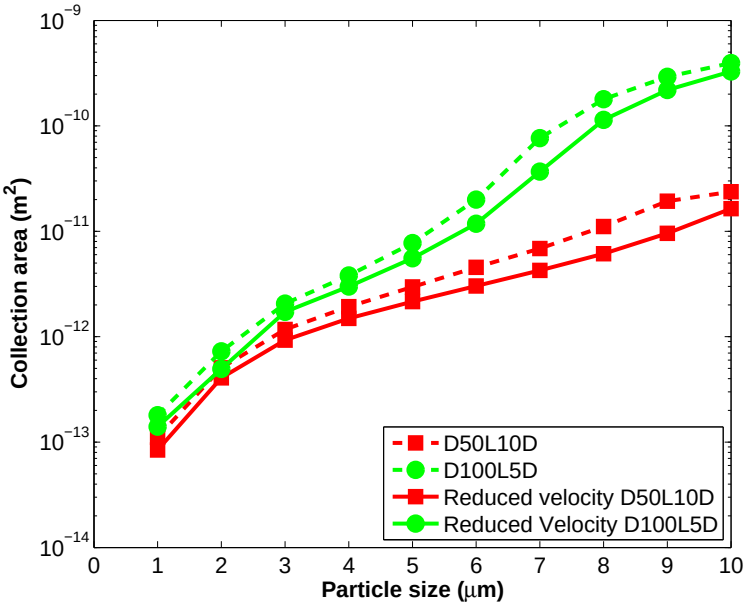

(a)

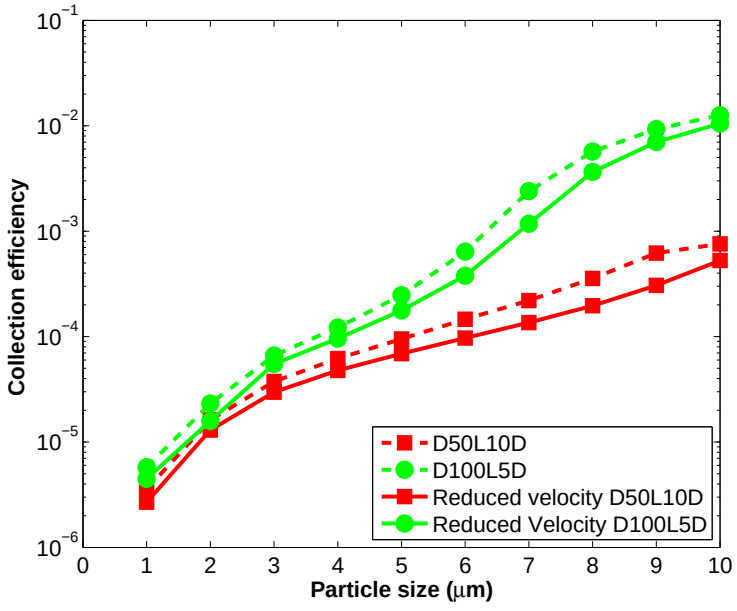

(b)

Figure 4.11: The inertial effect results from 500 μm droplet distance and a 1-10 μm particle with and without velocity hindrance consideration (Case 500 μm droplet L=10D and 100 μm droplet L=5D) (a) the collection area plot (b) the collection efficiency plot

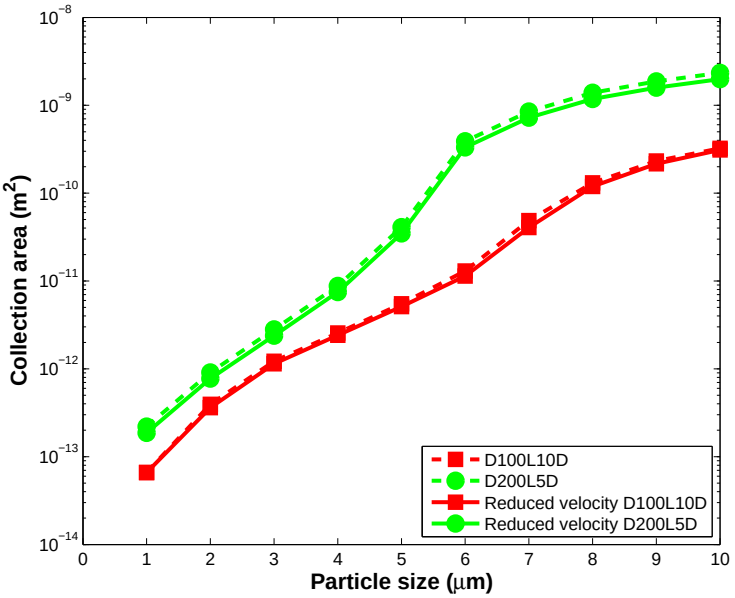

(a)

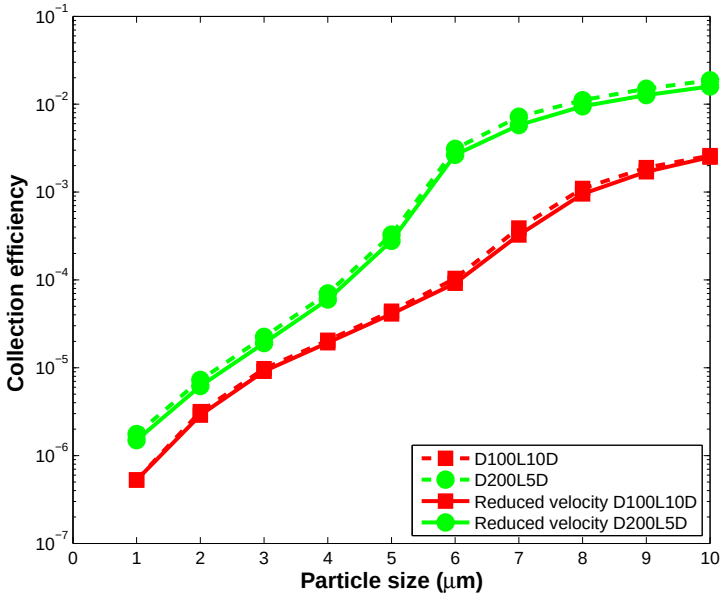

(b)

Figure 4.12: The inertial effect results from a 1000 μm droplet distance and a 1-10 μm particle with and without velocity hindrance consideration (Case 100 μm droplet L=10D and 200 μm droplet L=5D) (a) the collection area plot (b) the collection efficiency plot

Figure 4.14 to 4.16 show the model validation results. The single droplet and multiple droplet results are compared to published single droplet numerical results. Most results come from Pinsky's result in 2000 [59]. For 100 and 200 μm droplet cases, the results from Lin and Lee [6] in 1975 are also included. Pinsky achieved the flow field solutions by using both the Stokes solution and Hamielec and Johnson's results [60]. The Stokes solution is applicable for creeping flow ($Re << 1$). It is also proved that Hamielec and Johnson's results are valid for an intermediate Re number up to 100. Pinsky took the stream function average of two flow solutions by using the Re number as the weight coefficient. Once the flow field was achieved, Pinsky used the fifth-order Runge-Kutta method to solve the equation of particle motion. Similar to this study, Pinsky calculated the collection area and the collection efficiency by summarizing the fates of particles. Lin and Lee also utilized a similar approach except that they used their own numerical flow field solution.

Most of the previous single droplet studies including Pinsky and Lin's work defined the collection efficiency using the collection area normalized by the droplet and particle projection area as shown in Equation 4.2

$$E = \frac{A_{collection}}{\pi(R+r)^2} \tag{4.2}$$

where R and r are the droplet and particle radii respectively. As described in the pervious chapter, this study defined the collection efficiency using the collection area normalized by the inlet area related to the droplet distance. To avoid confusion, all comparisons are made on the collection area instead of the collection efficiency. It should also be noted that the collection area in this study only represents one-eighth of a 360-degree full three-dimensional domain. The single droplet collection areas from Pinsky and Lin were also scaled down by a factor of eight for comparison purposes.

Overall, the single droplet results in this study have good agreement with Pinsky's results. For the 50 μm droplet, there is little difference between this study and Pinsky's. The two results match better for the 100 and 200 μm cases. This is because Pinsky's approach on acquiring the flow fields is more accurate at the intermediate Re range. Lin's results are higher than the results of both this study and Pinsky's. This discrepancy might come from Lin's numerical solutions of the flow field.

Comparison is also made between the single droplet and multiple droplet results.

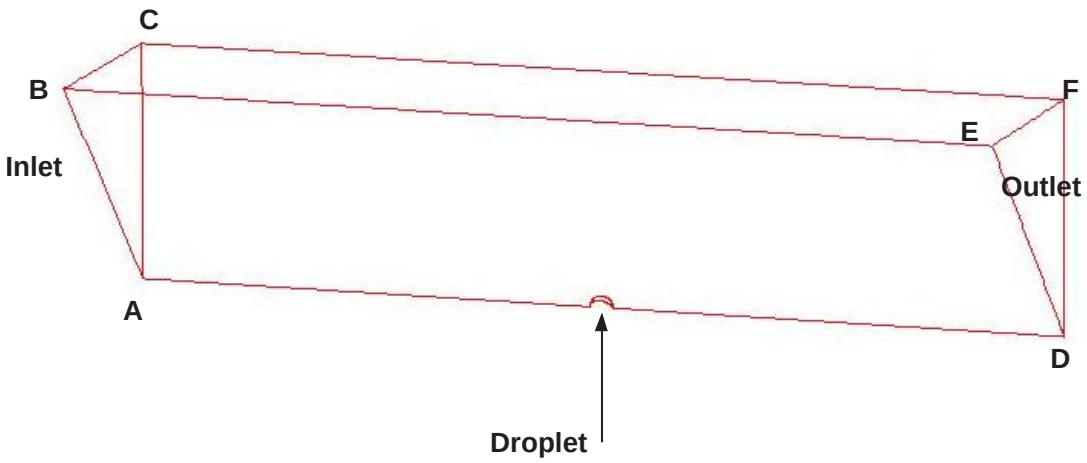

Figure 4.13: The single droplet model domain

For the 50 μm droplet case, it is obvious that the collection areas for the multiple droplet system are higher than that of the single droplet because of the flow acceleration caused by surrounding droplets. Although the smaller droplet spacing slows down the whole system velocity, the acceleration effect is still dominant to acquire larger collection area for a 50 μm droplet. For larger droplet sizes such as 100 and 200 μm , the droplet distance $10D$ or even $5D$ is far enough so that the acceleration is not obvious. As a consequence, both the single droplet and the multiple droplet models predict the similar collection areas. It should also be noted that a group of condensed large droplets are not necessary to provide high collection areas at some particle sizes because of the system velocity hindrance. This can be seen in the cases of 100 and 200 μm droplet and $2D$ droplet distances at certain ranges of the particle size.

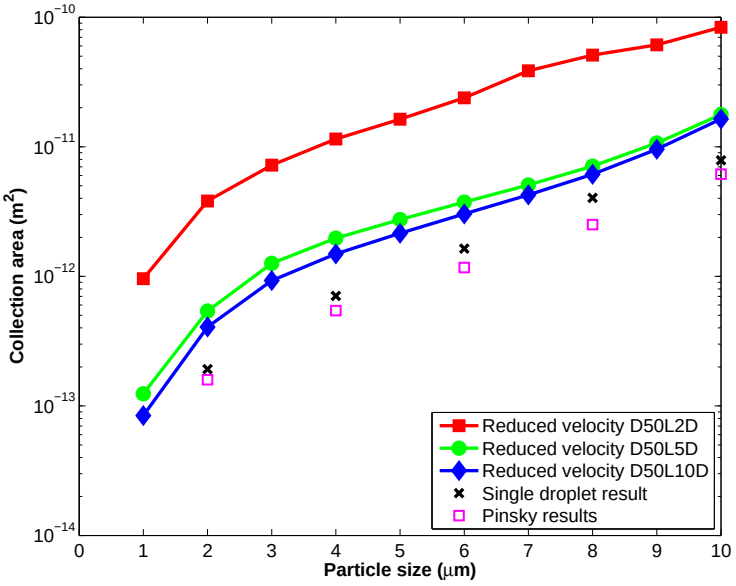

Figure 4.14: The inertial effect validation for a 50 μm droplet and a 1-10 μm particle, collection areas for single droplet, $L = 2D, 5D$ and $10D$ with velocity hindrance effect and published data

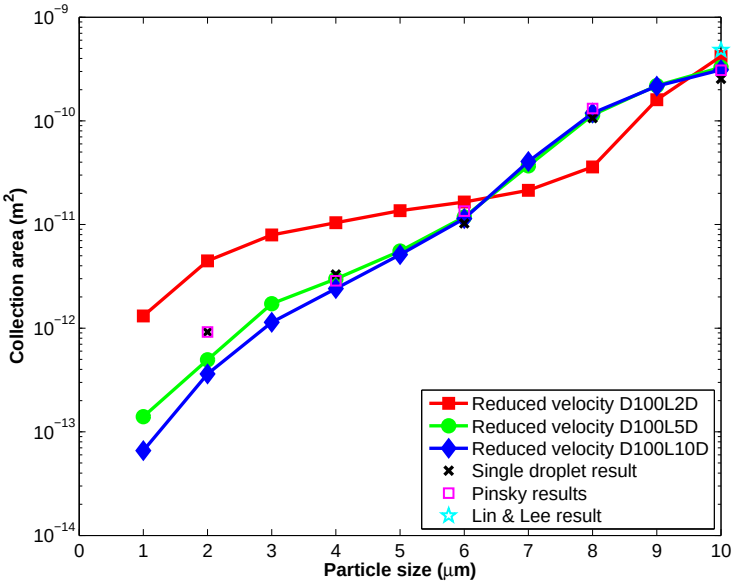

Figure 4.15: The inertial effect validation for a 100 μm droplet and a 1-10 μm particle, collection areas for single droplet, $L = 2D, 5D$ and $10D$ with velocity hindrance effect and published data

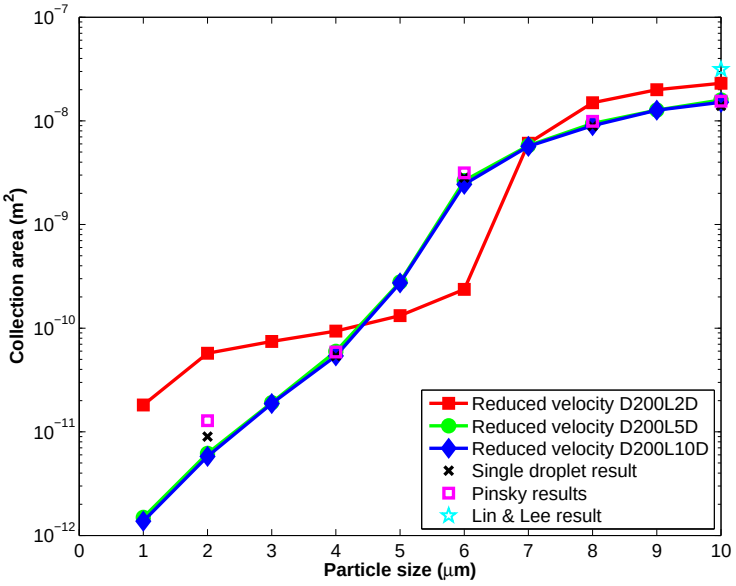

Figure 4.16: The inertial effect validation for a 200 μm droplet and a 1-10 μm particle, collection areas for single droplet, $L = 2D, 5D$ and $10D$ with velocity hindrance effect and published data

Chapter 5

The influence of the electrostatic effect on collection efficiency

5.1 Overview

In atmospheric environments, particles are very seldom neutral. Most particles carry some electric charge, and some may be highly charged. Therefore, it is necessary to take the electrostatic effect into account when studying the physics of atmospheric particle interaction. Moreover, nowadays one of the scavenging technologies is to highly charge droplets to improve collection efficiency. All of those need to study the influences of the electrostatic effect on scavenging. This chapter will discuss a model that predicts collection efficiency while considering the electrostatic effect.

5.2 Electrostatic effect

For a given size, there is a limit of the maximum charge on a liquid particle. The electric charges can generate a repulsion force acting on the liquid particle. Alternatively, surface tension keeps the liquid particle together. When the repulsion force exceeds the surface tension, the particle can be broken into smaller particles. The limiting charge is called the Rayleigh limit and given by

$$n_L = (\frac{2\pi\gamma D^3}{K_E e^2}) \tag{5.1}$$

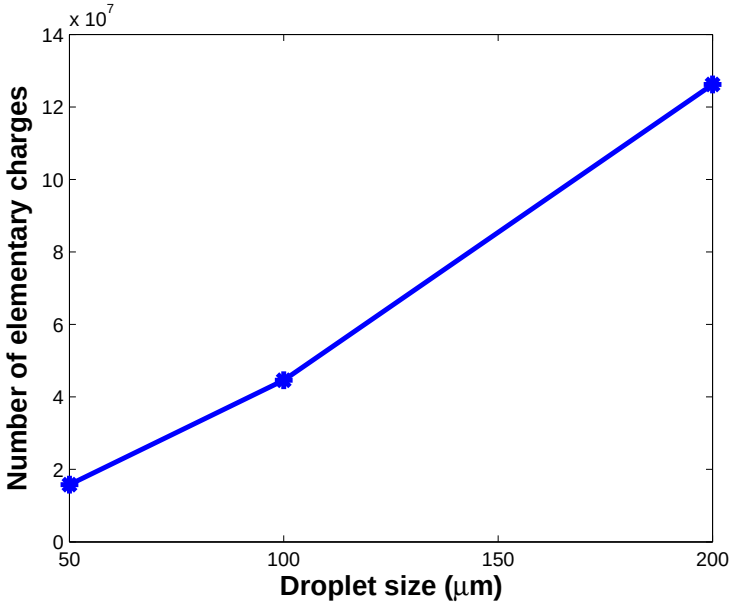

Figure 5.1: Charging Rayleigh limit for water droplets (Surface tension $\gamma = 0.073\ N/m$)

where γ is the surface tension,K_E is the Coulomb constant and e is the elementary charge.

Figure 5.1 and 5.2 show the Rayleigh limits for the water droplet and particle of the certain sizes. The surface tension γ is assumed to be 0.073 N/m. In this study, the Rayleigh limits of a 200 μm droplet and a 1 μm particle are used as a reference to quantify the charges on a droplet and a particle. For simplicity, a scale factor (SF) is introduced to describe the varying charges. SF is defined as the ratio of the charge multiple of a droplet and a particle over the product of the Rayleigh limits of a 200 μm droplet and a 1 μm particle. For example, the maximum charge of a 200 μm droplet is $2.019e^{-11}\ C$, and the maximum charge of a 1 μm particle is $7.1e^{-15}\ C$. If the scale factor SF is $1e^{-6}$, then the total charge multiple is $1e^{-6} \times 2.019e^{-11} \times 7.1e^{-15} = 1.43e^{-31}\ C^2$. The selected values of SF in this study are checked to guarantee that the total charge multiple does not exceed the product of the Rayleigh limits of the droplet and the particle for each case.

Figure 5.3 shows the influences of electrostatic effect on the collection area and the collection efficiency. The case is for the 200 μm droplet and $L = 2D$. The particle size

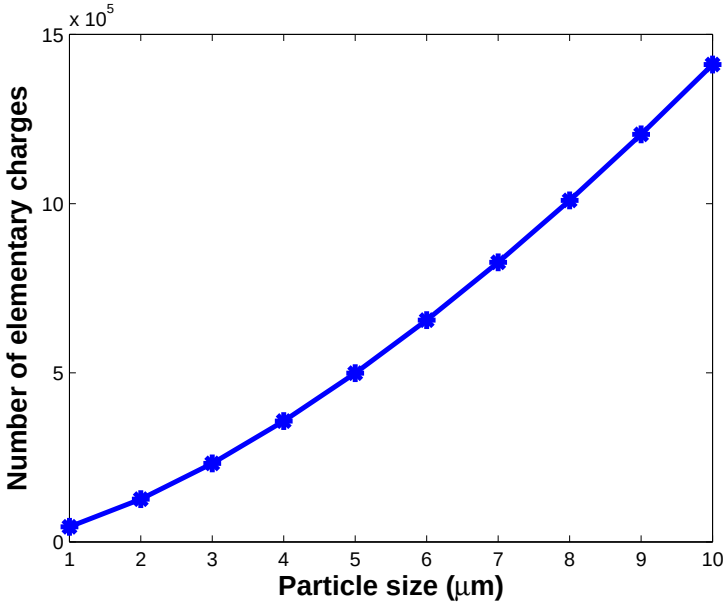

Figure 5.2: Charging Rayleigh limit for particles (Surface tension $\gamma = 0.073\ N/m$)

varies from 1 to 10 μm . It should be noted that the flow field is for a group of settling droplets including the velocity hindrance effect. It can be seen from the results that the collection area and the collection efficiency increase with increasing charges for all sizes of particles. At lower charge, the inertial effect is dominant, so larger particles have higher collection efficiency because of their larger inertia. As charge increases, the electrostatic effect becomes more important. When SF approaches $5e^{-4}$, the electrostatic effect begins to overcome the inertial effect. The electrostatic effect becomes dominant at SF $1e^{-2}$ for most particle sizes. Another important point is that a smaller particle is more easily influenced by the electrostatic effect than a larger one. The trend of the curves shows that a smaller particle responds faster on the collection area and the collection efficiency to the increase of SF than a lager one.

All of the results above are for a group of settling droplets including the velocity hindrance effect (See Chapter 4 for the explanation of velocity hindrance effect). The results are also compared to those without the consideration of the velocity hindrance effect. The comparison can demonstrate the effects of relative velocity of the particle and the droplet on collection efficiency with varying charges. Figure 5.4 shows the velocity hindrance effect for a 200 μm droplet, $L = 2D$, 1 and 10 μm particles. For 10 μm particles, when the SF is low ($SF < 1e^{-3}$) and therefore the inertial effect is dominant, the results with the velocity hindrance effect has lower collection area and collection efficiency than that without the velocity hindrance effect. Once the electrostatic effect becomes dominant ($SF > 1e^{-3}$), the collection area and the collection efficiency with velocity reduction become larger. This is because the lower the relative velocity, the longer time the particle needs to approach the droplet. As a consequence, the electrostatic force can have more effect on the particle trajectory and increase the collection probability because of longer traveling time. This is quite evident for 1 μm particles, which have lower inertia. It can be seen that the electrostatic effect for 1 μm particles has become dominant beginning at $SF > 10e^{-6}$. As already discussed, for smaller particles, since the electrostatic effect overcomes the inertial effect easily, the collection area and the collection efficiency for lower relative velocity becomes larger than those for higher relative velocity even at very low charges. It can also be observed that once the charges are large enough the collection efficiencies for both higher and lower relative velocities are identical and approaching 1.

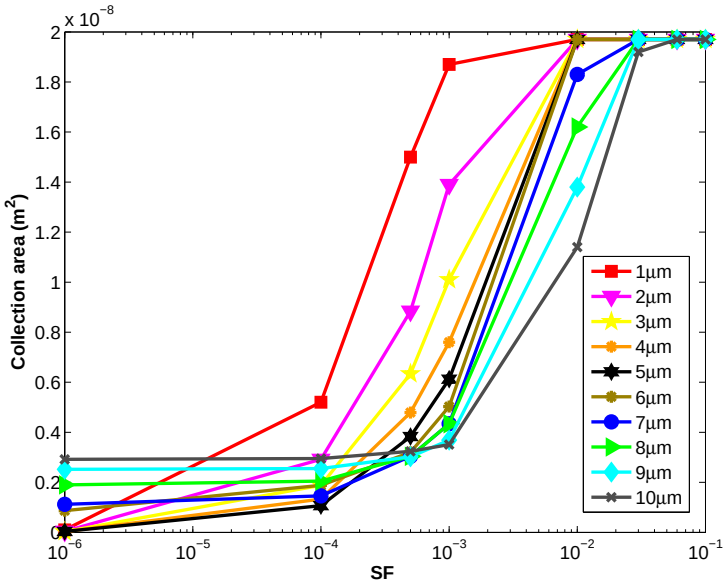

(a)

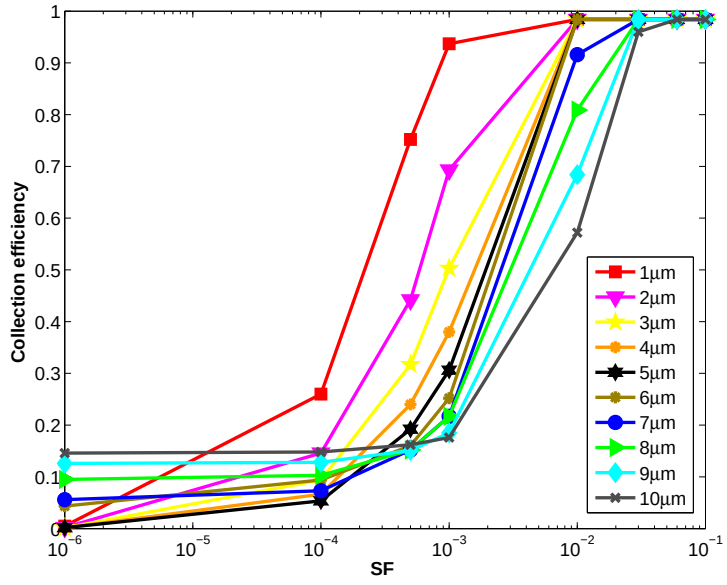

(b)

Figure 5.3: The effect of varying charge for a 200 μm droplet, L = 2D (droplet distance equals two times of droplet diameter) and a 1-10 μm particle ($SF = \frac{Qq}{(RL_{200\mu m})\times(RL_{1\mu m})}$, where $RL_{200\mu m}$ and $RL_{1\mu m}$ are the Rayleigh limits for 200 μm and 1 μm water droplets respectively) (a) the collection area plot (b) the collection efficiency plot

Figure 5.5 shows the effects of varying droplet distance on the collection area and the collection efficiency for the case of a 200 μm droplet and a 10 μm particle. When the SF is less than $1e^{-3}$, the inertial effect is dominant and the smaller droplet distance L results in a larger collection area and collection efficiency. This is because the air velocity accelerates more at a smaller droplet distance, which makes the collection occur more easily. However, when the electrostatic effect becomes dominant ($SF > 1e^{-3}$), the larger droplet distance has the larger collection area. This can still be explained by considering the particle and droplet relative velocity. A larger droplet distance causes the air to accelerate less and the particle to approach the droplet at a relatively lower speed. Consequently, it takes longer traveling time for the particle to approach the droplet. The force of electrostatic attraction can thus have more influence on the particle trajectory when the traveling time is longer. Therefore, it increases the probability of collection to cause a larger collection area. However, this trend cannot be seen on the collection efficiency, because the collection efficiency is the collection area normalized by an area related to the droplet distance L. For the same idea, Figure 5.6 shows the effects of varying droplet distance for the case of a 200 μm droplet and a 1 μm particle. Compared with Figure 5.5, it can be seen that the electrostatic effect is more easily dominant over the inertial effect compared to a 10 μm particle.

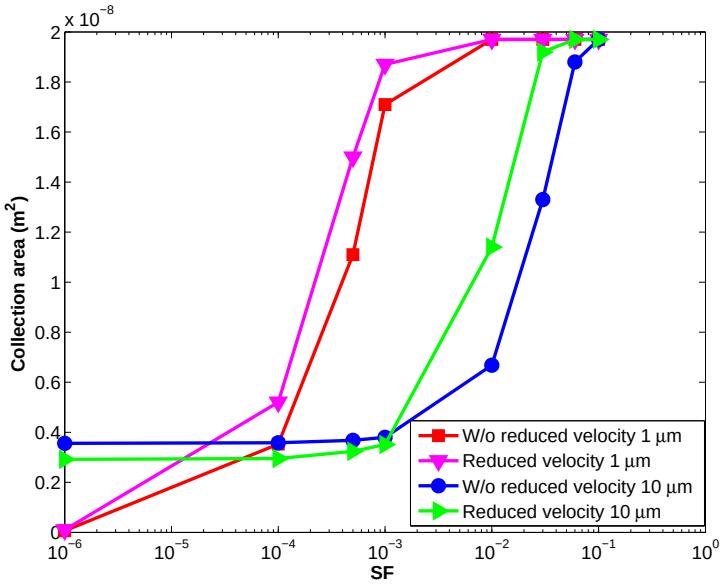

(a)

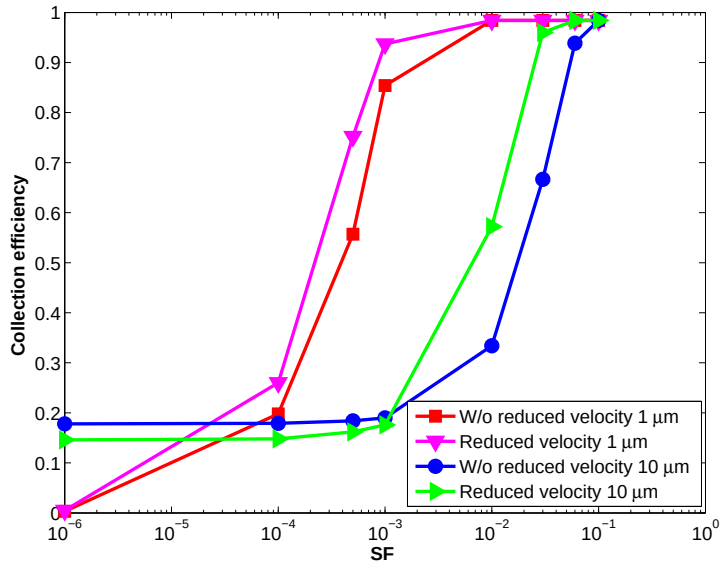

(b)

Figure 5.4: Velocity hindrance effect on particle collection for a 200 μm droplet, L = 2D (droplet distance equals two times of droplet diameter), 1 and 10 μm particle in diameter ($SF = \frac{Qq}{(RL_{200\mu m})\times(RL_{1\mu m})}$, where $RL_{200\mu m}$ and $RL_{1\mu m}$ are the Rayleigh limits for 200 μm and 1 μm water droplets respectively) (a) the collection area plot (b) the collection efficiency plot

Figure 5.7 shows the effect of droplet diameter on the collection area and the collection efficiency. The results include two cases, a 100 μm droplet $L = 10D$ and a 200 μm droplet $L = 5D$. Both cases have the the same droplet distance 1000 μm and the particle size is 10 μm , so the only difference between the two cases is the droplet diameter. When the charge on the particle and the droplet is low ($SF < 10^{-3}$), a 200 μm droplet has a larger collection area and the collection efficiency than 100 μm droplet. This is because the inertial effect is dominant at this range. When SF exceeds 10^{-3}, the collection area and the collection efficiency for 100 μm droplet increases faster and becomes larger than that of a 200 μm droplet. This is because a 100 μm droplet has lower particle and droplet relative velocity than a 200 μm droplet. Therefore, it causes the particle to spend a longer time traveling to the droplet. The force of electrostatic attraction can have more influence when the traveling time is longer. Suppose that two particles begin at the same location relative to either a 200 μm droplet or a 100 μm droplet. The particle approaching the 100 μm droplet will have a longer traveling time, and it causes the particle to travel more distance in radial location. Therefore, the chance of collection is enhanced. This explains why smaller droplets have larger collection efficiency when they are highly charged. In conclusion, the smaller droplet has a relatively larger collection efficiency at the same droplet distance when the charge is large enough to make the electrostatic effect dominant.

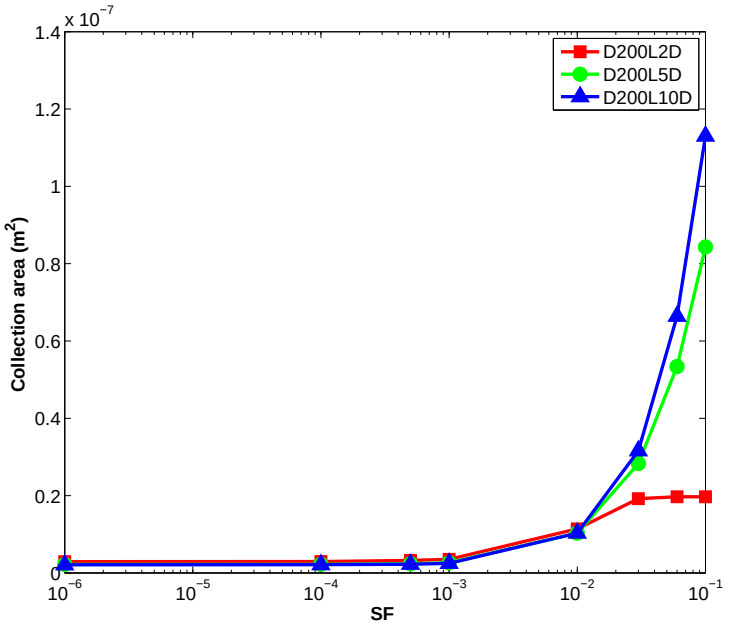

(a)

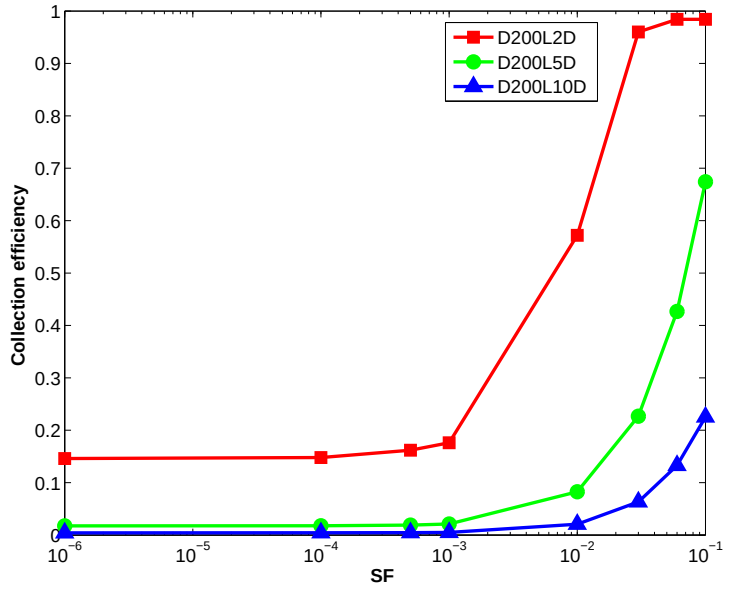

(b)

Figure 5.5: The effect of varying droplet distance ($L = 2D, 5D, 10D$) for a 200 μm droplet and a 10 μm particle ($SF = \frac{Qq}{(RL_{200\mu m})\times(RL_{1\mu m})}$, where $RL_{200\mu m}$ and $RL_{1\mu m}$ are the Rayleigh limits for 200 μm and 1 μm water droplets respectively) (a) the collection area plot (b) the collection efficiency plot

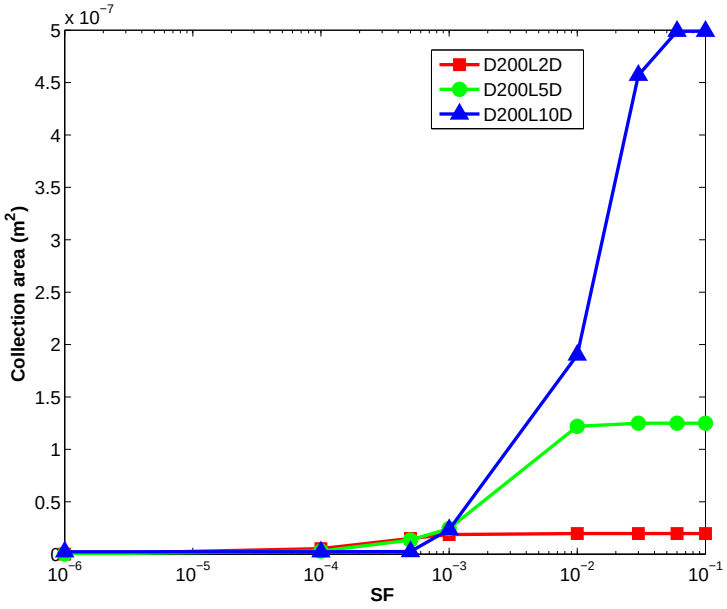

(a)

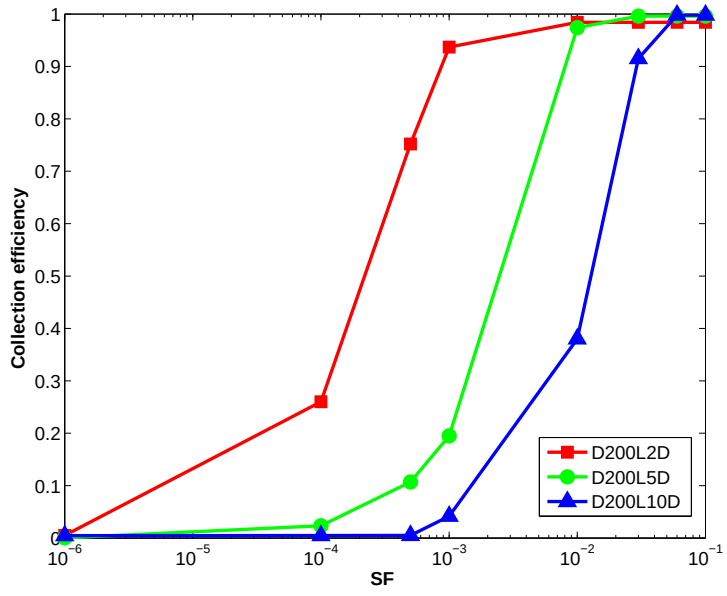

(b)

Figure 5.6: The effect of varying droplet distance ($L = 2D, 5D, 10D$) for a 200 μm droplet and a 1 μm particle ($SF = \frac{Qq}{(RL_{200\mu m})\times(RL_{1\mu m})}$, where $RL_{200\mu m}$ and $RL_{1\mu m}$ are the Rayleigh limits for 200 μm and 1 μm water droplets respectively) (a) the collection area plot (b) the collection efficiency plot

5.3 Validation

Similar to the validation approach for the inertial effect described in Chapter 4, a single droplet model has been used to validate the electrostatic effect as well. As described in Chapter 4, the flow field solution is achieved for the case of a single droplet. The only difference compared to the inertial effect validation is the particle tracking step. Not only is the inertial force included in the particle motion equation but also the electrostatic force.

In 2004, Khain numerically calculated the particle collection efficiency with the electrostatic effect. Khain's model concentrated on the microphysics of a single droplet and a single particle. The flow field caused by a moving droplet is assumed to obey the Stokes solution because all of the cases in his study have small Reynolds numbers. The equation of particle motion was solved to determine if the particle can be collected. Eventually, the collection area and the collection efficiency were calculated.

To compare with Khain's result [10], a model for a 40 μm single droplet has been set up. The geometry was achieved by scaling from the single droplet model of 200 μm described in Chapter 4. The inlet was applied with a uniform velocity, and the magnitude equaled the settling velocity of 40 μm droplet (0.0484 m/s). The steady state flow field was achieved when the iteration converged. The particle tracking methodology was similar to the approach of inertial effect validation described in Chapter 4 except that the electrostatic force was included here.

$$\frac{dV_p}{dt} = g^* + (\frac{C_D Re_p}{24\tau})(V_p - U) + \frac{Fe}{M} \tag{5.2}$$

$$\frac{dS_p}{dt} = V_p \tag{5.3}$$

where V_p is the particle velocity and U is the flow velocity, S_p is the particle position, $g^* = \frac{(\rho_p - \rho)g}{\rho_p}$ is the net gravitational acceleration, ρ_p is the particle density, ρ is the fluid density, M is the mass of a particle, $Re_p = \frac{\rho|V_p - U|d}{\mu}$ is the particle relative Reynolds number, d is the particle diameter, C_D is the drag coefficient, F_e is the electrostatic force and τ is the characteristic relaxation time.

Khain's study concentrated on the electrostatic effect between a highly charged droplet and a neutral particle. When a highly charged droplet is adjacent to a neutral

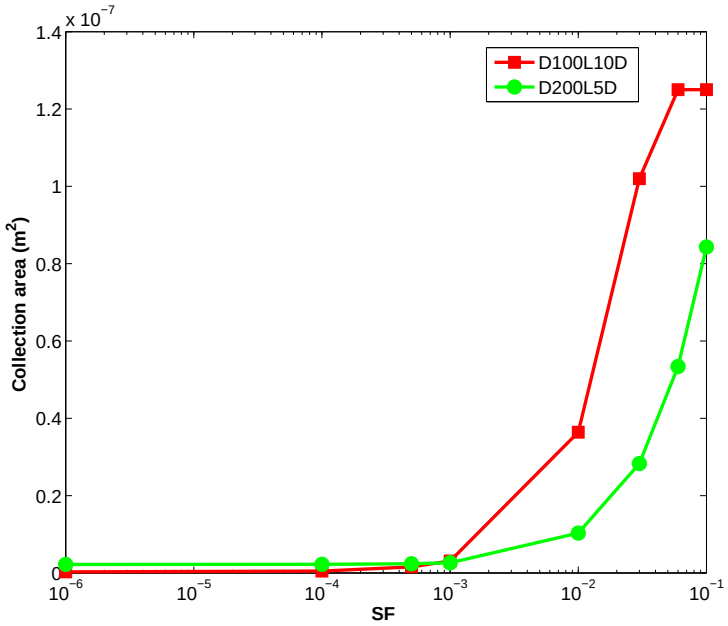

(a)

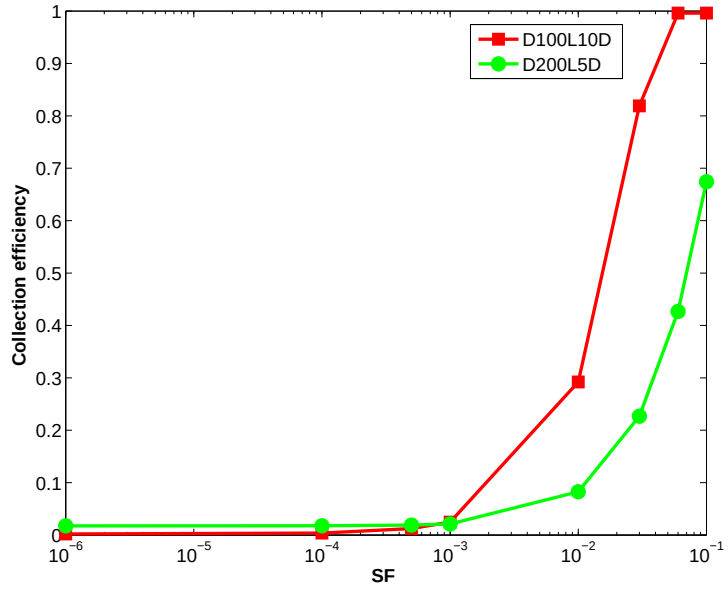

(b)

Figure 5.7: The effect of droplet size on particle collection for a 10 μm particle with the same droplet distance 1000 μm (Case 100 μm droplet $L = 10D$ and 200 μm droplet $L = 5D$, $SF = \frac{Qq}{(RL_{200\mu m})\times(RL_{1\mu m})}$, where $RL_{200\mu m}$ and $RL_{1\mu m}$ are the Rayleigh limits for 200 μm and 1 μm water droplets respectively)(a) the collection area plot (b) the collection efficiency plot

particle, electrons inside the particle can be relocated. The electron relocation can cause an attraction between the droplet and the particle. The electrostatic force can be represented by the following formula:

$$\begin{aligned} F_e = \frac{Qq}{4\pi\varepsilon_0 S^2} + \frac{1}{4\pi\varepsilon_0} Q^2 r[\frac{1}{S^3} - \frac{S}{(S^2-r^2)^2}] + \frac{1}{4\pi\varepsilon_0} q^2 R[\frac{1}{S^3} - \frac{S}{(S^2-R^2)^2}] \\ + \frac{1}{4\pi\varepsilon_0} QqRr[\frac{1}{S^4} + \frac{1}{(S^2-R^2-r^2)^2} - \frac{1}{(S^2-R^2)^2} - \frac{1}{(S^2-r^2)^2}] \end{aligned} \tag{5.4}$$

where Q and q are the charges on the droplet and the particle respectively, R and r are the radii of the droplet and the particle respectively, ε_0 is the dielectric permittivity of free space and S is the distance between the droplet and the particle. The first term in Equation 5.4 represents the Coulomb force, the next two terms represent interaction between point charges and the dipole. The last term describes interaction between induced imaginary charges. In this case of a charged droplet and a neutral particle, the first, third and fourth terms are zero.

Rather than the Rayleigh limit, Khain used a different type of charging limit called corona discharging limit. The maximum possible charge is a function of the droplet radius and given by Equation 5.5. Basically, if the charge of a droplet is higher than the limit, a corona discharge occurs suddenly.

$$Q_{max} = 4\pi U_b \varepsilon_0 R^2 \tag{5.5}$$

where U_b is called the air breakdown voltage and equals $3 \times 10^6\ V/m$ [91].

Figure 5.8 shows the comparison of collection areas between this study and Khain's. The results are for 2 μm neutral particles collected by a 40 μm droplet with varying charges. Both of the results clearly show the trend of increasing collection area with increasing charges on the droplet. The results of this study have good agreement with Khain's, which shows the accuracy of the developed models in this study.

5.4 Numerical uncertainty discussion

Since the results of collection area and collection efficiency in this study come from the flow field results solved by CFD, CFD uncertainty will be one of the major error sources. There have been many studies about CFD uncertainty [92, 93, 94, 95]. One

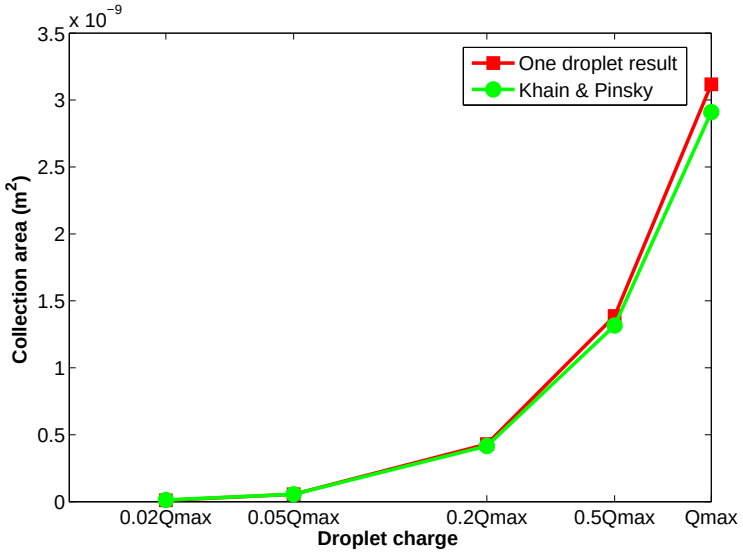

Figure 5.8: Comparison of collection area between one droplet result and the Khain and Pinsky result, a 40 μm droplet with varying charge from 0.02 to 1 Q_{max} and a 2 μm neutral particle (where Q_{max} is the corona discharging limit of 40 μm droplet)

of approaches to estimate the iteration error is to use the range of max and min values for a period of iterations [93]. Another method was proposed by Richardson [96] to estimate discretization error. This method is similar to the approach used in this study. Basically, it needs three sets of CFD results with different grid resolutions to achieve grid independent results. However, there is no standard method for evaluating numerical uncertainty currently accepted by the CFD community. Moveover, for this particular study, the difficulty also exists on how to propagate the CFD error to the collection efficiency. The collection efficiency is based on statistical results of the particle fate which is individually affected by the CFD error. To control the numerical accuracy, this study followed the guidelines published by *Journal of Fluids Engineering* [97], which is most typically used by most CFD studies. This study strictly obeyed the guidelines where those are applicable. The numerical computations in this study are second order accurate in space. The mesh sensitivity study has been performed to prove the grid independence. The numerical methods and proof of convergence were also provided. At last, the results were validated by comparing to the existing studies.

5.5 Particle electroscavenging suggestion

1. Collection mechanism selection

   The study shows the electrostatic effect can easily increase the collection efficiency by 90%. Therefore, using the electrostatic effect instead of the inertial effect is suggested. It is already approved in industry that a conventional inertial scrubber needs relatively high droplet speed to guarantee the collection efficiency. Alternatively, electrostatic scrubbers require lower water rate and lower pressure drop through the equipment,achieving the same collection efficiencies as inertial scrubbers.

2. Droplet size selection

   For any given size of particle, the first step is to choose the droplet size. Basically, as for electroscavenging, the smaller the droplet size, the larger the collection efficiency. Smaller droplets have lower settling velocity, which increases the chance of collection . In this study, the droplets and particles move in the same direction. There are cross-flow electrostatic scrubbers, which are used in industry as well. For similar reason, the smaller droplets still provide more time for the interaction between droplets and particles. As a consequence, the collection efficiency can be improved. However, the cost of breaking up droplets with smaller size needs to be considered in the electroscavening design.

3. Droplet charge selection

   Obviously, highly charged particles and droplets to opposite polarities can benefit collection efficiency. As shown in the study, the collection efficiency increases rapidly at a certain range of SF, and levels off once the SF passes that range. It is recommended that SF can be chosen at the upper bound of that range to guarantee high collection efficiency without wasting the charging cost. As an example, Table 5.1 shows the cutoff SF for the 200 μm droplet and $L = 2D$ case. For each particle size, it can be found that the minimum SF can still achieve the high efficiency above 0.90.

4. Droplet distance selection

Table 5.1: Cutoff SF for a 200 μm droplet and $L = 2D$

Particle size (μm)	SF	Collection efficiency
1	$1e^{-3}$	0.94
2	$1e^{-2}$	0.99
3	$1e^{-2}$	0.99
4	$1e^{-2}$	0.98
5	$1e^{-2}$	0.98
6	$1e^{-2}$	0.97
7	$3e^{-2}$	0.98
8	$3e^{-2}$	0.98
9	$6e^{-2}$	0.98
10	$6e^{-2}$	0.98

Table 5.2: Combined effect of charging and droplet distance on a 200 μm droplet and a 1 μm particle

Droplet distance	SF	Collection efficiency
$L = 2D$	$1e^{-3}$	0.94
$L = 5D$	$1e^{-2}$	0.97
$L = 10D$	$3e^{-2}$	0.92

This study suggests that a smaller droplet distance improves the collection efficiency. Although a single droplet in a group of droplet with larger droplet distance has a larger collection area, a group of droplets with a smaller droplet distance can cover a greater portion of a particular sweeping volume. Droplet distance is directly related to liquid consumption. Therefore, choosing droplet distance is one concern in practical use of the electrostatic scrubbers. Another point that needs to be emphasized here is to evaluate the combined effect of charging and droplet distance. As shown in Table 5.2, the different combinations of charging amount and droplet distance achieve almost the same high efficiency. Therefore, choosing the right combination simply becomes a cost issue.

Chapter 6

Conclusion

6.1 Summary

The study of microphysics of droplet-and-particle interaction are needed in many areas to estimate particle collection efficiency by droplets (e.g., atmospheric study, industrial and military applications). There are a few experimental studies related to this topic. However, those experimental data are discrete because only certain sizes of particle and droplet and certain charges have been measured. In addition, the collection mechanisms during those experiments were complicated and occurred at the same time. Hence, it was difficult to investigate the contribution of each mechanism. There have been many numerical studies in past years. Most numerical studies are 2D analyses and only concentrate on the interaction of a single droplet and a single particle. In reality, it is always a group of droplets falling through a space filled with aerosol particles. To overcome those deficiencies, a new numerical model for predicting the particle collection efficiency by a group of droplets has been developed in this study. The 3D model simulates the scenario where an individual particle travels through a matrix of droplets each time. Then the behavior of each particle starting from different locations has been statistically recorded, and eventually used to predict the collection efficiency. This study also investigates the situation where both droplets and particles are highly charged. The impact of collection efficiency by the sizes of particle and the droplet,the charges of particle and droplet, and inter-droplet distance have also been studied. The results have been compared to existing numerical studies at certain ranges and achieved good

agreement. The following summarizes all the conclusions in this study.

- When the inertial effect is the only collection mechanism, the collection area and the collection efficiency increase as particle size increases. This conclusion holds true whether considering the settling velocity reduction or not.
- When the inertial effect is the only collection mechanism, the collection area and the collection efficiency increase as droplet size increases. This conclusion holds true whether considering the settling velocity reduction or not. Increasing droplet size has more effect on larger particles than smaller particles in terms of the collection area and the collection efficiency.
- When the inertial effect is the only collection mechanism, the larger the droplet distance is, the smaller the collection area and the collection efficiency are. This holds true until the droplet distance is large enough and has no influence on the inertial effect. At that moment, the increase of droplet distance cannot cause the collection area to decrease anymore. However, the collection efficiency will continue to decrease because it is inversely proportional to the square of the droplet distance.
- A group of droplets usually settles at lower velocity than a single droplet. With the velocity hindrance, there is a reduction of the collection area and the collection efficiency. This reduction is more evident for a smaller droplet distance than for a larger one. At a certain range of droplet and particle sizes, the collection area and the collection efficiency for smaller droplet distance can be even smaller than those for larger droplet distance.
- For the sake of validation, a single droplet model has been developed using the same approach as the multi-droplet model. The results of collection efficiency predicted by the single droplet model have good agreement with published numerical results.
- Basically, the collection area and the collection efficiency increase with increasing charges on the droplet or the particle. As charges continue increasing, the collection area is eventually approaching a constant and the collection efficiency is equal to 1.

- A smaller particle is more easily influenced by the electrostatic effect. When charges are low, the larger particle has a larger collection area and collection efficiency than the smaller particle with all other conditions remaining equal. However, as charges increase, the smaller particle will have a larger collection area and collection efficiency because of the electrostatic effect.

- The reduction of velocity caused by group settling under the electrostatic effect has also been studied. When charges are low, the collection area and the collection efficiency are smaller when considering the velocity hindrance. When charges become large, the collection area and the collection efficiency become larger when considering the velocity hindrance than those without considering the velocity hindrance.

- When the electrostatic effect is dominant over the inertial effect, a larger droplet distance causes a larger collection area. The larger droplet distance causes locally lower air velocity, and the force of electrostatic attraction can have more influence on the particle in this situation. Hence, it increases the probability of collection. The collection efficiency might not necessarily increase with increasing droplet distance.

- Generally, the larger droplet has a larger collection area and a larger collection efficiency at the inertial effect dominant region when other conditions are the same. This trend changes when the electrostatic effect becomes dominant over the inertial effect. A group of smaller droplets settles at relatively lower velocity, which causes particles to be influenced more by the force of electrostatic attraction. Hence, the collection efficiency can be improved.

- Similar to inertial effect validation, a single droplet model including the electrostatic effect has been developed. The results have been compared to the published data and have good agreement. Since the single droplet model shares the same approaches with the multi-droplet model, this agreement provides confidence in the multi-droplet model.

- Based on the results of this study, parameter selection to benefit particle electroscavenging has been discussed. Those parameters include the amount of charging, the droplet size, and distance. The contribution from one individual parameter or combination of two parameters have been investigated. The relation between those parameters and the cost of an electrostatic scrubber has also been stated.

6.2 Future work

This work used a first-ever modeling approach and made important contributions to the study of particle scavenging. It also resulted in some other interesting topics for future work. Here is an outline of those topics.

In this dissertation, a group of droplets are assumed to form a simple cubic structure. It is a reasonable assumption considering the situation where a group of monodispersed droplets with the same charge have achieved a steady state in a certain volume. However, there are other formations including face-centered cubic (FCC) structure and body-centered cubic (BCC) structure that can also reach the steady state. It will be very interesting to see how those different formations make an effect on particle collection.

Is is assumed that particle collection occurs in still air in this study. However, in practice, still air is difficult to achieve. Most likely, in atmospheric environments, winds exist. In industrial applications, droplets might be formed by water jet breakup and atomization with a high-speed gas stream. Under those situations, the droplets could have a velocity higher than their settling velocity. Investigating the effects of the velocity on the collection efficiency will be the future work. Once the velocity is high enough to cause turbulence, how the turbulence affects particle collection should be investigated.

In this study, the minimum particle diameter is 1 μm . It is appealing to investigate the collection of particles smaller than 1 μm . In that situation, the Brownian effect on particle collection cannot be avoided. To consider the Brownian effect, a statistical approach can be included to the current model. Specifically, a random Brownian force can be introduced to the equation of particle motion, and then the Monte Carlo method can be used to estimate the behavior of a large amount of particles.

References

[1] W. Hinds. *Aerosol technology.* Joohn Wiley and Sons, 2nd edition, 1999.

[2] A.P.T.I. classroom. Lesson 2: Operating principles of scrubbers. *http ://yosemite*1.*epa.gov/oaqps/EOGtrain.nsf/DisplayView/SI*$_4$12C_0 − 5?*OpenDocument*, 2011.

[3] S. Kojevnikova and Y. Zimmels. Mechanism of collection of aerosols by an array of oppositely charged drops. *Journal of Aerosol Science*, 31:437–461, 1999.

[4] D. M. Chate and A. K. Kamra. Collection efficiencies of large water drops collecting aerosol particles of various densities. *Atmospheric Environment*, 31:1631–1635, 1997.

[5] T. Andersson. Small scale variations of the contamination of rain caused by washout from the low layers of the atmosphere. *Tellus*, 21:685–692, 1969.

[6] C. L. Lin and S. C. Lee. Collision efficiency of water drops in the atmosphere. *Journal of Atmospheric Sciences*, 32:1412–1415, 1975.

[7] K. V. Beard and S. N. Grover. Numerical collision efficiencies for small raindrops colliding with micron size particles. *Journal of Atmospheric Sciences*, 31:543–550, 1974.

[8] P. K. Wang, S. N. Grover, and H. R. Pruppacher. On the effect of electric charges on the scavenging of aerosol particles by clouds and small raindrops. *Journal of the Atmospheric Sciences*, 35:1735–1743, 1978.

[9] S. N. Grover, H. R. Pruppacher, and A. E. Hamielec. A numerical determination of the efficiency with which spherical aerosol particles collide with spherical water drops due to inertial impaction and phoretic and electrical forces. *Journal of Atmospheric Sciences*, 34:1655–1662, 1977.

[10] A. Khain, V. Arkhipov, M. Pinsky, Y. Feldman, and Ya. Ryabov. Rain enhancement and fog elimination by seeding with charged droplets. part i: theory and numerical simulations. *Journal of Applied Meteorology*, 43:1513–1529, 2004.

[11] B. A. Silverman and W. Sukarnjanaset. Results of the thailand warm-cloud hygroscopic particle seeding experiment. *Journal Applied Meteor*, 39:1160–1175, 2000.

[12] G. W. Penney. *U. S. Patent 2, 357 354*, 25, 1944.

[13] M. J. Pilat, S. A. Jaasund, and L. E. Sparks. Collection of aerosol particles by electrostatic droplet spray scrubbers. *Environment and Science Technology*, 8:360–362, 1974.

[14] M. Schmidt and F. Loffler. Investigations of fine particle separation using an electrostatic nozzle scrubber. *Journal of Aerosol Science*, 23 Suppl.1:773–777, 1992.

[15] A. Krupa, A. Jaworek, T. Czech, M. Lackowski, and J. Luckner. Dust particles removal by wet-type electrostatic scrubber. *In: Electrostatics, Institution of Physics Conference Series*, 178:349–354, 2003.

[16] A. Jaworek, A. Krupa, and K. Adamiak. Submicron charged dust particle interception by charged drops. *IEEE Transactions on Industry Applications*, 34:985–991, 1998.

[17] A. Jaworek, W. Balchandran, M. Lackowski, J. Kulon, and A. Krupa. Multi-nozzle electrospray system for gas cleaning process. *Journal of Electrostatics*, 64:194–202, 2006.

[18] H. F. Kraemer and H. F. Johnstone. Collection of aerosol particles in presence of electrostatic fields. *Industrial Engineering Chemistry Fundamentals*, 47:2426–2434, 1955.

[19] K. A. Nielsen and J. C. Hill. Collection of inertialess particles on spheres with electrical forces. *Industrial Engineering Chemistry Fundamentals*, 15:149–157, 1976.

[20] L. Theodore and A. J. Buonicore. *Air pollution control equipment.* Prentice-Hall, New Jersey, 1st edition, 1982.

[21] S. Calvert. *A. C. stern, scrubbing, air pollution.* Academic Press, New York, 3rd edition, 1982.

[22] S. C. Yung, H. F. Barbarika, and S. Calvert. *JAPCA.* 1977.

[23] D. Leith, D. W. Cooper, and S. N. Rudnick. Venturi scrubbers: pressure loss and regain. *Aerosol Science and Technology*, 4:239–243, 1985.

[24] H. E. Hesketh. Atomization and cloud behavior in wet scrubbers. In *Proceedings of the US-USSR Symposium on Control Fine Particulate Emissions*, pages 15–18, 1974.

[25] R. H. Boll. Particle collection and pressure drop in venturi scrubbers. *Industrial Engineering Chemistry Fundamentals*, 12:50–60, 1973.

[26] B. J. Azzopardi and A. H. Govan. Modeling of venturi scrubbers. *Filtration and Separation*, 67:196–200, 1984.

[27] B. J. Azzopardi, S. F. C. F.Teixeira, A. H. Govan, and T. R. Bott. Improved model for pressure drop in venturi scrubbers. *Process Safety and Environmental Protection: Transactions of the Institution of Chemical Engineers, Part B*, 69:237–245, 1991.

[28] M. Van Werven, H.R.E. Van Maanen, G. Ooms, and B. J. Azzopardi. Modeling wet-gas annular/dispersed flow through a venturi. *AIChE Journal*, 49:9–18, 2003.

[29] R. A. Pulley. Modeling the performance of venturi scrubbers. *Chemical Engineering Journal*, 67:9–18, 1997.

[30] C. Tsai, K. Chung, and C. Wang. Considerations for cleanroom control in different climatic regions. In *Semiconductor Manufacturing Technology Workshop Proceedings, 2004*, pages 59–62, 2004.

[31] H. Wakamatsu, M. Matsuki, N. Tanaka, H. Ogata, H. Iba, and K. Murata. High efficiency airborne molecular contaminants removal technology by a new cooled-type 2-stage high-speed air washer method. In *The Ninth international symposium on semiconductor manufacturing, 2004*, pages 289–291, 2004.

[32] K. Schaber, A. Schenkel, and A. Koch. Growth of acid aerosol droplets in humid air. *Journal of Aerosol Science*, 25:449–450, 1994.

[33] J. Sun, B. Y. H. Liu, P. H. McMurry, and S. Greenwood. Method to increase control efficiencies of wet scrubbers for submicron particles and particulate metals. *Journal of the Air and Waste Management Association*, 25:184–185, 1994.

[34] K. S. Kumar and Pl L. Feldman. Fine particulate and trace element control in wet electrostatic precipitators. In *Proceedings of 87th Annual Meeting- Air and Waste Management Association*, volume 6A, pages 1–10, 1994.

[35] S. V. Sheppard. Ionizing wet scrubbers control plant emissions. *Mechanical Engineering*, pages 72–75, 1985.

[36] S. Greenfield. Rain scavenging of radioactive particulate matter from the atmosphere. *Journal of Meteor*, 14:115–125, 1957.

[37] W. Walton and A. Woolcock. The suppression of air-borne dust by water sprays. *International Journal of Air Pollutant*, 3:129–153, 1960.

[38] N. A. Fuchs. *The mechanics of aerosols.* Macmillan, New York, 1 edition, 1964.

[39] L. Z. Waldmann and K. H. Schmidt. Thermophoresis and diffusiophoresis of aerosols. *Aerosol Science*, pages 148–155, 1966.

[40] W. G. Slinn and J. M. Hales. Phoretic processes in scavenging: precipitation scavenging. *AEC Symposium Series*, pages 411–421, 1970.

[41] W. G. Slinn and J. M. Hales. A reevaluation of the role of thermophoresis as a mechanism of in and below cloud scavenging. *Journal of Atmospheric Sciences*, 28:1465–1471, 1971.

[42] H. M. Davenport and L. K. Peters. Field studies of atmospheric particulate concentration charges during precipitation. *Atmospheric Environment*, 12:997–108, 1977.

[43] H. T. Yang, S. Viswanathan, W. Balachandran, and M. B. Ray. Modeling and measurement of electrostatic spray behavior in rectangular throat of pease-anthony venturi scrubber. *Environmental Science and Technology*, 37:2547–2555, 2003.

[44] I. Langmuir and K.B. Blodgett. Mathematical investigation of water droplet trajectories. *General Electric research laboratory report*, RL225, 1946.

[45] S. Viswanathan. An improved single droplet collection efficiency for the intermediate flow regime. *Particle Science Technology*, 16:215–227, 1998.

[46] J. Kulon A. Jaworek, W. Balachandran. A. Krupa and M. Lackowski. Wet electroscurbbers for state of the art gas cleaning. *Environmental Science and Technology*, 40:6197–6207, 2006.

[47] H. R. Pruppacher and J. D. Klett. *Microphysics of clouds and precipitation*. D. Reidel publishing company, New Jersey, 2nd edition, 1997.

[48] L. M. Hocking. The collision efficiency of small drops. *Journal of Roy Meteor Society*, 85:44–50, 1959.

[49] L. M. Hocking and P. R. Jonas. The collision efficiency of small drops. *Journal of Roy Meteor Society*, 96:722–729, 1970.

[50] M. H. Davis. Collisions of small cloud droplets. *Journal of Atmospheric Sciences*, 29:911–915, 1972.

[51] M. H. Davis and J. D. Sartor. Theoretical collision efficiencies for small cloud droplets in Stokes flow. *Nature*, 215:1371–1372, 1967.

[52] S. Kim and S. J. Karrila. *Microhydrodynamics principles and selected applications*. Butterworth-Hemmann, New York, 1st edition, 1991.

[53] J. D. Klett and M. H. Davis. Theoretical collision efficiencies of cloud droplets at small Reynolds numbers. *Journal of Atmospheric Sciences*, 30:107–117, 1973.

[54] G.F. Carrier. On slow viscous flow final report. *Contract Nonr-653(00)*, 1953.

[55] G. Dau. Rear surface deposition of fine particles on spheres-eddy deposition or electrostatic effects. *Chemical Engineering and Technology*, 10:330–337, 1987.

[56] A. Jaworek K. Adamiak and A. Krupa. Deposition efficiency of dust particles on a single, falling and charged water droplet. *IEEE Transaction*, 37:734–750, 2001.

[57] B. P. Le Clair, A. E. Hamielec, and H. R. Pruppacher. A numerical study of the drag on a sphere at low and intermediate Reynolds numbers. *Journal of Atmospheric Sciences*, 27:308–315, 1970.

[58] R. J. Schlamp, S. N. Grover, and H. R. Pruppacher. A numerical investigation of the effect of electric charges and vertical external electric fields on the collision efficiency of cloud drops. *Journal of Atmospheric Sciences*, 33:1747–1755, 1976.

[59] M. Pinskyan A. Khain. Collision efficiency of drops in a wide range of Reynolds number: effects of pressure on spectrum evolution. *Journal of Atmospheric Sciences*, 58:742–764, 2000.

[60] A. E. Hamielec and A. I. Johnson. Viscous flow around fluid spheres at intermediate Reynolds numbers. *Journal of Chemical Engineering*, 40:41–45, 1962.

[61] M. Pinsky, A. Khain, and M. Shapiro. Collision of small drops in a turbulence flow. part i: collision efficiency. problem formulation and preliminary results. *Journal of Atmospheric Sciences*, 56:2585–2600, 1999.

[62] B. A. Tinsley, R. P. Rohrbaugh, and M. Hei. Effects of image charges on the scavenging of aerosol particles by cloud droplets and on droplet charging and possible ice nucleation processes. *Journal of Atmospheric Sciences*, 57:2118–2134, 1999.

[63] A. Jaworek, K. Adamiak, W. Balachandran, A. Krupa, and P. Castle. Numerical simulation of scavenging of small particles by charged droplets. *Aerosol Science and Technology*, 36:913–924, 2002.

[64] S. Kojevnikova and Y. Zimmels. Mechanism of aerosol collection by two- and three-dimensional inhomogeneous arrays of charged drops. *Chemical Engineering Science*, 55:4839–4855, 2002.

[65] Y. Zimmels and S. Kojevnikova. Use of electric image forces for collection of aerosols by array of drops. *Aerosol Science and Technology*, 36:697–713, 2002.

[66] O. Vohl, S. K. Mitra, K. Diehl, G. Huber, S. C. Wurzler, K. L. Kratz, and H. R. Pruppacher. A wind tunnel study of turbulence effects on the scavenging of aerosol particles by water drops. *Journal of the Atmospheric Sciences*, 58:3064–3072, 2001.

[67] N. Song and D. Lamb. Experimental investigations of ice in supercooled clouds. part ii: Scavenging of an insoluble aerosol. *Journal of the Atmospheric Sciences*, 51:104–116, 1993.

[68] N. V. Krasnogorskaya. Experimental investigation of the collision efficiency of charged droplets of comparable size. *Advances in Aerosol Physics*, 6:61–67, 1993.

[69] V. Hampl, M. Kerker, D. D. Cooke, and E. Matijevic. Scavenging of aerosol particles by a falling water droplet. *Journal of the Atmospheric Sciences*, 28:1211–1221, 1971.

[70] J. R. Adam and R. G. Semonin. Collection efficiencies of raindrops for submicron particulates. *Journal of the Atmospheric Sciences*, 35:151–160, 1993.

[71] K. Y. Lai, N. Dayan, and M. Kerker. Scavenging of aerosol particles by a falling water drop. *Journal of the Atmospheric Sciences*, 35:674–682, 1993.

[72] P. K. Wang and H. R. Pruppacher. An experimental determination of the efficiency with which aerosol particles are collected by water drops in subsaturated air. *Journal of the Atmospheric Sciences*, 34:1664–1669, 1977.

[73] C. E. Abbott. Charged droplet collision efficiency measurements. *Journal of the Applied Meteorology*, 14:87–90, 1974.

[74] K. H. leong, K. V. Beard, and H. T. Ochs. Laboratory measurements of particle capture by evaporating cloud drops. *Journal of the Atmospheric Sciences*, 39:1130–11140, 1982.

[75] J. Stukel H.C. Wang, K. H. Leong and P. Hopke. Collection of hydrophilic and hydrophobic charged submicron particles by charged water droplets. *Journal of Aerosol Science*, 14:703–712, 1983.

[76] S. Sumiyoshitani M. Hara and M. Akazaki. Fundamental processes of fine particle collection by charged water droplets. *2nd International Conference Electrostatic Precipitation*, 1984.

[77] V. Sminov. Electrostatic collection of aerosol particles on a sphere at intermediate reynolds numbers. *Journal of Aerosol Science*, 7:473–477, 1976.

[78] *Gambit 2.3 documentation*. Fluent Inc., 2006.

[79] S. Taneda. Experimental investigation of the wake behind a sphere at low reynolds numbers. *Journal of Physics Society Japan*, 11:1104–1108, 1956.

[80] *FLUENT 6.3 user's guide*. Fluent Inc., 2006.

[81] S. Patankar. *Numerical heat transfer and fluid flow*. Taylor and Francis, 1st edition, 1980.

[82] J. Butcher. *Numerical methods for ordinary differential equations*. Joohn Wiley and Sons, 1st edition, 2003.

[83] J. Grace R. Clift and M. Weber. Bubbles, drops and particles. *Academic Press*, page 112, 1978.

[84] T. Mertes and H. Rhodes. Liquid-particle behavior. *Chemical Engineering Progress*, 51:429–432, 1955.

[85] J. Richardson and W Zaki. Sedimentation and fluidization. *Transactions of the Institution of Chemical Engineers*, 32:35–53, 1954.

[86] D. Oliver. The sedimentation of suspensions of closely sized spherical particles. *Chemical Engineering Science*, 15:230–242, 1961.

[87] S. Kuwabara. The forces experienced by randomly distributed parallel circular cylinders or spheres in a viscous flow at small Reynolds numbers. *Journal of the Physical Society of Japan*, 14:527–532, April 1959.

[88] H. Hasimoto. On the periodic fundamental solutions of the stokes equations and their application to viscous flow past a cubic array of spheres. *Journal of Fluid Mechanics*, 5:317–328, 1959.

[89] H. Happel. Viscosity of suspensions of uniform spheres. *Journal of Applied Physics*, 28:1288–1328, 1957.

[90] E. Barnea and J. Mizrahi. A generalized approach to the fluid dynamics of particulate systems part 1. general correlation for fluidization and sedimentation in solid multiparticle systems. *The Chemical Engineering Journal*, 5:171–189, 1973.

[91] J. M. Meek and J. D. Craggs. *Electrical breakdown of gases*. Clarendon press, New York, 1st edition, 1953.

[92] P. Newman M. Putko and A. Taylor. Employing sensitivity derivatives to estimate uncertainty propagation in cfd. *9th ASCE Specialty Conference on Probabilistic Mechanics and Structural Reliability*, pages 1–6, 2004.

[93] R. Wilson F. Stern and J. Shao. Quantitative V&V of cfd simulations and certification of cfd codes. *International Journal of Numerical Methods in Fluids*, 50:1335–1355, 2006.

[94] P. Roche. Conservatism of the GCI in finite volume computations on steady state fluid flow and heat transfer. *Journal of Fluids Engineering*, 125:731–732, 2003.

[95] I. Celik and O. Karatekin. Numerical experiments on application of richardson extrapolation with nonuniform grids. *Journal of Fluids Engineering*, 119:584–590, 1997.

[96] L. Richardson and J. Gaunt. The deferred approach to the limit. *Transactions of the Royal Society of London*, 226:291–361, 1927.

[97] N. Ghia P. Roche and M. White. Editorial policy statement on the control of numerical accuracy. *Journal of Fluids Engineering*, 108:2–4, 1986.

Appendix A

Computer programs

A.1 UDF code for the inertial effect

```
/*****************************************************************
  UDF for computing  particle trajectoriers while considering
  size of diameter
*****************************************************************/
#include "udf.h"
/*#include "surf.h"*/
/*#include "dpm.h"*/
/*#include "stdio.h"*/
/*#include "string.h"*/

#define D 0.0001

 static real bottomx=0;   /*define droplet position*/
 static real bottomy=0;
 static real bottomz=0;
 /*static real topx=0.0004330127;
 static real topy=0.0005;*/
 int counter=0, tcounter=0, bcounter=0;
```

```
/* top or bottom counter for recording the number of particles
hitting on the top or bottom droplet */
int inicounter=0, pinicounter=5;  /*counting how many time scalar
update function initialized, refelect how many particles set out*/
int elsecounter,stopnumber,tracknumber; /*elsecounter is to count
how many times one  particle enters from inlet */
int current_stream=0;
float  ppZ;



DEFINE_DPM_SCALAR_UPDATE(Mycollision,cell,thread,initialize,p)
{


  real R1,R2,cd; /*R1 and R2 are the distance from particle to two
  droplet center respectively, cd is collision judge distance  */

  FILE *fp2,fp3;

  double beg; /*scaled particle x position*/


 if (initialize)
    {
      elsecounter=0;
      stopnumber=0;
      ppZ=-1;
      tracknumber=0;
      inicounter=1;

         printf( "inicounter = %d \n", inicounter);
```

```
        printf( "ppZ = %f \n", ppZ);
        printf( "elsecounter = %d \n",elsecounter);
    }

 else
    {


        if(ppZ < p->state.pos[2])
 {
   ppZ = p->state.pos[2];
   /* printf("I was here 1\n");*/
 }
         else
         {
        elsecounter = elsecounter +1;
printf("elsecounter = 2\n");
         }

       R2 = sqrt(SQR( p->state.pos[0]-bottomx)+SQR(

       p->state.pos[1]-bottomy)+SQR(p->state.pos[2]-bottomz) );

       cd = 0.5* P_DIAM(p)+0.5*D;


       fp2 = fopen("Onedrop.dat", "a");
      if(!fp2)
       {
         printf("can not open myupdatefile.txt for writing.\n");
         return;
       }
```

```
   if (R2<=cd && inicounter==1)
  {

    bcounter= bcounter+1;

fprintf(fp2,"%e %.9f %.9f %.9f  %d %.9f %.9f %.9f
    %f %f %f %d\n",

    P_TIME(p), p->state.pos[0],p->state.pos[1],
    p->state.pos[2],bcounter,

    P_INIT_POS(p)[0],P_INIT_POS(p)[1],P_INIT_POS(p)[2],
    P_INIT_VEL(p)[0],

    P_INIT_VEL(p)[1],P_INIT_VEL(p)[2],p->stream_index);

    /*printf("Bottom counter equals %d\n", bcounter );
printf("I am here \n");

    printf("R2 = %f, cd = %f, particle postion is %f
    %f %f\n ", R2,

    cd,p->state.pos[0],p->state.pos[1],p->state.pos[2]);*/

    stopnumber=1.0;
    current_stream=current_stream+1;
    pinicounter=inicounter;
    /*printf("previous inicounter = %d \n",pinicounter);*/
    inicounter=0;
```

```
   p->stream_index=-1;
         }


          if (elsecounter>0)
          /* judge if this is the second time the particle

          passed the inlet, if yes, then stop the particle
          motion. */
         {
       p->stream_index=-1;
       /*printf("particle out of domain %d",elsecounter);*/

  printf(fp2, "particle out of domain %d %n",
          elsecounter);
          }

         fclose(fp2);

         } /*end of else */

}        /*end of scalar_update*/
```

A.2 UDF code for the electronic effect

```
/************************************************************
  UDF for computing  particle trajectoriers when considering size
  of diameter and electrical charge
************************************************************/
#include "udf.h"
/*#include "surf.h"*/
```

```
/*#include "dpm.h"*/
/*#include "stdio.h"*/
/*#include "string.h"*/


#define D 0.0002
#define L  5*D
#define N 5
#define M (2*N+1)*(2*N+1)*(2*N+1)

 static real Ke = 9.0e9;  /*define constant*/
 static real e= 1.6e-19; /* %C */
 static real Gamma = 0.073; /*%N/m surface tension*/

 static real bottomx=0;   /*define droplet position*/
 static real bottomy=0;
 static real bottomz=0;
 /*static real topx=0.0004330127;
 static real topy=0.0005;*/
 int counter=0, tcounter=0, bcounter=0;
 /* top or bottom counter for recording the number
 of particles hitting on the top or bottom droplet */
 int inicounter=0, pinicounter=5;  /*counting how
 many time scalar update function initialized,
 refelect how many particles set out*/
 int elsecounter,stopnumber,tracknumber;
 /*elsecounter is to count how many times one
 particle enters from inlet */
 int current_stream=0;
 float  ppZ;
 static real myFe=0.0;
```

```
DEFINE_DPM_SCALAR_UPDATE
(Mycollision,cell,thread,initialize,p)
{


  real R1,R2,cd; /*R1 and R2 are the distance
  from particle to two droplet center respectively,
  cd is collision judge distance  */

  FILE *fp2,fp3;

  double beg; /*scaled particle x position*/


 if (initialize)
    {
      elsecounter=0;
      stopnumber=0;
      ppZ=-1;
      tracknumber=0;
      inicounter=1;

         printf( "inicounter = %d \n", inicounter);

         printf( "ppZ = %f \n", ppZ);

         printf( "elsecounter = %d \n",elsecounter);
     }

  else
```

```
   {


       if(ppZ < p->state.pos[2])
{
  ppZ = p->state.pos[2];
  /* printf("I was here 1\n");*/
}
        else
        {
        if (p->state.pos[2] < 0)
{ elsecounter = elsecounter +1; }
else
{ ppZ = p->state.pos[2];        }
   /*printf("elsecounter = 2\n");*/
        }

      R2 = sqrt(SQR( p->state.pos[0]-bottomx)+SQR(

       p->state.pos[1]-bottomy)+SQR(p->state.pos[2]-bottomz) );

      cd = (0.5* P_DIAM(p)+0.5*D));


      fp2 = fopen("Onedrop.dat", "a");
     if(!fp2)
      {
        printf("can not open myupdatefile.txt for writing.\n");
        return;
      }
```

```
   if (R2<=cd && inicounter==1)
  {

    bcounter= bcounter+1;

fprintf(fp2,"%e %.9f %.9f %.9f  %d %.9f %.9f %.9f %f

    %f %f %d %f %f %f\n", P_TIME(p),

     p->state.pos[0],p->state.pos[1],p->state.pos[2],

     bcounter,P_INIT_POS(p)[0],P_INIT_POS(p)[1],

     P_INIT_POS(p)[2],

     P_INIT_VEL(p)[0], P_INIT_VEL(p)[1],P_INIT_VEL(p)[2],

     p->stream_index, P_VEL(p)[0],P_VEL(p)[1],P_VEL(p)[2] );

    /*printf("Bottom counter equals %d\n", bcounter );

printf("I am here \n");

    printf("R2 = %f, cd = %f, particle postion is

    %f %f %f\n ", R2,

    cd,p->state.pos[0],p->state.pos[1],p->state.pos[2]);*/

    stopnumber=1.0;
    current_stream=current_stream+1;
```

```
          pinicounter=inicounter;

          /*printf("previous inicounter = %d
          \n",pinicounter);*/
          inicounter=0;
   p->stream_index=-1;
        }


       if (elsecounter>0)
       /* judge if this is the second time the particle
       passed the inlet, if yes, then stop the particle motion. */
       {

     /*printf("particle out of domain %d",elsecounter);*/

 /*fprintf(fp2, "my particle out of domain %d %n",

        elsecounter);*/

        p->stream_index=-1;

        }



  fclose(fp2);

      } /*end of else */

}     /*end of scalar_update*/
```

```
DEFINE_DPM_BODY_FORCE(My_particle_body_force,p,i)
{
        real bforce,sumFex=0,sumFey=0,sumFez=0;

        real a,A,R,RtoC,Q_D,q_p,Fe,Term1,Term2,Term3,Term4;

/*real DM[3][pow((2*N+1),3)];*/

        real DM[3][M],AllFe[M], AllFexyz[3][M];

         /*define droplet position matrix */
real xx, yy,zz;
int DMcounter=0;
        /*FILE *fp4;
fp4 = fopen("bodyforce.dat", "a"); */
      /* if(!fp4)
        {
          printf("can not open myupdatefile.txt for writing.\n");

          return;
        }*/

    /*fprintf(fp4,"i am here\n"),*/
a = 0.5* P_DIAM(p);

        A = D/2;

         RtoC = sqrt(SQR( p->state.pos[0]-bottomx)+SQR(

         p->state.pos[1]-bottomy)+SQR(p->state.pos[2]-bottomz) );
```

```
         /*distance to the center (0,0,0) */
 Q_D = 0.2019e-10;  /*Coulomb* Raleign limit/
 /*q_p = 0.0071e-12;*/  /*CoulombRaleign limit*/
         q_p = 0.0071e-15;



         for  (zz = -N*L ; zz <= N*L ; zz = zz +L )

         /* Total (2N+1)^3 droplet, for each droplet,

         calculate electric force */
for (yy = -N*L ; yy <= N*L ; yy = yy +L )
for (xx = -N*L ; xx <= N*L ; xx = xx +L )
         {
                 DM[0][DMcounter]= xx;

                 /* Total (2N+1)^3 droplet positions are
                 saved to array DM,  0 1 2 represent x y z */

                 DM[1][DMcounter]= yy;

                 DM[2][DMcounter]= zz;

                 R = sqrt(SQR( p->state.pos[0]-DM[0]

                 [DMcounter])+SQR(

                 p->state.pos[1]-DM[1][DMcounter])+

                 SQR(p->state.pos[2]
```

```
-DM[2][DMcounter]) );

/*calculate the distance from the

particle to each droplet*/

/* Term2= Ke*SQR(Q_D)*a*( 1/pow(R,3) -
R/SQR(SQR(R)-SQR(a)));

 Term3= Ke*SQR(q_p)*A*(

 1/pow(R,3) - R/SQR(SQR(R)-SQR(A)));

 Term4= Ke* SQR(Q_D)*a*SQR(q_p)*A*(

1/pow(R,4)+ 1/SQR(SQR(R)-SQR(a)-SQR(A))

- 1/SQR(SQR(R)-SQR(a)) -1/SQR(SQR(R)-SQR(A))); */

 Term1 = Ke*Q_D*q_p/SQR(R);

   AllFe[DMcounter] =  Term1;

   /* This is array stores all Fe forces

   from each droplet,

   size is (2N+1)^3*/

   AllFexyz[0][DMcounter]=((DM[0][DMcounter]

   -p->state.pos[0]
```

```
)/R)*AllFe[DMcounter];

 AllFexyz[1][DMcounter]=((DM[1][DMcounter]

 -p->state.pos[1])

/R)*AllFe[DMcounter];

/*Dissect Fe to x y z, save to a 3 x

(2N+1)^3 array AllFexyz*/

 AllFexyz[2][DMcounter]=((DM[2][DMcounter]

 -p->state.pos[2])/R)

 *AllFe[DMcounter];


sumFex= sumFex + AllFexyz[0][DMcounter];

sumFey= sumFey + AllFexyz[1][DMcounter];

/*Calculate sum Fe*/


sumFez= sumFez + AllFexyz[2][DMcounter];

DMcounter++;
}
```

```
 if(i==0) bforce= sumFex;

           else if(i==1) bforce=sumFey;
   else if (i==2) bforce=sumFez;


         if( i==2 )
{

               /*fprintf( fp4,"%e %d %e %e %e %e %.9f \n"

                 ,P_TIME(p),

              i, bforce,Term1,Term2,Term3,Term4, R);*/

                /*fprintf( fp4,"%d %e \n", i, bforce);*/
}
 else
{
/*fprintf( fp4,"%d %e ", i, bforce);*/

}


         /*fprintf( fp4,"%e %d %e %.9f %.9f %.9f %.9f

          %.9f %.9f

         %.9f %.9f \n",P_TIME(p),
```

```
        i, bforce,Fe, p->state.pos[0],p->state.pos[1],

        p->state.pos[2], P_VEL(p)[0],P_VEL(p)[1],

        P_VEL(p)[2], R);*/

        /*fclose(fp4);*/

       /* an acceleration should be returned */

       return (bforce/P_MASS(p));

}
```

Appendix B

Tables of results for the electrostatic effect

Table B.1: The inertial effect results from a 50 μm droplet, a 1-10 μm particle, and $L = 2D, 5D$ and $10D$ without velocity hindrance consideration.

Particle size (μm)	Collection area (m^2) L = 2D	Collection efficiency L=2D	Collection area (m^2) L=5D	Collection efficiency L=5D	Collection area (m^2) L=10D	Collection efficiency L=10D
1	$1.64E^{-12}$	0.0013	$1.90E^{-13}$	$2.43E^{-05}$	$1.11E^{-13}$	$3.56E^{-06}$
2	$6.05E^{-12}$	0.0048	$7.56E^{-13}$	$9.68E^{-05}$	$5.06E^{-13}$	$1.62E^{-05}$
3	$1.16E^{-11}$	0.0095	$1.79E^{-12}$	$2.29E^{-04}$	$1.17E^{-12}$	$3.75E^{-05}$
4	$1.94E^{-11}$	0.0155	$3.00E^{-12}$	$3.84E^{-04}$	$1.93E^{-12}$	$6.19E^{-05}$
5	$3.05E^{-11}$	0.0244	$4.74E^{-12}$	$6.06E^{-04}$	$2.97E^{-12}$	$9.49E^{-05}$
6	$4.97E^{-11}$	0.0398	$7.37E^{-12}$	$9.44E^{-04}$	$4.55E^{-12}$	$1.46E^{-04}$
7	$8.81E^{-11}$	0.0705	$1.11E^{-11}$	$1.50E^{-03}$	$6.87E^{-12}$	$2.20E^{-04}$
8	$1.43E^{-10}$	0.1142	$2.03E^{-11}$	$2.60E^{-03}$	$1.11E^{-11}$	$3.56E^{-04}$
9	$1.95E^{-10}$	0.1556	$3.53E^{-11}$	$4.50E^{-03}$	$1.93E^{-11}$	$6.19E^{-04}$
10	$2.33E^{-10}$	0.1867	$5.66E^{-11}$	$7.20E^{-03}$	$2.37E^{-11}$	$7.58E^{-04}$

Table B.2: The inertial effect results from a 100 μm droplet, a 1-10 μm particle, and $L = 2D, 5D$ and $10D$ without velocity hindrance consideration.

Particle size (μm)	Collection area (m^2) L = 2D	Collection efficiency L=2D	Collection area (m^2) L=5D	Collection efficiency L=5D	Collection area (m^2) L=10D	Collection efficiency L=10D
1	$1.80E^{-12}$	$3.59E^{-04}$	$1.80E^{-13}$	$5.76E^{-06}$	$6.62E^{-14}$	$5.29E^{-07}$
2	$6.17E^{-12}$	0.0012	$7.26E^{-13}$	$2.32E^{-05}$	$3.95E^{-13}$	$3.16E^{-06}$
3	$1.11E^{-11}$	0.0022	$2.06E^{-12}$	$6.61E^{-05}$	$1.22E^{-12}$	$9.76E^{-06}$
4	$1.81E^{-11}$	0.0036	$3.81E^{-12}$	$1.22E^{-04}$	$2.56E^{-12}$	$2.05E^{-05}$
5	$3.67E^{-11}$	0.0073	$7.73E^{-12}$	$2.47E^{-04}$	$5.50E^{-12}$	$4.40E^{-05}$
6	$1.41E^{-10}$	0.0282	$2.00E^{-11}$	$6.40E^{-04}$	$1.30E^{-11}$	$1.04E^{-04}$
7	$4.43E^{-10}$	0.0886	$7.65E^{-11}$	$2.40E^{-03}$	$4.87E^{-11}$	$3.89E^{-04}$
8	$6.34E^{-10}$	0.1267	$1.79E^{-10}$	$5.70E^{-03}$	$1.31E^{-10}$	$1.10E^{-03}$
9	$9.05E^{-10}$	0.181	$2.92E^{-10}$	$9.30E^{-03}$	$2.32E^{-10}$	$1.90E^{-03}$
10	$8.65E^{-10}$	0.173	$3.94E^{-10}$	$1.26E^{-02}$	$3.24E^{-10}$	$2.60E^{-03}$

Table B.3: The inertial effect results from a 200 μm droplet, a 1-10 μm particle, and $L = 2D, 5D$ and $10D$ without velocity hindrance consideration.

Particle size (μm)	Collection area (m^2) L = 2D	Collection efficiency L=2D	Collection area (m^2) L=5D	Collection efficiency L=5D	Collection area (m^2) L=10D	Collection efficiency L=10D
1	$3.34E^{-12}$	$1.67E^{-04}$	$2.20E^{-13}$	$1.76E^{-06}$	$1.91E^{-13}$	$3.83E^{-07}$
2	$9.51E^{-12}$	$4.76E^{-04}$	$9.10E^{-13}$	$7.28E^{-06}$	$8.04E^{-13}$	$1.36E^{-06}$
3	$1.39E^{-11}$	$6.93E^{-04}$	$2.81E^{-12}$	$2.25E^{-05}$	$2.60E^{-12}$	$5.20E^{-06}$
4	$2.25E^{-11}$	$1.10E^{-03}$	$8.79E^{-12}$	$7.03E^{-05}$	$7.50E^{-12}$	$1.50E^{-05}$
5	$6.88E^{-11}$	$3.40E^{-02}$	$4.10E^{-11}$	$3.28E^{-04}$	$3.80E^{-11}$	$7.60E^{-05}$
6	$1.61E^{-09}$	$8.06E^{-02}$	$3.90E^{-10}$	$3.10E^{-03}$	$3.39E^{-10}$	$6.78E^{-04}$
7	$2.46E^{-09}$	$1.23E^{-01}$	$8.50E^{-10}$	$7.20E^{-03}$	$7.89E^{-10}$	$1.58E^{-03}$
8	$2.95E^{-09}$	$1.48E^{-01}$	$1.39E^{-09}$	$1.11E^{-02}$	$1.25E^{-09}$	$2.50E^{-03}$
9	$3.33E^{-09}$	$1.66E^{-01}$	$1.87E^{-09}$	$1.50E^{-02}$	$1.76E^{-09}$	$3.50E^{-03}$
10	$3.52E^{-09}$	$1.76E^{-01}$	$2.34E^{-09}$	$1.87E^{-02}$	$2.10E^{-09}$	$4.20E^{-03}$

Table B.4: The inertial effect results from a 50 μm droplet, a 1-10 μm particle, and $L = 2D, 5D$ and $10D$ with velocity hindrance consideration.

Particle size (μm)	Collection area (m^2) L = 2D	Collection efficiency L=2D	Collection area (m^2) L=5D	Collection efficiency L=5D	Collection area (m^2) L=10D	Collection efficiency L=10D
1	$9.60E^{-13}$	0.0008	$1.24E^{-13}$	$1.59E^{-05}$	$8.42E^{-14}$	$2.69E^{-06}$
2	$3.81E^{-12}$	0.0031	$5.40E^{-13}$	$6.91E^{-05}$	$4.07E^{-13}$	$1.30E^{-05}$
3	$7.21E^{-12}$	0.0058	$1.26E^{-12}$	$1.61E^{-04}$	$9.27E^{-13}$	$2.97E^{-05}$
4	$1.15E^{-11}$	0.0092	$1.97E^{-12}$	$2.52E^{-04}$	$1.49E^{-12}$	$4.77E^{-05}$
5	$1.63E^{-11}$	0.0131	$2.74E^{-12}$	$3.51E^{-04}$	$2.15E^{-12}$	$6.90E^{-05}$
6	$2.39E^{-11}$	0.0191	$3.74E^{-12}$	$4.79E^{-04}$	$3.03E^{-12}$	$9.68E^{-05}$
7	$3.86E^{-11}$	0.0309	$5.07E^{-12}$	$6.49E^{-04}$	$4.25E^{-12}$	$1.36E^{-04}$
8	$5.10E^{-11}$	0.0408	$7.09E^{-12}$	$9.08E^{-04}$	$6.13E^{-12}$	$1.96E^{-04}$
9	$6.11E^{-11}$	0.0489	$1.07E^{-11}$	$1.40E^{-03}$	$9.57E^{-12}$	$3.06E^{-04}$
10	$8.36E^{-11}$	0.0669	$1.77E^{-11}$	0.0023	$1.64E^{-11}$	$5.26E^{-04}$

Table B.5: The inertial effect results from a 100 μm droplet, a 1-10 μm particle, and $L = 2D, 5D$ and $10D$ with velocity hindrance consideration.

Particle size (μm)	Collection area (m^2) L = 2D	Collection efficiency L=2D	Collection area (m^2) L=5D	Collection efficiency L=5D	Collection area (m^2) L=10D	Collection efficiency L=10D
1	$1.31E^{-12}$	$2.61E^{-04}$	$0.14E^{-12}$	$4.48E^{-06}$	$6.59E^{-14}$	$5.27E^{-07}$
2	$4.46E^{-12}$	$8.92E^{-04}$	$4.95E^{-13}$	$1.58E^{-05}$	$3.62E^{-13}$	$2.89E^{-06}$
3	$7.94E^{-12}$	0.0016	$1.72E^{-12}$	$5.5E^{-05}$	$1.14E^{-12}$	$9.14E^{-06}$
4	$1.04E^{-11}$	0.0021	$2.99E^{-12}$	$9.57E^{-05}$	$2.41E^{-12}$	$1.93E^{-05}$
5	$1.36E^{-11}$	0.0027	$5.54E^{-12}$	$1.77E^{-04}$	$5.12E^{-12}$	$4.10E^{-05}$
6	$1.65E^{-11}$	0.0033	$1.18E^{-11}$	$3.78E^{-04}$	$1.14E^{-11}$	$9.16E^{-05}$
7	$2.14E^{-11}$	0.0043	$3.68E^{-11}$	$1.18E^{-03}$	$4.06E^{-11}$	$3.25E^{-04}$
8	$3.59E^{-11}$	0.0072	$1.14E^{-10}$	$3.65E^{-03}$	$1.19E^{-10}$	$9.52E^{-04}$
9	$1.60E^{-10}$	0.0321	$2.19E^{-10}$	$7.01E^{-03}$	$2.16E^{-10}$	$1.70E^{-03}$
10	$4.19E^{-10}$	0.0839	$3.28E^{-10}$	$1.05E^{-02}$	$3.11E^{-10}$	$2.50E^{-03}$

Table B.6: The inertial effect results from a 200 μm droplet, a 1-10 μm particle, and $L = 2D, 5D$ and $10D$ with velocity hindrance consideration.

Particle size (μm)	Collection area (m^2) L = 2D	Collection efficiency L=2D	Collection area (m^2) L=5D	Collection efficiency L=5D	Collection area (m^2) L=10D	Collection efficiency L=10D
1	$2.27E^{-12}$	$1.13E^{-04}$	$1.87E^{-13}$	$1.50E^{-06}$	$1.72E^{-13}$	$3.43E^{-07}$
2	$7.16E^{-12}$	$3.58E^{-04}$	$7.74E^{-13}$	$6.19E^{-06}$	$7.24E^{-13}$	$1.48E^{-06}$
3	$9.31E^{-12}$	$4.66E^{-04}$	$2.39E^{-12}$	$1.91E^{-05}$	$2.34E^{-13}$	$4.68E^{-06}$
4	$1.17E^{-11}$	$5.85E^{-04}$	$7.47E^{-12}$	$5.98E^{-05}$	$6.75E^{-12}$	$1.35E^{-05}$
5	$1.65E^{-11}$	$8.27E^{-04}$	$3.49E^{-11}$	$2.79E^{-04}$	$3.42E^{-11}$	$6.84E^{-05}$
6	$2.96E^{-11}$	$1.50E^{-03}$	$3.32E^{-10}$	$2.65E^{-03}$	$3.05E^{-10}$	$6.10E^{-04}$
7	$7.60E^{-10}$	$3.80E^{-02}$	$7.26E^{-10}$	$5.78E^{-03}$	$7.10E^{-10}$	$1.42E^{-03}$
8	$1.87E^{-09}$	$9.34E^{-02}$	$1.18E^{-09}$	$9.45E^{-03}$	$1.13E^{-09}$	$2.25E^{-03}$
9	$2.50E^{-09}$	$1.25E^{-01}$	$1.59E^{-09}$	$1.27E^{-02}$	$1.58E^{-09}$	$3.17E^{-03}$
10	$2.88E^{-09}$	$1.44E^{-01}$	$1.99E^{-09}$	$1.59E^{-02}$	$1.89E^{-09}$	$3.78E^{-03}$

Appendix C

Tables of results for the electrostatic effect

Table C.1: The collection area results for the electrostatic effect from a 200 μm droplet, a 1-10 μm particle, and $L = 2D$.

Particle size (μm)	Collection area (m^2) $SF = 1E^{-6}$	Collection area (m^2) $SF = 1E^{-4}$	Collection area (m^2) $SF = 5E^{-4}$	Collection area (m^2) $SF = 1E^{-3}$	Collection area (m^2) $SF = 1E^{-2}$	Collection area (m^2) $SF = 3E^{-2}$	Collection area (m^2) $SF = 6E^{-2}$	Collection area (m^2) $SF = 1E^{-1}$
1	$9.85E^{-11}$	$5.20E^{-09}$	$1.50E^{-08}$	$1.87E^{-08}$	$1.97E^{-08}$	$1.97E^{-08}$	$1.97E^{-08}$	$1.97E^{-08}$
2	$4.13E^{-11}$	$2.92E^{-09}$	$8.84E^{-09}$	$1.39E^{-08}$	$1.97E^{-08}$	$1.97E^{-08}$	$1.97E^{-08}$	$1.97E^{-08}$
3	$2.90E^{-11}$	$1.88E^{-09}$	$6.34E^{-09}$	$1.01E^{-08}$	$1.97E^{-08}$	$1.97E^{-08}$	$1.97E^{-08}$	$1.97E^{-08}$
4	$2.90E^{-11}$	$1.33E^{-09}$	$4.79E^{-09}$	$7.60E^{-09}$	$1.97E^{-08}$	$1.97E^{-08}$	$1.97E^{-08}$	$1.97E^{-08}$
5	$3.84E^{-11}$	$1.07E^{-09}$	$3.83E^{-09}$	$6.12E^{-09}$	$1.97E^{-08}$	$1.97E^{-08}$	$1.97E^{-08}$	$1.97E^{-08}$
6	$8.67E^{-10}$	$1.88E^{-09}$	$3.20E^{-09}$	$5.03E^{-09}$	$1.97E^{-08}$	$1.97E^{-08}$	$1.97E^{-08}$	$1.97E^{-08}$
7	$1.12E^{-09}$	$1.46E^{-09}$	$3.04E^{-09}$	$4.34E^{-09}$	$1.83E^{-08}$	$1.97E^{-08}$	$1.97E^{-08}$	$1.97E^{-08}$
8	$1.90E^{-09}$	$2.05E^{-09}$	$3.04E^{-09}$	$4.34E^{-09}$	$1.62E^{-08}$	$1.97E^{-08}$	$1.97E^{-08}$	$1.97E^{-08}$
9	$2.52E^{-09}$	$2.55E^{-09}$	$3.02E^{-09}$	$3.69E^{-09}$	$1.38E^{-08}$	$1.97E^{-08}$	$1.97E^{-08}$	$1.97E^{-08}$
10	$2.92E^{-09}$	$2.95E^{-09}$	$3.24E^{-09}$	$3.51E^{-09}$	$1.14E^{-08}$	$1.92E^{-08}$	$1.97E^{-08}$	$1.97E^{-08}$

Table C.2: The collection efficiency results for the electrostatic effect from a 200 μm droplet, a 1-10 μm particle, and $L = 2D$.

Particle size (μm)	Collection efficiency $SF = 1E^{-6}$	Collection efficiency $SF = 1E^{-4}$	Collection efficiency $SF = 5E^{-4}$	Collection efficiency $SF = 1E^{-3}$	Collection efficiency $SF = 1E^{-2}$	Collection efficiency $SF = 3E^{-2}$	Collection efficiency $SF = 6E^{-2}$	Collection efficiency $SF = 1E^{-1}$
1	$4.90E^{-03}$	$2.60E^{-02}$	$7.52E^{-02}$	$9.37E^{-02}$	$9.84E^{-02}$	$9.84E^{-02}$	$9.84E^{-02}$	$9.84E^{-02}$
2	$2.10E^{-03}$	$1.46E^{-02}$	$4.42E^{-02}$	$6.93E^{-02}$	$9.84E^{-02}$	$9.84E^{-02}$	$9.84E^{-02}$	$9.84E^{-02}$
3	$1.50E^{-03}$	$9.40E^{-02}$	$3.17E^{-02}$	$5.03E^{-02}$	$9.84E^{-02}$	$9.84E^{-02}$	$9.84E^{-02}$	$9.84E^{-02}$
4	$1.40E^{-03}$	$6.64E^{-02}$	$2.40E^{-02}$	$3.80E^{-02}$	$9.84E^{-02}$	$9.84E^{-02}$	$9.84E^{-02}$	$9.84E^{-02}$
5	$1.90E^{-03}$	$5.35E^{-02}$	$1.92E^{-02}$	$3.06E^{-02}$	$9.84E^{-02}$	$9.84E^{-02}$	$9.84E^{-02}$	$9.84E^{-02}$
6	$4.34E^{-02}$	$9.40E^{-02}$	$1.60E^{-02}$	$2.52E^{-02}$	$9.84E^{-02}$	$9.84E^{-02}$	$9.84E^{-02}$	$9.84E^{-02}$
7	$5.60E^{-02}$	$7.32E^{-02}$	$1.52E^{-02}$	$2.17E^{-02}$	$9.16E^{-02}$	$9.84E^{-02}$	$9.84E^{-02}$	$9.84E^{-02}$
8	$9.50E^{-02}$	$1.03E^{-02}$	$1.52E^{-02}$	$2.17E^{-02}$	$8.09E^{-02}$	$9.84E^{-02}$	$9.84E^{-02}$	$9.84E^{-02}$
9	$1.26E^{-02}$	$1.28E^{-02}$	$1.51E^{-02}$	$1.85E^{-02}$	$6.84E^{-02}$	$9.84E^{-02}$	$9.84E^{-02}$	$9.84E^{-02}$
10	$1.46E^{-02}$	$1.48E^{-02}$	$1.62E^{-02}$	$1.76E^{-02}$	$5.72E^{-02}$	$9.60E^{-02}$	$9.84E^{-02}$	$9.84E^{-02}$

Table C.3: The collection area results for the electrostatic effect from a 200 μm droplet, a 1 μm particle, and $L = 2D, 5D, 10D$.

Droplet distance	Collection area (m^2) $SF = 1E^{-6}$	Collection area (m^2) $SF = 1E^{-4}$	Collection area (m^2) $SF = 5E^{-4}$	Collection area (m^2) $SF = 1E^{-3}$	Collection area (m^2) $SF = 1E^{-2}$	Collection area (m^2) $SF = 3E^{-2}$	Collection area (m^2) $SF = 6E^{-2}$	Collection area (m^2) $SF = 1E^{-1}$
$L = 2D$	$9.85E^{-11}$	$5.20E^{-09}$	$1.50E^{-08}$	$1.87E^{-08}$	$1.97E^{-08}$	$1.97E^{-08}$	$1.97E^{-08}$	$1.97E^{-08}$
$L = 5D$	$2.78E^{-11}$	$2.94E^{-09}$	$1.34E^{-08}$	$2.44E^{-08}$	$1.22E^{-07}$	$1.25E^{-07}$	$1.25E^{-07}$	$1.25E^{-07}$
$L = 10D$	$2.27E^{-09}$	$2.33E^{-09}$	$2.50E^{-09}$	$2.35E^{-08}$	$1.90E^{-07}$	$4.57E^{-07}$	$4.99E^{-07}$	$4.99E^{-07}$

Table C.4: The collection efficiency results for the electrostatic effect from a 200 μm droplet, a 1 μm particle, and $L = 2D, 5D, 10D$.

Droplet distance	Collection efficiency $SF = 1E^{-6}$	Collection efficiency $SF = 1E^{-4}$	Collection efficiency $SF = 5E^{-4}$	Collection efficiency $SF = 1E^{-3}$	Collection efficiency $SF = 1E^{-2}$	Collection efficiency $SF = 3E^{-2}$	Collection efficiency $SF = 6E^{-2}$	Collection efficiency $SF = 1E^{-1}$
$L = 2D$	$4.90E^{-03}$	$2.60E^{-02}$	$7.52E^{-02}$	$9.37E^{-02}$	$9.84E^{-02}$	$9.84E^{-02}$	$9.84E^{-02}$	$9.84E^{-02}$
$L = 5D$	$2.22E^{-04}$	$2.35E^{-02}$	$1.07E^{-02}$	$1.95E^{-02}$	$9.74E^{-02}$	$9.96E^{-02}$	$9.96E^{-02}$	$9.96E^{-02}$
$L = 10D$	$4.50E^{-03}$	$4.70E^{-03}$	$5.00E^{-03}$	$4.17E^{-02}$	$3.80E^{-02}$	$9.15E^{-02}$	$9.98E^{-02}$	$9.98E^{-02}$

Table C.5: The collection area results for the electrostatic effect from a 200 μm droplet, a 10 μm particle, and $L = 2D, 5D, 10D$

Droplet distance	Collection area (m^2) $SF = 1E^{-6}$	Collection area (m^2) $SF = 1E^{-4}$	Collection area (m^2) $SF = 5E^{-4}$	Collection area (m^2) $SF = 1E^{-3}$	Collection area (m^2) $SF = 1E^{-2}$	Collection area (m^2) $SF = 3E^{-2}$	Collection area (m^2) $SF = 6E^{-2}$	Collection area (m^2) $SF = 1E^{-1}$
$L = 2D$	$2.92E^{-09}$	$2.95E^{-09}$	$3.24E^{-09}$	$3.51E^{-09}$	$1.14E^{-08}$	$1.92E^{-08}$	$1.97E^{-08}$	$1.97E^{-08}$
$L = 5D$	$2.19E^{-09}$	$2.22E^{-09}$	$2.36E^{-09}$	$2.62E^{-09}$	$1.03E^{-08}$	$2.83E^{-08}$	$5.34E^{-08}$	$8.43E^{-08}$
$L = 10D$	$2.10E^{-09}$	$2.13E^{-09}$	$2.27E^{-09}$	$2.49E^{-09}$	$1.03E^{-08}$	$3.16E^{-08}$	$6.64E^{-08}$	$1.13E^{-07}$

Table C.6: The collection efficiency results for the electrostatic effect from a 200 μm droplet, a 10 μm particle, and $L = 2D, 5D, 10D$.

Droplet distance	Collection efficiency $SF = 1E^{-6}$	Collection efficiency $SF = 1E^{-4}$	Collection efficiency $SF = 5E^{-4}$	Collection efficiency $SF = 1E^{-3}$	Collection efficiency $SF = 1E^{-2}$	Collection efficiency $SF = 3E^{-2}$	Collection efficiency $SF = 6E^{-2}$	Collection efficiency $SF = 1E^{-1}$
$L = 2D$	$1.46E^{-02}$	$1.48E^{-02}$	$1.62E^{-02}$	$1.76E^{-02}$	$5.72E^{-02}$	$9.60E^{-02}$	$9.84E^{-02}$	$9.84E^{-02}$
$L = 5D$	$1.75E^{-02}$	$1.77E^{-02}$	$1.89E^{-02}$	$2.10E^{-02}$	$8.25E^{-02}$	$2.27E^{-02}$	$4.27E^{-02}$	$6.74E^{-02}$
$L = 10D$	$4.20E^{-03}$	$4.30E^{-03}$	$4.50E^{-03}$	$5.00E^{-03}$	$2.06E^{-02}$	$6.33E^{-02}$	$1.33E^{-02}$	$2.25E^{-02}$

Table C.7: The collection area results for the electrostatic effect from a 10 μm particle, and $L = 1000\mu m$.

Cases	Collection area (m^2) SF =$1E^{-6}$	Collection area (m^2) SF =$1E^{-4}$	Collection area (m^2) SF =$5E^{-4}$	Collection area (m^2) SF =$1E^{-3}$	Collection area (m^2) SF =$1E^{-2}$	Collection area (m^2) SF =$3E^{-2}$	Collection area (m^2) SF =$6E^{-2}$	Collection area (m^2) SF =$1E^{-1}$
100 μm droplet $L = 10D$	$2.61E^{-10}$	$4.69E^{-10}$	$1.56E^{-09}$	$3.10E^{-09}$	$3.64E^{-08}$	$1.02E^{-07}$	$1.25E^{-07}$	$1.25E^{-07}$
200 μm droplet $L = 5D$	$2.19E^{-09}$	$2.22E^{-09}$	$2.36E^{-09}$	$2.62E^{-09}$	$1.03E^{-08}$	$2.83E^{-08}$	$5.34E^{-08}$	$8.43E^{-08}$

Table C.8: The collection efficiency results for the electrostatic effect from a 10 μm particle, and $L = 1000\mu m$.

Cases	Collection efficiency $SF = 1E^{-6}$	Collection efficiency $SF = 1E^{-4}$	Collection efficiency $SF = 5E^{-4}$	Collection efficiency $SF = 1E^{-3}$	Collection efficiency $SF = 1E^{-2}$	Collection efficiency $SF = 3E^{-2}$	Collection efficiency $SF = 6E^{-2}$	Collection efficiency $SF = 1E^{-1}$
100 μm droplet $L = 10D$	$2.10E^{-03}$	$3.80E^{-03}$	$1.25E^{-02}$	$2.48E^{-02}$	$2.92E^{-02}$	$8.19E^{-02}$	$9.96E^{-02}$	$9.96E^{-02}$
200 μm droplet $L = 5D$	0.0175	0.0177	0.0189	0.021	0.0825	0.2267	0.4268	0.6743

Table C.9: Comparison of the collection areas between one droplet results and Khain and Pinsky's results, a 40 μm droplet with varying charge from 0.02 to 1 Q_{max} and a 2 μm neutral particle (where Q_{max} is the corona discharging limit of 40 μm droplet.)

Cases	Collection area (m^2) $0.02Q_{max}$	Collection area (m^2) $0.05Q_{max}$	Collection area (m^2) $0.2Q_{max}$	Collection area (m^2) $0.5Q_{max}$	Collection area (m^2) Q_{max}
This study's results	$9.93E^{-12}$	$5.55E^{-11}$	$4.30E^{-10}$	$1.29E^{-09}$	$3.12E^{-9}$
Khain and Pinsky [10]	$1.25E^{-11}$	$5.54E^{-11}$	$4.16E^{-10}$	$1.32E^{-9}$	$2.10E^{-9}$